A Quantitative Analysis of Cell-Cell Interaction Mechanisms

Emily Edith Brieger

München 2024

A Quantitative Analysis of Cell-Cell Interaction Mechanisms

Emily Edith Brieger

Dissertation
an der Fakultät für Physik
der Ludwig–Maximilians–Universität
München

vorgelegt von
Emily Edith Brieger
aus Leer

München, den 08.05.2024

Erstgutachter: Prof. Dr. Joachim O. Rädler
Zweitgutachter: Prof. Dr. Chase P. Broedersz
Tag der mündlichen Prüfung: 04.07.2024

Ludwig-Maximilian-University
Faculty of Physics

A Quantitative Analysis of Cell-Cell Interaction Mechanisms

Dissertation, 2024

Emily Edith Brieger

Quantitative Analyse von Zell-Zell Interaktionsmechanismen

Dissertation
an der Fakultät für Physik
der Ludwig-Maximilians-Universität
München

vorgelegt von
Emily Edith Brieger
aus Leer

München, den 08.05.24

Erstgutachter: Prof. Dr. Joachim O. Rädler
Zweitgutachter: Prof. Dr. Chase P. Broedersz
Tag der mündlichen Prüfung: 04.07.2024

Zusammenfassung

Kollektive Bewegung ist ein Phänomen, das bei einer Vielzahl von Systemen zu beobachten ist, von Zellverbänden über Tierschwärme bis hin zum Autoverkehr. Es beschreibt Systeme 'aktiver Materie', in denen sich aus eigenem Antrieb bewegende Einheiten durch Kräfte mit ihren Nachbarn interagieren und dadurch synchronisierte Bewegungen erzeugen. In biologischen Systemen ist die koordinierte Bewegung von Zellen für die Organisation des menschlichen Körpers und Prozesse wie Embryogenese, Wundheilung und Krebsentwicklung von entscheidender Bedeutung. Diese kollektiven Verhaltensweisen werden stark durch die Interaktionen bei Zellkontakten beeinflusst. In vorherigen Arbeiten wurden die Zell-Zell-Interaktionen in Mikrostrukturen mit Hilfe von Adhäsions- und Kohäsionskräften beschrieben. Es fehlen jedoch systematische Studien, die Zellkollisionen zwischen verschiedenen Zelltypen untersuchen. Die Entwicklung eines quantitativen theoretischen Models über ein breites Spektrum von Zelltypen ist von entscheidender Bedeutung für die Beschreibung des epithelialen bis hin zum mesenchymalen Motilitätsverhalten.
In dieser Arbeit haben wir die Zellmigrationsdynamik und die Zell-Zell-Interaktionen mit Hilfe von Zwei-Zustands-Mikrostrukturen untersucht. Diese hantelförmige Mikrostruktur bietet eine kontrollierte und standardisierte Umgebung für die Beobachtung wiederholter Kollision zweier Zellen. Wir analysierten eine Vielzahl von Zwei-Zell-Trajektorien verschiedener motiler Zellen, die entweder als epithelial oder mesenchymal klassifiziert wurden.
Wir untersuchten zunächst die Dynamik der Einzelzellmigration und stellten fest, dass fast alle untersuchten Zelllinien deterministisch in die Verengung der Mikrostruktur beschleunigt wurden. Darüber hinaus konnten wir zwei unterschiedliche Migrationsmuster je nach Zellphänotyp feststellen: Nicht-invasive epitheliale Zellen zeigten Bistabilität, während invasive mesenchymale Zellen Grenzzyklus-Oszillationen aufwiesen. Durch gezielte Inhibition oder Induktion bestimmter molekularer Merkmale, wie E-Cadherin oder microRNA200c, konnten wir zeigen, dass das Migrationsverhalten stark mit dem Phänotyp der Zellen korreliert und möglicherweise auch deren invasives Potenzial widerspiegelt.
Anschließend wurden die homotypischen Zell-Zell-Interaktionen verschiedener Zelllinien in der Mikrostruktur untersucht. Die Analyse der Zelltrajektorien zeigte eine Vielzahl unterschiedlicher Verhaltensweisen zwischen den Zelltypen. Mit Hilfe eines datengetriebenen theoretischen Ansatzes identifizierten wir verschiedene Muster von Kohäsions- und Reibungsinteraktionen, die von Anziehung und 'Anti-Reibung' bis hin zu starker Abstoßung und starker Reibung zwischen den Zellkernen reichten. Bemerkenswerterweise konnten die verschiedenen Interaktionen durch einen einzigen Mechanismus beschrieben werden, der auf der kontaktvermittelten Kopplung der Zellpolarität beruht. Experimentelle Manipulationen der Zelladhäsions- und Erkennungssignalwege zeigten, dass die Polaritätsausrichtung durch E-Cadherin beeinflusst wird und durch Inhibition von ephrinA2 und ROCK in Anti-Ausrichtungsinteraktionen verschoben werden kann.
Zusammenfassend tragen die in dieser Arbeit verwendeten datengetriebenen Ansätze zu einem umfassenderen Verständnis der Zellmigrationsdynamik bei und verdeutlichen die Variabilität der Interaktionsdynamik zwischen verschiedenen Zelltypen. Diese Erkenntnisse könnten auch Aufschluss über das kollektive Verhalten phänotypisch unterschiedlicher Zellen geben.

Summary

Collective motion is a phenomenon observed across a broad spectrum of life, from cell assemblies and animal flocks to car traffic. These 'active matter' systems are described as self-propelled agents, that interact with their neighbours through forces, and exhibit emerging large scale properties, such as synchronised movement. In biological systems, the coordinated and directed movement of cell collectives crucially supports the organisation and maintenance of the human body, impacting fundamental processes such as embryogenesis, wound healing, and cancer progression. These collective behaviours are critically determined by the way cell trajectories are altered during cell-cell contacts. In previous work cell-cell interactions in confined geometries have been modelled as interactions that include both effective adhesive and cohesive forces. However, there is a lack of systematic studies that explore cell collisions across different cell types, and a comprehensive quantitative theoretical framework has yet to be developed. Such a framework is essential for describing the diverse spectrum of motility behaviours, from epithelial to mesenchymal, potentially influenced by factors such as surface proteins.

In this thesis, we explored cell migration dynamics and cell-cell interactions using two-state micropattern. This dumbbell-shaped micropattern provides a controlled and standardised environment, that allows the observation of repeated cell collisions of two cells. We monitored a large amount of two-cell trajectories across distinct motile cells, classified as either epithelial or mesenchymal.

First, we analysed the single cell migration dynamics and discovered that almost all cell lines were deterministically driven into the constriction. Furthermore, we observed two distinct migratory behaviours among the phenotypes: non-invasive epithelial cells exhibited excitable bistability, whereas invasive mesenchymal cells demonstrated limit cycle oscillations on the dumbbell-shaped micropattern. By inhibiting or inducing several phenotypic traits in the cells, such as E-Cadherin or microRNA200c, we further demonstrated that the migration behaviour is closely linked to the phenotype of the cells, potentially also reflecting the invasive potential of these cells.

Next, we investigated the homotypic cell-cell interaction behaviour of these cell lines, repurposing the dumbbell-shaped micropattern as a 'cell collider'. The analysis of the coupled cell trajectories revealed a range of distinct interaction behaviours across the cell lines. Utilising a data-driven theoretical approach, we inferred distinct patterns of cohesion and friction interactions, spanning from attraction and anti-friction to strong repulsion and friction between the cell nuclei. Remarkably, although the effective interactions varied strongly among different cell lines, they could be uniformly described by a single interaction mechanism that involves contact-mediated coupling of cell polarity. We further discovered that polarity alignment interactions are influenced by E-Cadherin, while modifications in the polarisation machinery through ephrinA2 and ROCK inhibition effectively shifted polarity alignment to anti-alignment interactions.

Overall, the data-driven approaches used in this work contribute to a more general understanding of cell migration dynamics and highlight the emergence of variability in the interaction dynamics across distinct cell types. These findings provide a general basis for obtaining new insight into the underlying mechanisms of collective cell migration.

Contents

List of Publications and Manuscripts

P1 Unravelling the metastasis-preventing effect of miR-200c *in vitro* and *in vivo*
Bianca Köhler, **Emily Brieger**, Tom Brandstätter, Elisa Hörterer, Ulrich Wilk, Jana Pöhmerer, Anna Jötten, Philipp Paulitschke, Chase P. Broedersz, Stefan Zahler, Joachim O. Rädler, Ernst Wagner, Andreas Roidl
under revision at *Molecular Oncology*
bioRxiv doi: 10.1101/2023.11.14.566527

P2 Data-driven theory reveals universal cell-cell interactions across distinct motile cells
Tom Brandstätter*, **Emily Brieger***, David Brückner, Georg Ladurner, Joachim Rädler, Chase P. Broedersz
to be submitted to *Nature Communications*

M1 Patterns of collective cell migration driven by cell-cell interactions
Bram Hoogland*, Tom Brandstätter*, **Emily Brieger**, Joachim O. Rädler, Chase P. Broedersz
In preparation

* authors contributed equally to the work

1. Introduction

Collisions between two moving objects occur across a broad spectrum of scales, from the microscopic interactions of molecules, atoms, and subatomic particles, to the macroscopic impacts between solid bodies. In every instance of collision, forces are exerted on the colliding objects, influencing their subsequent trajectories and states. For instance, the local motion of gas particles demonstrates how particles in motion interact through forces that alter their paths. In a biological setting, cells within a multicellular organism frequently collide, triggering a series of complex interaction mechanisms. These cellular interactions play a critical role in dictating the collective behaviour and fate of the organism [1–3].
For instance, during morphogenesis, cells must rearrange in a coordinated manner to facilitate the formation of complex structures [4]. Similarly, in tissue repair, epithelial cells migrate as wide sheets, with individual cells maintaining stable cell-cell junctions between neighbours [5]. These junctions are crucial for the transmission of signals and forces across the cell collective. Moreover, in cancer progression, the disruption or alteration of these cell-cell interactions often leads to unregulated cell growth and metastasis. Cancer cells can manipulate cell-cell adhesion to detach from the primary tumour mass and invade surrounding tissues, exploiting the body's normal mechanisms of cell migration and interaction [6, 7]. Therefore, an intricate understanding of how cells interact in various contexts could be crucial for comprehending disease progression, such as cancer.
At the heart of those behaviours are intricate inter- and intracellular molecular processes that control both single cell migration and cell-cell interactions. The single cell migration of most eukaryotic cell types can be described as a cyclic process of expansion and contraction driven by an actin-based machinery. Specifically, a cell polarises to form an active leading edge with dynamic protrusions extending outward, while the trailing edge retracts, propelling the cell forward [8–10]. This intricate process relies on numerous molecular components that interact with the cytoskeleton, which are broadly conserved across various cell types and different migration modalities [9–12].
Another crucial process influencing cell migration and interactions is the epithelial-to-mesenchymal transition (EMT). This program enables epithelial cells to acquire mesenchymal characteristics. The epithelial phenotype is characterised by its apicobasal polarity and its ability to form stable cell-cell adhesion via E-Cadherin, while mesenchymal cells lack the ability to form stable junctions, have a spindle like morphology and enhanced migratory capabilities [13, 14]. EMT is vital in numerous processes, including developmental stages and wound healing, where traditionally

stationary cells acquire the ability to move in order to fulfill critical roles. In the context of epithelial cancer, the transition to a mesenchymal, invasive phenotype via EMT is critical as it facilitates metastasis, thereby affecting patient prognosis significantly [15–17]. The migratory capabilities and invasiveness of cells are closely linked to their phenotype; however, existing studies often limit their focus to one or two similar cell lines. Moreover, traditional methods for assessing invasiveness, such as transwell assays or Boyden chambers, do not provide insights into the dynamic migration patterns of phenotypically diverse cells. In this thesis, we want to address this issue and try to connect the single cell dynamics of phenotypically different cell lines with their invasive potential.

Initially, the study of single cell migration was conducted *in vitro* on plane adhesive substrates. The analysis of the cell trajectories revealed that cells on those unstructured 2D surfaces perform persistent random motion [18, 19]. While these studies were insightful for unravelling fundamental mechanisms of cell migration, they often lacked physiological relevance. Additionally, such setups made it challenging to control environmental variables for individual cells, further complicated by the substantial heterogeneity observed across different cell populations. To overcome these limitations, standardised environments created through various micropatterning techniques have been developed [20–23]. These platforms allow for more precise control over the conditions affecting cell behaviour. For instance, confining cells on one dimensional lanes allows for simplifications of cell shape and revealed several characteristics of cell motion such as the universal correlation between speed and persistence (UCSP) [12].

Recently, dumbbell-shaped micropattern, creating a minimal two-state system, were employed to study how cells migrate through narrow constriction, mimicking a more physiological context, such as squeezing through thin pores [24]. The unique geometry of these patterns not only facilitates the differentiation between deterministic and stochastic contributions of single-cell dynamics, but also allows the micropattern to function as a cell collider. This setup enables the detailed study of repeated head-to-head collisions between cell pairs, providing a robust platform for analysing homotypic cell-cell interaction behaviours [25].

One of the most widely studied and observed interactions between cell pairs is the active repulsion of one cell by another, commonly referred to as contact inhibition of locomotion (CIL). [26–29]. Upon contact, cells retract and change their direction, indicating CIL to be a general mechanism of local inhibition of cell protrusions. To induce this repulsive response and effectively redirect the cell's polarisation machinery, a complex network of surface proteins is required. Most contact mediated cell-cell interactions involve two core mechanisms that rely on two sets of distinct molecular machineries: cell recognition and adhesion. Recognition between cells is primarily facilitated through various ligand and receptor interactions. For example, the Ephrin family plays a critical role in affecting cell polarity, often triggering a repulsive response upon engagement [30]. Following recognition, cell contact is stabilised through the formation of adherens junctions, typically mediated by E-Cadherin. This adhesion protein not only helps in maintaining physical contact but is also crucial for its mechanosensing capabilities, allowing the transmission of

mechanical forces between cells [31–33]. In controlled experiments, such as those conducted on 1D lanes or dumbbell shaped patterns, several modes of cell-cell interactions have been observed, ranging from classical CIL following head-to-head collisions, to following or flocking behaviours after head-to-tail collisions, and 'walk past' of cells, exchanging positions [25,34,35]. However, unravelling the mechanisms behind these interactions remains challenging due to the complexity of the molecular processes involved. Cell-cell interactions are driven by the intricate coupling of each cell's migratory machinery, which encompasses a broad network of molecular markers. Among these, a large network of Rho GTPases plays a pivotal role in regulating cell polarisation [36–38].
Recently, those dumbbell-shaped pattern were employed to study the cell-cell interaction behaviour, facilitating a high-throughput of interacting trajectories. Using a data-driven approach, effective interaction parameters such as effective cell-cell adhesion and effective cell-cell friction were inferred from the experimental observed trajectories [25]. However, a more phenomenological description of the underlying mechanisms employed by interacting cells remains elusive.

In this thesis, we adopt a data-driven approach to explore the dynamics of single cells confined within dumbbell-shaped micropatterns, focusing on how these dynamics vary among phenotypically distinct motile cell lines. This analysis aims to broaden our understanding of the correlation between invasive capabilities and migratory behaviours. Building on this, we aim to elucidate the coupling between cell-cell interactions and cellular behaviour across a diverse range of motile cell lines, each reflecting unique molecular architectures and collective morphodynamics. We employ a top-down data-driven strategy to develop a phenomenological model for cell-cell interactions by systematically constraining model candidates using experimental observations. Additionally, we pharmacologically target molecular components crucial for cell adhesion and recognition to deepen our understanding of how these molecular processes influence interactive behaviours in various physiological settings.

The structure of this thesis is organised to systematically explore the dynamics of cell migration and cell-cell interactions, aiming to uncover the underlying biophysical mechanisms.
Chapter 2 sets the foundation by discussing the essential aspects of cell migration and cell-cell interactions. It explains key physical and biological properties of single and collective cell migration, as well as the mechanisms involved in cell-cell interaction. Additionally, this chapter introduces various theoretical frameworks and modelling approaches used to study these phenomena.
In **Chapter 3** the methodologies employed in the study are described, starting with the micropatterning techniques used to study cell migration. Followed by the microscopy techniques utilised, including light microscopy and confocal microscopy.
Chapter 4 presents research findings on the single cell dynamic behaviours exhibited by various cell types when constrained within a dumbbell shaped pattern. This chapter specifically analyses the impact of cellular phenotypic traits on these single cell dynamics. It further discusses how processes such as epithelial-to-mesenchymal

transition (EMT) and the modulation of the miRNA200c expression influence cell behaviour, providing deeper insights into how genetic and phenotypic modifications can alter single cell dynamics.
The focus in **Chapter 5** shifts to cell-cell interactions in a dumbbell-shaped pattern, where the transient collision behaviour of various motile cell lines is studied. This chapter discusses how polarity alignment and anti-alignment emerge as universal interaction modes among cells. The detailed discussion of these findings enhances understanding of the intricate mechanisms governing cell-cell interactions.
Chapter 6 explores the impact of specific molecular perturbations, such as protein inhibition, protein overexpression and cytoskeletal modifications, on cell-cell interaction dynamics. It explores how alterations in contact-mediated adhesion affect polarity alignment and how the cellular phenotype influences interaction dynamics. This chapter also delves into the roles of the cell recognition system and polarisation machinery in shaping these dynamics, with a particular focus on the implications of EMT.
An outlook and general discussion of the topics studied in this thesis is given in **Chapter 7**. Experimental details can be found in **Appendix A** and a detailed description of the data analysis is given in **Appendix B**.

2. Fundamental Concepts

2.1 Cell Migration

Cell migration plays a crucial role in various physiological and pathological processes. Processes such as embryogenesis, tissue regeneration, and wound healing heavily depend on the directed and coordinated movement of cells [4,5,39]. However, errors or mutation to the cell migration machinery can also contribute to diseases, including chronic inflammation and the progression of cancer through metastasis [2,6]. The basic mechanism by which cells migrate is similar over a range of distinct cell types and regulated by a combination of structural, chemical, and biological factors [12,40]. Yet, the migration process is incredibly complex due to the involvement of intricate molecular networks and signalling pathways. This complexity makes achieving a comprehensive understanding of cell migration challenging [2,41].
Depending on cellular phenotype and function, cells can undergo different modes of cell migration, which can be categorised as either single cell migration or collective cell migration (Fig. 2.1). Single cell migration is characterised through a lack of cell-cell adhesion and can be divided into two groups, amoeboid and mesenchymal migration. Amoeboid migration is defined through blebbing and rapid movement, often observed in leukocytes during the immune response [42]. In contrast, cells undergoing mesenchymal migration exhibit robust stress fibers and establish leading edges marked by actin-rich protrusions [43]. Collective cell migration is characterised through the coordinated movement of a group of cells guided through interaction between neighbouring cells [1,44]. In epithelial tissues, cells maintain stable cell-cell adhesion through Cadherin junctions. In contrast, cells in mesenchymal tissues only form transient adherens junctions between neighbours, which are still effective in polarising the cells [44,45].
In this thesis, we mainly focus on motile cell lines that can undergo mesenchymal migration. The molecular and physical basics of this migration mode are introduced in the following sections.

2.1.1 Physical and Biological Properties of Single Cell Migration

Single cells frequently engage in persistent random motion, yet when confronted with specific environmental cues, they have the capacity to transition into a more directed movement. This directed migration is mostly universal across different con-

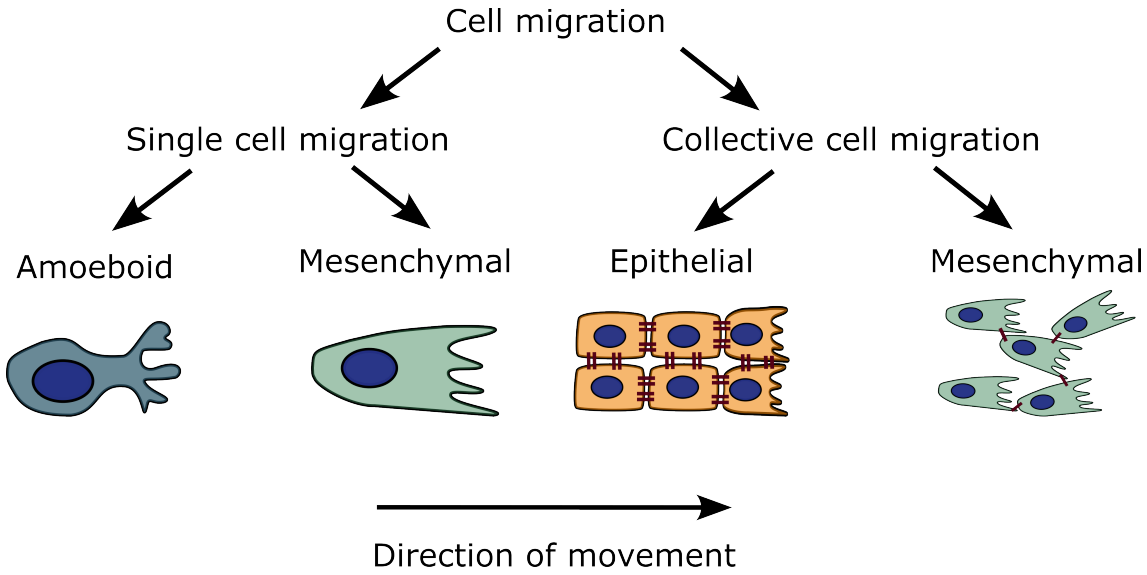

Figure 2.1: Display of the different migration modes. Cell nucleus is coloured in blue and cell adhesion contacts are displayed as red bars.

texts and is marked by repeated cycles of cell front extension, cell body contraction, and rear end retraction (Fig. 2.2) [3, 8, 10]. Upon stimulation with external cues, cells adapt an asymmetrical polarised morphology with a clear distinction between cell front and cell rear.
At the molecular level, this polarisation is initiated by the activation of G-protein coupled receptors, triggering a cascade involving various GTPases of the Rho family (Cdc42, Rac1, phosphoinositide 3-kinase (PI3K)) [41, 46, 47]. Cdc42, in particular, instigates the polarisation process, leading to a dynamic rearrangement of the cytoskeleton [48]. This restructuring results in the active extension of the cell membrane, forming broad and flat protrusions known as lamellipodia or slender and spike-like extensions called filopodia [49]. In lamellipodia, actin are cross-linked into lattice-like meshworks, whereas in filopodia, actin is organised in long parallel bundles. However, actin filaments, being long and flexible in vitro, cannot sustain a pushing force without buckling. Therefore, the Arp2/3 complex stimulates actin polymerisation in lamellipodia by creating new nucleation cores, promoting the assembly of a dense network of short, branched actin filaments (Fig. 2.2B - inset) [10]. Nevertheless, the question of how polymerisation can generate a pushing force is still open. The elastic Brownian ratchet model, proposed by Mogilner and Oster in 1996, addresses this issue by envisioning the actin filament as a spring-like wire continually bending due to thermal energy [50]. The propulsive force is generated by the unbending of the filaments against the surface [51]. However, in order for a cell to move forward, the protrusions must be stabilised by adhering to the surface, as otherwise the propulsive force would drive the filaments backwards and not forwards on the surface.
The formation of adhesions between cell and substrate is guided by several trans membrane receptors [52, 53]. Integrins are the key players regulating the dynamic

interactions between the actin cytoskeleton and the extracellular matrix (ECM). During cell migration, integrins dynamically engage with ECM components, forming molecular linkages between substrate and actin network through proteins like talin, vinculin, or α-actinin (Fig. 2.2C - insets). This process establishes anchor points crucial for generating traction forces. These forces, arising from the interaction between the cell and its substrate, enable the cell to exert the necessary pull for forward movement [54, 55].
Addionally, a contractile force is needed to push the cell forward, leading to cell body contraction and the retraction of the rear end. The motor protein non-muscle myosin II interacts with actin filaments and uses the energy of ATP hydrolysis to push neighbouring actin filaments past each other, resulting in contraction. This in turn promotes the depolymerisation of filamentous actin, causing actin filaments to move rearward toward the cell center. This rearward movement is what constitutes actin retrograde flow [52]. Furthermore, myosin directly interacts with the focal adhesions by facilitating their release and enabling the retraction of the cell's rear end [56].

2.1.2 Molecular Basis of Cell Polarisation

The ability of cells to polarise is crucial for the proper functioning of numerous biological processes. Cellular polarisation refers to the asymmetrical organisation of cellular components, which allows cells to have distinct structural and functional domains. It is necessary during cell division, neuronal development, immune response and cell migration [37, 57, 58]. An intricate network of polarity proteins, conserved throughout evolution, assemble into multiprotein complexes that induces downstream signalling in order to break cellular symmetry [3, 59]. One of the key molecular players are the small GTPases of the Ras superfamily that function as molecular switches in the polarisation signalling pathways. A vast number of those Rho GTPase effector proteins have been discovered, adding to the challenge in understanding cell polarisation.
In this section, the focus lies on the main players guiding the polarisation machinery - the Rho (Ras homologous) family proteins of the Ras superfamily [47]. Specifically, the proteins Cdc42, Rac1 and RhoA regulate and coordinate cytoskeleton remodelling through inducing the polymerisation of actin filaments to linear fibres or branched networks [36, 60]. To establish protrusions at the leading front, Rac1 and Cdc42 stimulate the Arp2/3 complex by binding to proteins of the WAVE or WASP family respectively [46]. This induces the branchend actin network in lamellipodia necessary for cell movement. Furthermore, in the early stages of adhesion, activity of Rac1 at the front of the cell leads to an inhibition of RhoA at the rear end. During later stages of adhesion and protrusion formation, Rac1 expression decreases leading to an increase of RhoA which accumulates at the rear end of the cell. RhoA in turn suppresses the activity of Rac1, known as the Rho-Rac antagonism [38, 61]. The main effector responsible for activating Rho are the Rho-associated coiled-coil-containing protein kinases (ROCKI and ROCKII), orchestrating the phosphorylation of the myosin light chain [36]. This phosphorylation event subsequently upreg-

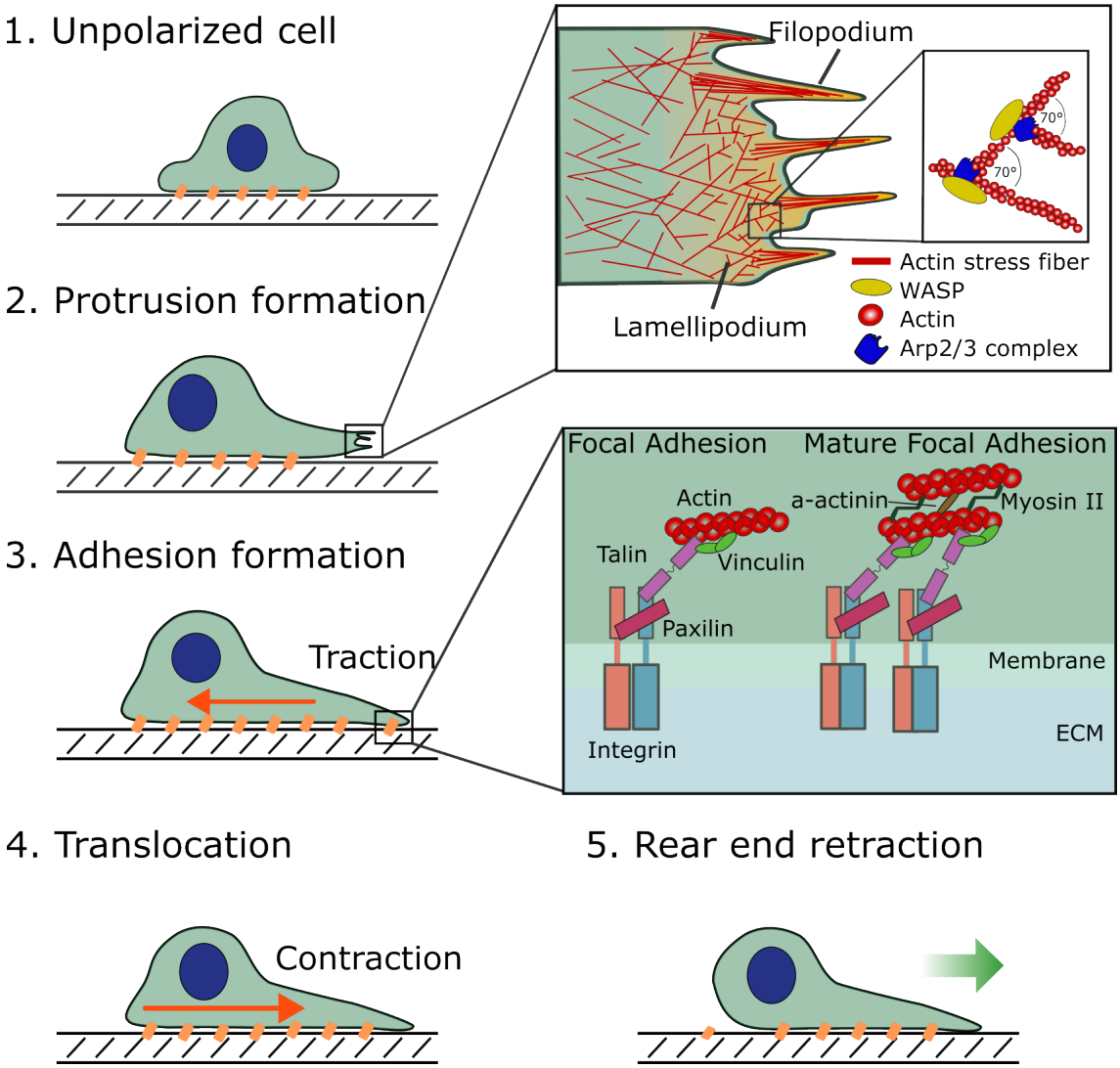

Figure 2.2: Overview of the 5 step cycle in single cell migration. A) Unpolarised cell is attached to the substrate or extracellular matrix (ECM) via focal adhesion (FA). B) Through external cues, cell symmetry is broken and protrusions are formed. On the right, the molecular details of filopodia and lamellipodia are shown. C) New adhesions are formed, which leads to a traction force against the substrate. Molecular details of focal adhesion are shown on the right. D) Translocation of the cell through a contraction force mediated through myosin II. E) Rear end retraction and forward movement of the cell.

ulates actomyosin activity, inducing the contraction of stress fibers and resulting in the retraction of the cell.

2.1.3 Cytoskeleton in Cell Migration

The cytoskeleton is a crucial component of every cell, acting as both a structural framework and a scaffold that shapes the cell and organises the cytoplasm. Con-

sisting of an extensive network of protein filaments, the cytoskeleton plays a pivotal role in cell movement, including the intracellular transport of organelles and the segregation of mitotic chromosomes [62]. This network, which includes actin filaments, intermediate filaments, and microtubules, is supported by a diverse array of proteins that connects these cytoskeletal polymers to subcellular organelles and the plasma membrane. As a dynamic structure, the cytoskeleton generates coordinated forces that allow it to rapidly adapt, reorganising itself to enable the cell to move and alter its shape in response to various stimuli [63, 64]. This adaptability is critical for processes such as navigating through tight spaces or altering course following cell-cell interactions [65].

The three primary structural polymers of the cytoskeleton each possess distinct properties that enable them to form varied architectures and respond appropriately to external and internal cues. These differences include variations in mechanical stiffness and polarity, as well as unique assembly and disassembly dynamics that allow each type of filament to function in specific cellular contexts [64]. Moreover, they are associated with specific molecular motors that facilitate movement along these structures using chemical energy derived from ATP. Kinesins and dyneins move along microtubules, often transporting organelles and vesicles, while myosins navigate along actin filaments, crucial for muscle contraction and cell crawling [8].

Microtubules are the most rigid components of the cytoskeleton, constructed from tubulin subunits arranged in a cylindrical structure [66]. This configuration provides substantial compressive and tensile strength, enabling microtubules to withstand bending forces. Despite their rigidity, microtubules can buckle under compressive loads and are susceptible to breaking under extreme elongational strains. These filaments exhibit an intrinsic polarity, typically with the minus end anchored at the microtubule-organising center (MTOC), from which they project outward. This polarity is crucial for their function, as it directs the assembly and disassembly of tubulin subunits. Moreover, their dynamic instability allows for rapid growth and shrinkage through polymerisation and depolymerisation at their ends necessary for cell migration. Furthermore, the dynamic behaviour of microtubules is intricately linked to actin dynamics within the cell through the mediation of Rho GTPase signalling pathways [67, 68].

Intermediate filaments, while providing tensile strength, are the most elastic and deformable components of the cytoskeleton, enabling them to withstand mechanical stress. These filaments are classified into three main subclasses: Class I and II comprise keratins, typically expressed in cells with an epithelial phenotype, whereas Class III includes vimentin, which is predominantly found in cells exhibiting a mesenchymal phenotype. Lamins represent a third category of intermediate filaments, which are crucial for maintaining the mechanical integrity of the eukaryotic nucleus. These types of polymers are not polarised, which precludes them from supporting directional movement of molecular motors. However, they are capable of extensive cross-linking with each other, enabling them to form higher-order structures [64].

Actin filaments, recognised for their semi-flexibility, are capable of forming complex dendritic and cross-linked structures, commonly observed in structures like lamellipodia [49, 64]. Their semi-flexible nature allows them to be actively bent by

thermal fluctuations, making them the most dynamic of the cytoskeletal polymers. Instead of switching between polymerised und depolymerised states, actin filaments typically exhibit steady growth. This continuous assembly process enables them to generate the necessary forces for propelling the cell forward during migration. In addition to their role in cellular protrusions, actin filaments can assemble into contractile actomyosin bundles forming so called stress fibers. Stress fibers play a critical role in maintaining cell shape, enabling contraction, and stabilising cell-substrate adhesions [69, 70]. They are crucial for transmitting mechanical signals and forces across the cell, thereby influencing cell behaviour in response to external mechanical stimuli [71].

2.1.4 Collective Cell Migration

Collective cell migration is characterised by a coordinated movement of a group of cells in which they move forward together and remain in constant contact through stable cell-cell adhesion [1, 45, 72]. This adhesion is evident in various forms, including adherens junctions (AJs), tight junctions (TJs), desmosomes, and gap junctions. Furthermore, the collective behaviour of cells involves the chemical or physical crosstalk between individual cells inside the collective [44, 73]. For collective migration to occur, each individual cell within the group must undergo polarisation, employing the same molecular mechanisms observed in single-cell migration. However, the cell-cell interactions inside the collective modify the classical features of polarisation found in individual migrating cells. There is a distinction in morphology and polarity proteins expressed in cells at the front of the cluster compared to cells inside or at the back [3]. Cells at the front are often referred to as leader cells, while the others are called follower cells [74, 75]. The leader cells can sense the microenvironment and dictate the direction and velocity of the collective. They adapt mesenchymal properties and establish lamellipodia at the front of the cell cluster. Leader cells communicate and influence the follower cells through mechanical coupling and biochemical signals [73, 74, 76]. Follower cells show increased contractility through enhanced actomyosin activity similar to the rear end of a single cell [45, 72, 77].

2.2 Cell-Cell Interaction

Cell-cell interactions play a crucial role in orchestrating the coordinated movement of cells during key biological processes such as embryogenesis, morphogenesis, and cancer progression [4, 6, 77]. In order for these physiologically diverse processes to function, the cells must adapt their response accordingly upon contact with another cell. This response can be roughly divided into three interaction modes. When cells collide, they can exhibit a repulsive response, leading to a separation of the cells in opposite direction. This phenomenon is known as contact inhibition of locomotion (CIL) [29, 78]. Alternatively, they can stick together by forming adhesion bonds and move collectively, referred to as contact following of locomotion (CFL) [79]. Another

mode is characterised by cells walking past each other, termed contact sliding of locomotion (CSL) [25]. In general, the contact-mediated response of cells is largely dependent on the collision angle between the cells. The underlying mechanisms are complex and extensive, guided by force transmission and signalling pathways, which are mediated by a vast network of cell receptors and surface proteins [29].
The most extensively studied contact response is CIL, which has been discovered and characterised in 1953 by Abercombie and Heaysman [26]. CIL is a fundamental cellular process exhibited by a large variety of phenotypically different cells during developmental processes (e.g. in *Drosophila* [28]) and tissue organization (e.g. neural crest of *Xenopus* [80]). When cells collide, CIL orchestrates a repulsive response, preventing them from overlapping or moving in the same direction [29]. In contrast, the loss of CIL is frequently observed in cancer progression, where cells lose their ability to repel each other upon contact. This breakdown in CIL allows cancer cells to move past one another, contributing to invasive and uncontrolled cell migration [81]. The mechanism of CIL can be divided into four main steps (Fig. 2.3) [78]:

1. establishment of cell-cell contact
2. inhibition of protrusive activities at contact sites
3. repolarisation of cells and formation of new protrusion pointing away from the site of contact
4. separation and migration away from each other

The molecular mechanisms navigating CIL are largely unknown. However, a set of molecular markers involved in the process has been identified [29, 78, 81]. In order for cells to transmit signals between each other, they have to build transient adhesion points upon contact. Those adhesions are facilitated by members of the cadherin family. Cadherins are transmembrane proteins that mediate Ca^{2+}-dependent homophilic cell–cell adhesion and tightly regulate the actin cytoskeleton. E-Cadherin has been identified to be required for CIL in migratory cells and epithelial sheets [82, 83]. In neural crest cells, N-Cadherin is essential for functioning CIL responses [84]. In the following stage, cell recognition and transduction of signals is mediated by another group of surface proteins, the Eph-ephrin family. This receptor-ligand system signals bidirectionally into both the Eph-receptor-expressing cells and the ephrin-expressing cells targeting the actin cytoskeleton through inhibiting or activating members of the small RhoGTPase family [30].

2.2.1 Cell Adhesion

Cell adhesion plays a critical role in both cellular communication and migration, encompassing two primary forms: cell-substrate adhesion via focal adhesions and cell-cell adhesion through adherens junctions. Focal adhesions, mediated by integrins, facilitate complexes between the cell and the extracellular matrix (ECM), anchoring cells to their substrates [44]. These adhesions act as a mechanical link

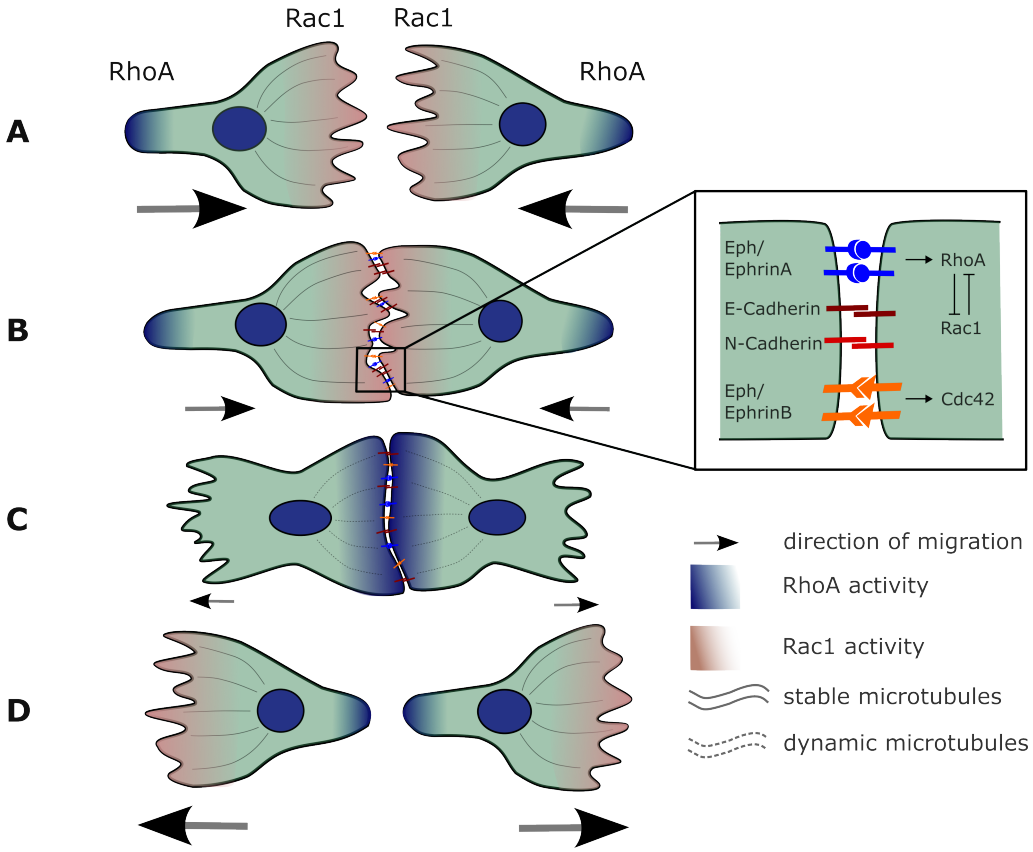

Figure 2.3: Mechanism of contact inhibition of locomotion. A) Polarised cells, with an accumulation of Rac1 at the front and RhoA at the rear, move towards each other. B) Upon contact cells establish adhesions mediated by ephrins and Cadherins. Inset on the right shows a small set of involved surface proteins and their influence on the small GTPases. C) Cells repolarise by an increase of RhoA activity at the cell contact site. D) Cells migrate in opposite direction.

that transmit forces generated by the actin cytoskeleton to the ECM, facilitating cell motility. During migration, focal adhesions exhibit mechanosensitive behaviour, enabling cells to spread and move along substrates [85, 86]. This dynamic adjustment of focal adhesions is essential for cells to respond to their physical environment, which influences direction and speed of movement. Notably, a reduction in cell adhesiveness is frequently observed in cancerous cells, allowing them to circumvent normal cellular constraints and thereby enhancing their metastatic potential [55]. Adhesions between two or more cells occur in nearly all tissues and cell types and take various forms, such as [87]:

- **Adherens Junctions:** Primarily mediated by cadherins, these junctions connect the cytoskeleton of one cell to another, enabling the transmission of tension and signals between cells. This is crucial for maintaining tissue integrity and responding to environmental changes.

- **Tight Junctions:** Intercellular adhesion complexes necessary to control para-

cellular permeability, mediated by the transmembrane proteins occludins and claudins.

- **Desmosomes:** These connect intermediate filaments of neighbouring cells, providing crucial mechanical strength to tissues.

In epithelial tissues, the integrity and function of cell-cell adhesion complexes are predominantly mediated by E-Cadherin. This transmembrane protein not only establishes a physical linkage between cells, but is also instrumental in transmitting mechanical signals that regulate cellular forces and maintain tissue stability [31,32]. For instance, E-Cadherin-based adherens junctions are essential for the polarisation of epithelial cells, aiding in the segregation of apical and basal membrane compartments, and facilitating the organisation of organelles and the directionality of intracellular trafficking [33]. Furthermore, E-Cadherin-mediated cell-cell adhesion can facilitate cell polarisation, leading to a redirection of the cellular migration machinery away from cell contact [88]. This linkage between E-Cadherin and the actin cytoskeleton not only initiates polarity cues such as Rac1 and Cdc42 [88, 89], but also serves as a mechanosensor at cell-cell junctions [32]. This emphasises that E-Cadherin is integral not just for mechanical cohesion but also for signalling pathways that direct cell behaviour.

2.2.2 Cell Recognition System

In order to direct the response upon cell collision, cells first have to sense and recognise each other. This cell-cell recognition is critical for various physiological functions and involves the specific interaction of receptors on one cell's surface with complementary ligands on another, triggering downstream signalling processes [90]. One of the major receptor familys involved in cell-cell recognitions and signal initiations is the Ephrin family [91].
The Eph receptors represent the largest known family of receptor tyrosine kinases in a variety of cell types [30, 92]. The receptors can be divided into two subclasses consisting of 9 different EphA and 5 EphB members. The structure of the receptors is largely conserved and both classes share the same structural features and domains. The receptors are activated by binding to the membrane-bound ligands called ephrins, which causes a bidirectional signalling cascade. The ligands are also divided into ephrinA and ephrinB ligands. Unlike the receptors, the ligands show structural differences between the classes. EphrinA ligands are characterised by glycosylphosphatidylinositol (GPI) anchors that bind them to the membrane. EphrinB ligands have a short transmembrane domain followed by a conserved cytoplasmic tail [93]. In most cases, ephrinA ligands bind to EphA receptors and ephrinB to EphB. However, there can be a potential cross-talk between the groups. While the Eph/ephrin system is an important cell recognition and signalling tool involved in developmental and differentiation processes [94], neuronal pathfinding and topographic mapping [95], it also plays a role in tumour development. In many types of cancer, Eph receptors are upregulated [92, 96]. In breast cancer, EphA2 and EphB4 are overexpressed leading to oncogenic transformation and enhancement of tumour

cell proliferation and motility [97]. These receptor-ligand interactions have a significant influence on cell polarity by modulating the expression of Rho GTPases, playing a pivotal role in the migratory machinery during cell-cell contacts [81]. For instance, EphB receptors have been observed to stimulate Cdc42 expression, which may promote attractive migration. In contrast, when ephrinA2 ligands interact with EphA2 and EphA4 receptors, activation of RhoA at sites of cell-cell adhesion is triggered. This in turn leads to a reduction in forward migration, which is primarily driven by actomyosin contraction regulated by Rho-GTPases [53].

2.2.3 Role of EMT in Cell Migration

During the earliest stages of embryonic development, epithelial cells have to change their molecular composition and migratory behaviour in order to differentiate into a diverse array of cell types, contributing to the development of different tissues and organs [13,98]. This process is known as epithelial-to-mesenchymal transition (EMT) which denotes a cellular program during which epithelial cells acquire mesenchymal phenotypes and behaviour. EMT is characterised by loss of cell-cell adhesion and cellular polarity, remodelling of the cytoskeleton resulting in a change of the cellular morphology, as well as increased migratory capacity (Fig. 2.4A) [14, 15]. The enhanced migratory abilities are often found in cancer cells undergoing EMT, thus this transformation is a promoter of metastasis and cancer progression [16].
Several intracellular signalling pathways, often mediated through transcription factors (TFs), can induce EMT in epithelial cells [17, 99]. One major pathway in controlling EMT is governed by the transformation growth factor β (TGFβ). Expression of TGFβ leads to the induction of several SMAD complexes, which in turn migrate to the nucleus and transcriptionally activate mesenchymal genes like vimentin and fibronectin [17, 100]. Furthermore, several TFs, specifically SNAIL, SLUG, ZEB1 and TWIST, are upregulated and enable the establishment of autocrine signalling. This creates a positive feedback loop to maintain the expression of the EMT programmes [100]. TFs also lead to the downregulation of E-Cadherin and several other adhesion proteins, while simultaneously promoting N-Cadherin. This Cadherin switch is often observed in cells undergoing EMT and is used as one of the major hallmarks that characterises this process. However, studies have shown that while loss of E-Cadherin expression is almost always observed in EMT, it is not sufficient to induce EMT [101]. Therefore other key players have to be involved, such as the large and intricate network of microRNAs (miRNAs), especially the miRNA200 family [14]. The miRNA200c is inhibiting the synthesis of ZEB1, which, reciprocally, can repress the transcription of miRNA200c. This negative feedback-loop involves other miRNAs (e.g. miRNA34) and is influenced by the presence of TGFβ, which promotes TFs, thus leading to an inhibition of miRNAs (Fig. 2.4B) [102]. Other signalling pathways like the Notch pathway or canonical WNT-signalling also influence and initiate EMT in epithelial cells [15].
However, it is noteworthy that EMT is not a bistable process between two states (E=epithelial and M=mesenchymal), but rather a spectrum of several intermediate E/M states [103]. Those cells show a hybrid phenotype, which is characterised by a

combination of epithelial and mesenchymal capabilities [104].

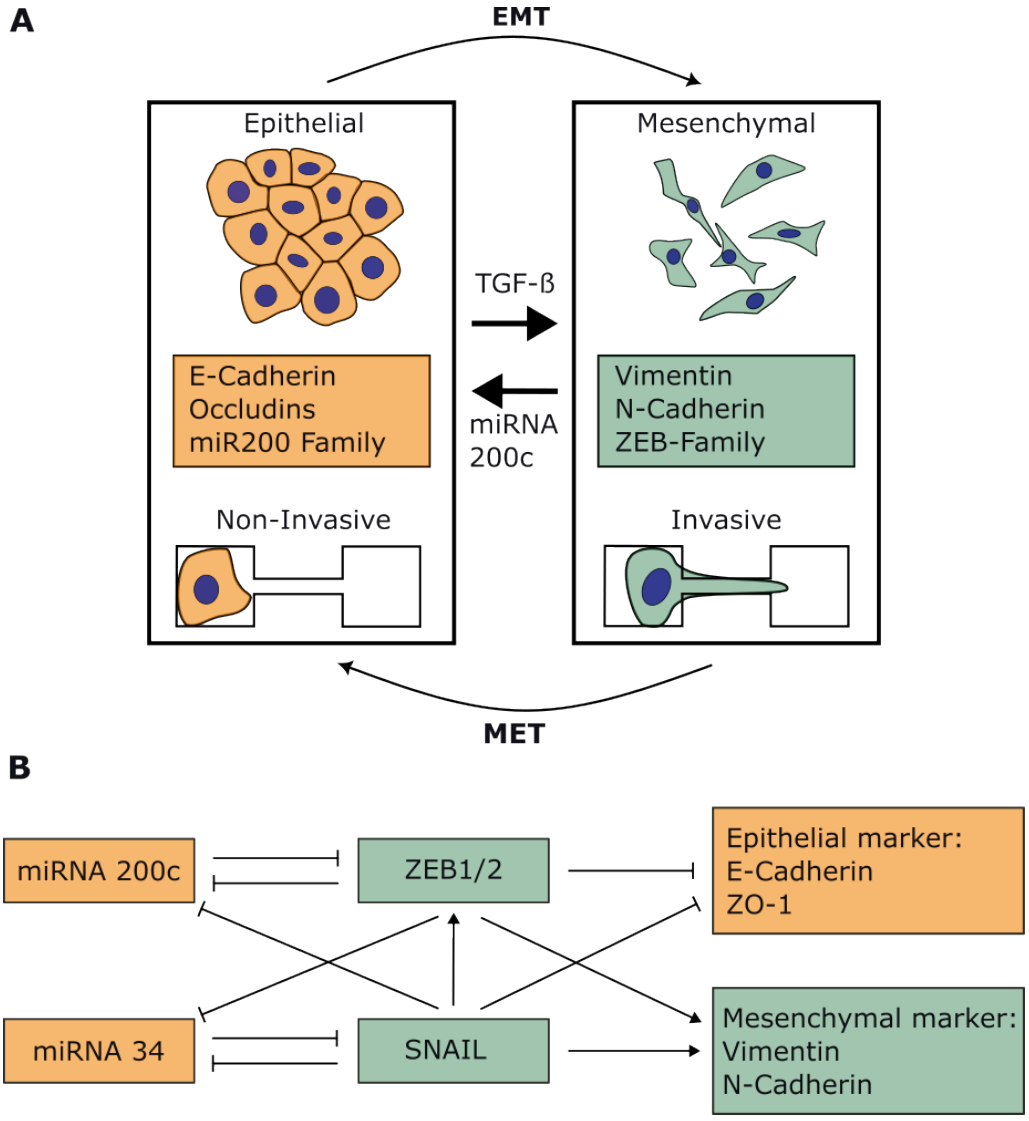

Figure 2.4: Overview of the epithelial-to-mesenchymal transition. A) EMT is initiated by TGFβ, which results in the loss of adhesion and the gain of motility in transitioned cells. MiRNA200c can induce the reverse transition, mesenchymal-to-epithelial transition (MET). B) Double negative feedback loop during EMT between transcription factors (TFs) and miRNAs. Arrows indicate activation and enhancement, inhibitory arrows indicate negative regulation and inhibition.

2.3 Theoretical Description of Cell Migration

In recent decades, extensive studies on cell motility and cell migration have led to the discovery of the intracellular signalling networks responsible for regulating the eukaryotic cell migration machinery. To transition from primarily descriptive

studies to a more quantitative science, mathematical and computational modelling have been increasingly integrated with experimental research [105]. These models provide the framework for achieving a quantitative understanding of the migratory behaviour. However, due to the inherent complexity of biological systems, mathematical models must selectively simplify the vast array of biochemical processes into minimal models. Hereby, it is crucial to choose an appropriate level of description and identify key degrees of freedom of cell migration that are not only simple enough but produce models with predictive power [106]. The theoretical analysis of biological phenomena not only provides deeper insights into underlying physical mechanisms, but also assists in identifying key parameters and variables that impact biological behaviours. This information is valuable for helping to design new experiments and focusing on the most critical factors that drive or inhibit cell movement [107].
Currently, the models employed in cell migration studies often tend to specialise only in one specific aspect of the field. At the smallest scale, models primarily focus on deciphering the intracellular signalling networks and their interactions with the actin cytoskeleton within a single cell. These models aim to provide a detailed understanding of the biochemical and mechanical processes that drive cell motility at the cellular level. At higher scales, the models expand their focus to encompass cell-cell interactions and the movement of larger groups of cells. These higher-level models seek to understand the collective behaviours and emergent properties of cell populations, such as tissue formation, wound healing, and cancer metastasis [79, 105, 108, 109].

2.3.1 Cell Migration Models

Persistent random walk

In 1920, while studying single-celled eukaryotes (protozoa), R. Fürth discovered that cells are not simply following a random Brownian motion, but have some directional persistence [18]. The persistent motion can be mathematically described as

$$P\frac{d\vec{v}}{dt} = -\vec{v} + \sqrt{2D}\vec{\eta} \tag{2.1}$$

with the velocity vector $\vec{v}$ and the diffusion coefficient D characteristic of Brownian motion. The timescale is represented by P, also called the persistence time and $\vec{\eta}$ is a normalised Gaussian white noise. This process is better known as the *Ornstein-Uhlenbeck process* (OU process) [19]. The mean square displacement (MSD), also referred to as Fürth's formula, is defined as

$$\langle d^2(t)\rangle = 2nD(t - P(1 - e^{-\frac{t}{P}})) \tag{2.2}$$

with n being the dimension of the space in which the motion takes place.
In 1970, Gail and Boone were the first to successfully interpret the locomotion of fibroblasts with this model, marking a significant advancement in cell motility studies [110]. Since then, this model has been widely applied across various systems to study cell movement [111–113], establishing itself as a standard framework.

Specifically, equation 2.2 has become the fundamental formula used to describe cell motility [114].
However, as technological advancements in data acquisition and processing, such as computer-aided cell tracking, high-resolution automated microscopy, and advanced image analysis have evolved, significant deviations from the original Ornstein-Uhlenbeck (OU) process described by the model have been observed. For example, the migration patterns of human fibroblasts and keratinocytes have been found to deviate from the OU process, revealing that these cell types retain a memory of past velocities [115]. These findings indicate that while the initial model has been instrumental in advancing our understanding of cell motility, it may no longer be sufficient to accurately describe cell motion. Consequently, the development of more specific models has become necessary to capture the complexities of cell motion to accurately reflect the dynamic and multifaceted nature of cellular behaviours in various biological contexts.

Particle Models

Active particle models are another theoretical framework used in physics and biophysics to describe the dynamics of self-propelled particles, such as cells. These particles are characterised by their ability to move persistently in one direction before randomising their direction after a certain period, known as the persistence time [116, 117].
In this framework, cells are represented as discrete particles or disks, which possess distinct attributes like position, velocity and interaction forces with neighbouring particles. In contrast to for example cellular potts models (CPMs), the cellular shape is largely overlooked [118, 119]. However, by adjusting the size of the particle or the radius of the disk, cell-shape anisotropy and head-tail asymmetry can still be captured. A central interparticle potential $V(|\vec{r_i} - \vec{r_j}|)$ implements positional cell-cell interactions [79]. The potential often features a repulsive part in order to prevent the cells to overlap. To account for cell adhesion, a mid-range attraction between cells is included in the potential. The dynamics in these systems are often dictated by force balance principles, where the equation of motion for interacting cells in a simple active particle model might take the form:

$$\gamma\vec{v_i} = T_a\vec{p_i} + \sum_{\langle i,j\rangle} \left[V(|\vec{r_i} - \vec{r_j}|) + \gamma_c[\vec{v_i} - \vec{v_j}]\right]. \tag{2.3}$$

Here, motility is accounted for by an active polar force $T_a\vec{p_i}$ with the polarity vector $\vec{p_i}$. This term describes the contribution to the velocity due to cell polarisation. Cell-substrate viscous friction is described by $-\gamma\vec{v_i}$ and cell–cell friction with the friction coefficient ξ_c [79]. The potential of interaction between cells is $V(|\vec{r_i} - \vec{r_j}|)$, which is capable of including the repulsion and adhesion between cells [120]. By incorporating additional terms, that for instance corresponds to the polarisation or repolarisation of cells at contacts, active particle models have been successfully employed in modelling CIL [88, 121]. Active particle models, despite their apparent simplicity, are remarkably effective at capturing a diverse array of phenomena

across various biological contexts. These models are particularly useful for explaining dynamics such as single cell migration and collective movements within cell populations [111, 120, 122]. Their flexibility allows for the incorporation of complex behaviours through relatively straightforward mechanisms, making them a powerful tool in both theoretical and applied studies of cellular processes.

Nonlinear equation of motion for confined cell migration

A more general approach to describe the stochastic migration of cells incorporates the application of generalised Langevin equations, enabling the prediction of both short ballistic motion and long random walk patterns [123]. Brückner *et al.* developed a theoretical framework to describe the stochastic migration of cells in structured environments [24]. Specifically, to mimic the challenge cells face while moving through the human body, such as the need to squeeze through thin pores, they employed a dumbbell-shaped micropattern to observe the stochastic dynamics of cancerous and non-cancerous breast cells. The pattern consists of two adhesive squares (islands) connected by a thin bridge. In this particular experimental set-up, cell nuclei are tracked over a certain time period (up to 48h). On the pattern, they can either be in a rest state on one of the islands or transition into the opposite island by squeezing over the small bridge. The time it takes one cell to complete a transition is dependent on bridge width and length and is in the range of a few hours depending on the cell line. The probability that a cell has not completed one transition is called the survival probability

$$S(t) = 1 - \int_0^t p(\tau)\, d\tau \tag{2.4}$$

that is defined by a probability distribution $p(\tau)$, with τ denoting the dwell time that a cell spends on one island. In order to describe the cell motion, a generalised Langevin equation is formulated:

$$\frac{dv}{dt} = F(x, v) + \sigma(x, v)\eta(t). \tag{2.5}$$

$F(x, v)$ is the deterministic effective force term and $\eta(t)$ represents a Gaussian white noise with zero mean $\langle \eta(t) \rangle = 0$ and correlation $\langle \eta(t)\eta(t') \rangle = \delta(t - t')$. Here, $F(x, v)$ does not directly capture the mechanical forces acting on the cells, but is rather an effective description of the nuclei trajectories. Contrary to persistent random motion described by the OU-process, the noise strength $\sigma(x, v)$ depends on both the velocity v and position x. The deterministic effective force term and noise term are inferred from experimental data by conditional averaging:

$$F(x, v) = \langle \dot{v} | x, v \rangle \tag{2.6}$$

$$\sigma(x, v) = \sqrt{\Delta t \langle [\dot{v} - F(x, v)]^2 | x, v \rangle} \tag{2.7}$$

with the experimental time resolution Δt. Importantly, the deterministic and stochastic contributions only depend on the acceleration $\dot{v}$ and are thus constrained

by the short-timescale behaviour of the measured trajectories. To gain a conceptual understanding of the underlying dynamics of cells hopping between two islands, a closer look at the deterministic contribution $F(x, v)$ is needed. Through plotting the characteristic landscapes in x-v-space, it is revealed that without noise the inferred system still exhibits regular transition. This implies that cells are deterministically driven into the bridge in order to transition. For the cancerous cell line MDAMB231 employed in [24], limit cycle oscillations between the islands around an unstable fix-point at $x, v = (0, 0)$ is observed, while the non-cancerous MCF10A cells exhibit excitable bistability with two stable fix-points at either side of the bridge.

2.3.2 Cell-Cell Interaction Model

To bridge the gap between single-cell behaviour and collective cellular dynamics, it is crucial to understand how cells interact with each other. One effective approach is to start by examining collisions between two individual cells. This could provide insights in the forces and molecular mechanisms at play during direct cell-cell interactions, which can then be extended to more complex scenarios involving larger groups of cells. In bottom-up models of cell-cell interactions, the dynamics are described in various ways. One common method is the use of repulsive potentials, which help model the excluded volume interaction. This means that the model takes into account the physical space occupied by cells, ensuring that they do not overlap or penetrate each other, thus maintaining a realistic representation of cellular boundaries. Additionally, these models often incorporate alignment terms, which help to simulate the way cells align their movement with neighbouring cells. For instance, Kulawiak *et al.* modelled cell-cell interaction by employing a computational phase field model including the mechanics of cell shape and a minimal chemical model for CIL, that focuses on Rac-signalling [124]. However, those models are often based on physical intuitions and not derived from experimental data.

The data-driven approach described in section 2.3.1 can be extended to study an interacting system consisting of two cells. Brückner *et al.* redefined the two state pattern as a minimal cell collider to develop a theoretical framework describing the dynamics of interacting cell pairs [25]. Again, in this setup the nuclei can be precisely tracked over long periods of time and most of the interacting behaviour is captured by the x-position of the cells. The cells are subsequently regarded as point-like particles characterised by a certain position and velocity. From the frequent stochastic collision events, three distinct types of behaviour are observed: reversal (CIL), sliding (CSL) and following (CFL). In order to detect underlying physical interaction to accurately describe the interaction dynamics of the cell pairs, Brückner *et al.* propose a stochastic equation of motion of the form

$$\frac{dv}{dt} = F(x, v) + f(|\Delta x|)\Delta x + \gamma(|\Delta x|)\Delta v + \sigma(x, v)\eta(t). \tag{2.8}$$

F(x,v) describes the interaction of each cell with the confinement similar to equation 2.5. Additionally, an effective interaction term is added consisting of two separate contributions. It has to be mentioned, that this equation of motion captures the

effective dynamics that describe cellular nucleus accelerations instead of mechanical forces acting on the cells. The effective positional interaction term $f(|\Delta x|)\Delta x$ captures the effective repulsion and attraction between the cell nuclei and the directional interaction term $\gamma(|\Delta x|)\Delta v$ captures the effective frictional interactions between the two nuclei. Both terms describe how, on average, the dependence of nuclear acceleration depends on the relative distance Δx and relative velocity Δv to the nucleus of the second cell. The last term accounts for intrinsic stochasticity with $\langle \eta(t) \rangle = 0$ and correlation $\langle \eta(t)\eta(t') \rangle = \delta(t - t')$. The effective friction between cell nuclei relies on a deceleration as they collide, while an acceleration of this process would be interpreted as anti-friction leading to sliding events. Using an underdamped Langevin inference (ULI) the functions for f and γ can be inferred from measured trajectories.

2.3.3 The Interaction Behaviour Space

To establish a link between the physical interaction terms and the cell-cell collision behaviour, the cell-cell interactions can be mapped onto a 2D phase space, spanned by the amplitudes of the cohesive and frictional contributions. This interaction behaviour space (IBS) provides a low dimensional representation of the inferred cohesion and friction interactions between the different cell pairs [25]. Specifically, every combination of possible parameters (for γ,f) is simulated and the dominant collision event is determined. Therefore, each parameter combination corresponds to a behaviour distribution, with varying proportions of the three main interaction events (reversal, sliding, following). The colours indicate the dominant collision event predicted from the pairs of cohesion and friction interactions (Fig. 2.5). In

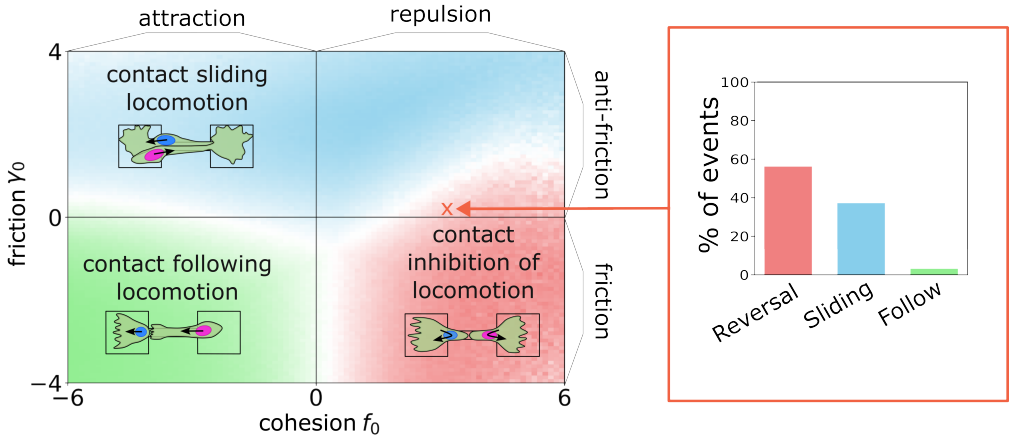

Figure 2.5: Interaction behaviour space (IBS). The IBS spanned by varying the amplitudes γ_0 and f_0 of the friction and cohesive interactions. For negative f_0 values cells show attraction, positive values correspond to repulsion. Negative γ_0 values indicate effective friction and positive values indicate effective anti frictional interactions. Colours indicate regions with one dominant interaction event. Sketches of the three interactions events are shown underneath each domain. Behaviour distribution from one specific point in the IBS is shown on the right.

the blue region, cell pairs show a predominantly sliding behaviour, in the red regions cell pairs are most likely to reverse upon contact and in the green region following events are dominant. White regions correspond to behaviour distribution where no single behaviour contributes more than 50% of events.

In this thesis, the theoretical framework developed by Brückner *et al.* for single cell migration and cell-cell interactions on a dumbbell-shaped confinement is employed. This approach is used to analyse the diversity in cell migration and interaction behaviours and to explore potential underlying mechanisms of these behaviours.

3. Experimental Setup

3.1 Micropatterning for Cell Migration

Within the human body, cells must navigate diverse geometries and environments. To investigate specific functions and address biological questions, it becomes essential to replicate these unique cellular microenvironments *in vitro*. Traditionally, cells are commonly studied *in vitro* by allowing them to adhere to homogeneous adhesive substrates. However, in such experimental setups, it is difficult to control the environmental parameters for individual cells, and the variability of cell behaviour makes it difficult to repeatedly observe certain phenomena. This makes it difficult to collect sufficient statistical data on specific processes to discover new mechanisms or develop insightful models. To overcome this challenge and improve comparability between experimental parameters, the experimental set up is often simplified by restricting cell movement to confined geometries. Several micropatterning techniques have been utilised to create such standardised cell environments [125, 126]. Dependent on the shape and structure of the confining micropattern, cell shapes and migratory behaviour differ greatly from freely moving cells on substrates. Those micropatterned environments can span a spectrum from long 1D lanes to intricate 2D structures and even extend to three-dimensional (3D) environments, such as nanofibers or cavities formed by hydrogel matrices [34, 127, 128]. Numerous microfabrication techniques have been developed and used to investigate cell mechanics and behaviour. Within the context of this thesis, the focus will be on 2D patterning techniques.

The most prominent fabrication methods are microcontact printing (μCP), microscale plasma-initiated protein patterning (μPIPP) and, more recently, photolithographic patterning techniques with and without the use of masks [126, 129, 130]. The basic principle underlying the production of cell-confining structures remains the same for all three methods: the entire substrate is made cell-repellent by chemically passivating the surface, leaving out or removing the passivation at the areas intended for the desired confinement geometry. These specific areas are then coated with proteins of the extracellular matrix (ECM), usually fibronectin, laminin or collagens.
For μCP a polydimethylsiloxane (PDMS) stamp in the shape of the desired structure is incubated with the coating protein of choice and then placed face down onto the substrate. To passivate the remaining surface area, the substrate is filled with a blocking solution, usually poly-ethylene glycol (PEG). This technique works on

a variety of different surfaces and for various ligands [20, 125, 131]. However, this method does not always provide a sharp and precise pattern, especially small structures are more challenging to produce.
μPIPP is another PDMS stamp based method [21]. The stamp is placed onto the substrate to exclude the desired structures from passivation. For passivation, the surface is oxygen plasma treated to activate the surface to promote the binding of poly-l-lysine (PLL), which is coupled to PEG. Upon removal of the stamp, the non-passivated areas can be coated with a protein to ensure cell adhesion. This technique has the advantage, that the patterned structures are visible in phase contrast imaging, while μCP and photopatterning methods rely on fluorophore labeled protein coatings.
Due to the fact that the stamps of the desired structures have to be fabricated in advance, changing the geometry is time consuming. As a result, photopatterning techniques have gained attention in recent years [22, 132, 133]. As a first step, the surface of the substrate is passivated with an anti-fouling component in a two-step process. PLL is incubated on the substrate. Following this, the surface is coated with Polyethylene Glycol-Succinimidyl Valerate (PEG-SVA). PEG-SVA can form covalent amide bonds with the amine groups of the PLL through its succinimidyl ester group. This layer serves to prevent cell adhesion due to PEG's hydrophilicity and resistance to protein adsorption. In order to selectively remove the passivation, a photoinitiator in form of a water-soluble benzophenone (i.e. 4-benzoylbenzyltrimethylammonium chloride - PLPP) is added. The substrate is then selectively illuminated by light emitting in an absorption band of benzophenone. For instance, emitting with a wavelength of 375 nm (UV). This illumination activates the benzophenone in the photoinitiator and triggers the photo-scission mechanism, leading to a cleavage of the amid bonds of the PEG-SVA-PLL layer [134]. In the following, those areas can be coated with ECM proteins for cell attachments. The UV light can by spatially modulated by deploying digital micromirror devices (DMD), enabling fast and precise patterning methods for many different and complex structures [23]. Moreover, the protein density depends on the illumination dose, which can be easily controlled.
In this thesis, a photopatterning technique with a UV laser and the PRIMO (alvéole) system is used. The technique and the resulting micropattern is shown in Fig. 3.1. As soon as cells adhere to the micropattern, they can adapt to the shape of the structure.
Smaller structures, such as rectangles, triangles or crosses, which accommodate only a single cell, are commonly employed to investigate phenomena like gene expression, cell death, or the cytoskeleton [103, 135–137]. Furthermore, these confined microenvironments allow for precise and focused examination of individual cellular behaviour in response to certain drugs or gene manipulations [138]. For studying cell migration, many different micropatterned structures have been employed [139–141]. Most prominent are long, thin lanes, where cell movement is restricted to one dimension [12, 127, 142]. This simplifies the analysis and allows for precise measurement of cell motility and actin network dynamics. Moreover, the adhesiveness of cells to certain ECM proteins can be studied by varying concentration and/or changing the

coating protein. By increasing the size of the patterns, collective migration can be investigated.

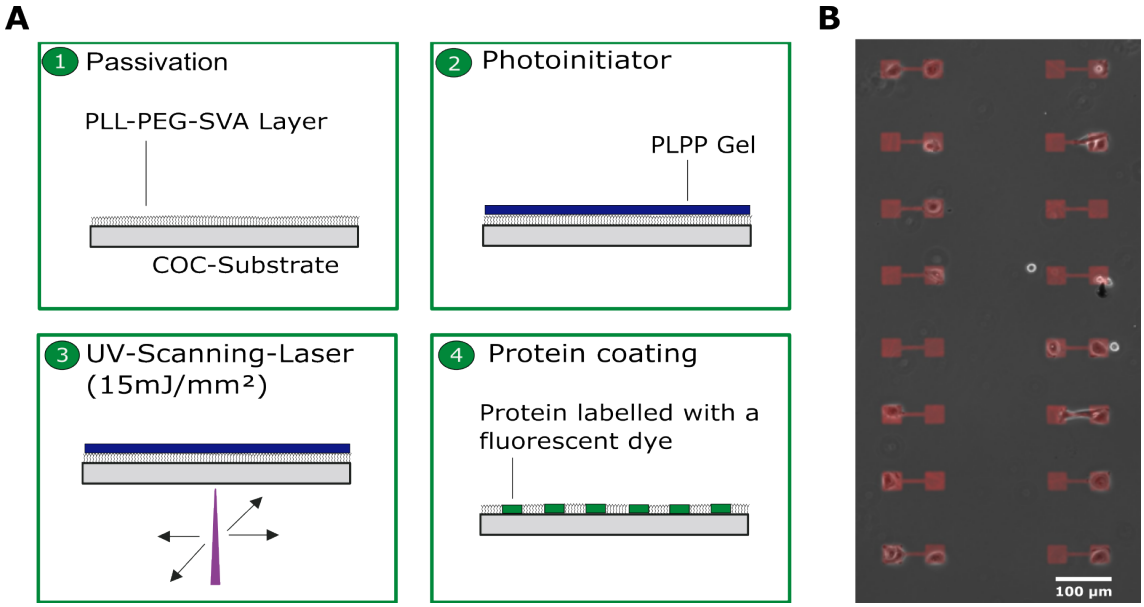

Figure 3.1: Micropatterning method using the PRIMO device. A) 1) Passivation is done on COC-substrates through a PLL-PEG-SVA coating. 2) PLPP is applied as a photoinitiator. 3) The UV light, directed by the PRIMO module, activates the PLPP resulting in the cleavage of the PLL-PEG-SVA layer. 4) The patterned areas can be coated with a protein to increase adhesiveness. B) Exemplary image of the pattern with adherent cells.

Advantages of a Dumbbell Pattern

In this thesis, a two-site pattern with a dumbbell shaped geometry is used in order to study single cell dynamics and the cell-cell interaction behaviour between two cells [24,25]. In further sections this micropattern will be referred to as the *dumbbell pattern*. The dumbbell consists of two 35 μm squares connected by a 7 μm wide and 40 μm long bridge. An image of the dumbbell structure is shown in Fig. 3.1B. In studying single cell dynamics, the dumbbell pattern functions as an invasion assay. A cell can either rest on one of the island or transition over the bridge into the opposite. Thus, the cell in the dumbbell pattern can be in a rest state (e.g. sitting on an island) or in a dynamic state (e.g. transitioning over the bridge). The frequency of transitions between the islands can serve as an indicator of invasiveness. Furthermore, the dumbbell pattern allows for precise tracking of the cellular velocity and acceleration.
When exploring interactions between two cells, the geometry of the dumbbell pattern induces head-to-head collisions, leading to specific responses based on the cell type involved. In this regard, the dumbbell pattern acts as a two-cell collider, facilitating high-throughput analysis of collision behaviour between cells. This innovative

approach provides significant insights into the fundamental dynamics governing cell motility and interaction, crucial for understanding more complex cellular behaviours in physiological and pathological contexts.

3.2 Light Microscopy

Light microscopy is a fundamental tool in biological research, providing insight into the structure, dynamics and behaviour of biological samples. This imaging technique uses visible light to illuminate samples, allowing researchers to observe cellular and subcellular structures in great detail [143]. Light microscopy spans different modalities, each tailored to specific applications and sample types. One of the most commonly used forms of light microscopy is brightfield microscopy (BF), in which samples are illuminated from above or below. The image is then created by collecting the transmitted or reflected light. The contrast in the image is formed by absorption of light in denser areas of the sample. This method uses a relatively simple optical setup and does not require special sample preparation or staining. However, low contrast in weakly absorbing samples and blurring of out-of-focus material are the limitations on this technique [144, 145].

Phase contrast microscopy (PC) is a technique employed to increase the contrast of images of transparent and colourless samples. This method effectively converts phase shifts resulting from differences in optical path length into amplitude shifts, which are perceptible to the human eye. To effectively separate and manipulate the illuminating light from the scattered light after interacting with the sample, a slightly modified setup compared to brightfield microscopy is required. A condenser annulus is positioned in the front polar focal plane to focus the light onto the sample. The light passing through the sample remains undeviated, while light that is diffracted and phase shifted by structures within the sample undergoes changes in phase. To enhance image contrast, constructive interference is generated between the diffracted and undeviated light. This is achieved by passing the background light through a phase ring, which shifts the light by one-quarter wavelength. Focusing the light on the image plane now causes destructive or constructive interference between diffracted and undeviated light resulting in darker or brighter regions in the sample compared to the background [146, 147].

Another powerful technique for generating contrast is fluorescence microscopy. This method utilises fluorescent molecules to label and visualise specific proteins or structures within the cell. When excited by light of a specific wavelength, these fluorescent molecules emit photons with a higher wavelength, providing contrast in the image. By employing different fluorescent molecules, multiplexing becomes possible, enabling the precise detection of multiple targets simultaneously. Furthermore, the development of synthetic molecules and the use of genetically encoded fluorescent proteins, such as those tagged with green fluorescent protein (GFP), allow for long-term live imaging of cellular dynamics with high spatial and temporal resolution [148, 149]. Additionally, many super-resolution techniques rely on the utilisation of fluorescent molecules within the cell [150–153].

3.3 Confocal Microscopy

Confocal microscopy was developed to enhance the optical resolution and contrast of images from cellular samples. This technique enables the imaging of optical sections from thicker specimens, while creating sharp images of the exact plane of focus. This is achieved by using a spatial pinhole that effectively blocks out-of-focus light from the background or other regions of the specimen. By stacking several images at different depths of a sample, a 3D image can be reconstructed and analysed. The main principle of a confocal microscope is outlined in Fig. 3.2.

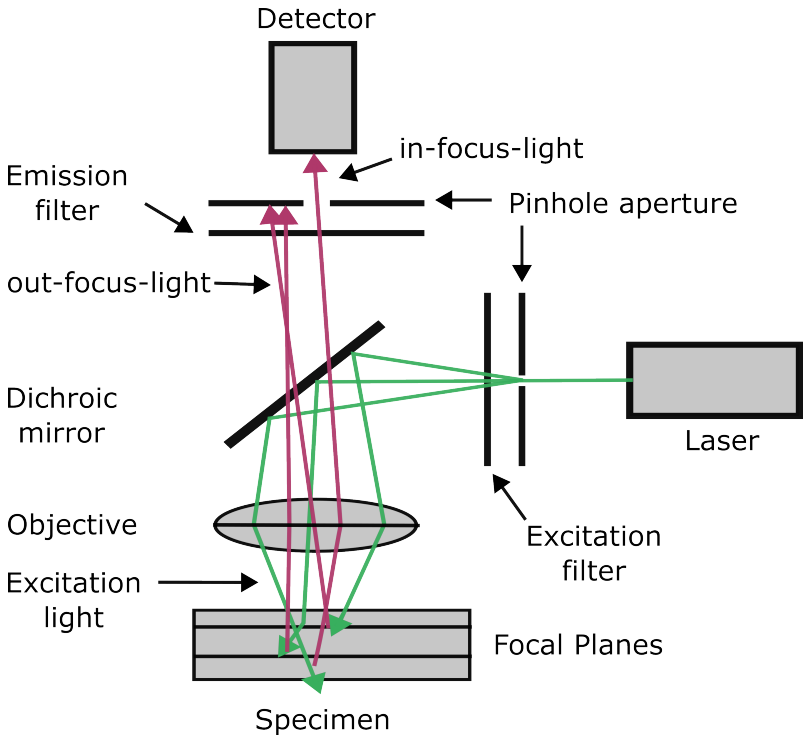

Figure 3.2: Confocal ligth path. The excitation light is shown in green and the emission light in dark red. Only in-focus-light passes through the pinhole aperture and reaches the detector.

An excitation source, typically a laser system, emits coherent light that passes through a pinhole aperture located in a plane conjugate to the scanning point on the specimen. The laser light is reflected by a dichroic mirror and focused by the objective lens onto a specific point at a certain depth within the specimen. This interaction induces the emission of fluorescent light from the focus point. The emitted light is collected by the same objective lens and directed back towards a second pinhole aperture located in front of a detector.The pinhole is strategically placed at a confocal plane, allowing only light emitted from the exact focal point to pass through to the detector. Light originating from out-of-focus areas of the specimen

will not be in focus at the pinhole and is thus blocked, preventing it from reaching the detector. This selective detection is crucial for enhancing image clarity and depth resolution. The detector, which is highly sensitive, is typically a photomultiplier tube (PMT) or an avalanche photodiode that converts the light into an electrical signal. This signal is then used to construct an image representing the optical section of the specimen [154–156].

A recent advancement in confocal microscopy is the development of a novel detector concept known as Airyscan, that significantly improves the resolution and sensitivity of imaging beyond the limits set by traditional confocal systems. The main principle is the implementation of a 32-channel gallium arsenide phosphide photomultiplier tube (GaAsP-PMT) area detector that captures a pinhole-plane image at every scan position. The Airyscan detector is placed in the conjugate focal plane and consists of a hexagonally packed detector array. In traditional confocal microscopy, higher resolution is typically achieved by decreasing the size of the pinhole. The diameter of the pinhole is usually set to one Airy Unit (AU), corresponding to the diameter of the central Airy disk of the diffraction pattern. Reducing this to 0.2 AU can increase spatial resolution by approximately 1.4x. However, this reduction leads to a substantial decrease in the amount of signal reaching the detector, impacting image quality due to lower light throughput. The Airyscan approach addresses this issue of retaining a high signal-to-noise ratio while also achieving a higher resolution. Each element in the detector array functions as a small 0.2-AU pinhole, arranged in a circular geometry that collectively covers a total detector area equivalent to 1.25 AU. This configuration not only allows for higher spatial resolution, akin to imaging with a 0.2 AU pinhole, but it also captures up to 50% more light compared to the conventional single-pinhole setting of 1 AU. Consequently, this leads to a significantly higher signal-to-noise ratio. By employing this method, the Airyscan technology effectively improves lateral resolution by up to 1.7 times and axial resolution by up to 1.4 times compared to standard confocal techniques [157, 158].

4. Single Cell Dynamics

Investigating cell dynamics is essential in understanding complex processes in tissue development, remodelling and cancer progression. In the field of single cell migration, various aspects have already been analysed to understand the behaviour and mechanics of individual cells as they migrate. For instance, the mechanical properties of migrating cells, such as cell stiffness, adhesion dynamics, and cytoskeletal organisation, have been investigated to understand how cells move and change shape during migration [139, 159, 160]. Other studies focused on the complex network of biochemical pathways and signalling events that regulate and coordinate the migration process at the molecular level. For instance, the control of the polymerisation and depolymerisation of actin filaments is carried out through proteins like Rho GTPases, such as Rac1, Cdc42, and RhoA [9, 10, 161]. In various studies, the cell motility is restricted to 1D motion in order to simplify the analysis by avoiding shape changes and to reduce the variety of migratory cell states. The analysis of the cellular trajectories on 1D lanes including speed, directionality, and persistence, has provided insights into the dynamics of single cell migration in different contexts. For example, Maiuri et al. analysed individual cell trajectories on 1D adhesive lanes across 54 different adherent cell types, revealing a universal coupling between cell speed and persistence (UCSP) [12, 40].
However, in more complex physiological contexts such as metastasis, cells cannot migrate on a straight line, but instead must navigate through tissues or pores to enter the bloodstream, facing higher degrees of confinement. Studies suggest that confined migration can enhance cancer metastasis by promoting increased invasiveness [162], highlighting the importance of understanding migratory behaviours within physiologically relevant environments that mimic tissue architecture.
The migratory behaviour of cells appears to be closely linked to their phenotype [163]. For example, during EMT, epithelial cells undergo changes in cellular morphology, molecular profiles and dynamic behaviour, acquiring motile and invasive characteristics essential for processes such as embryonic development, wound healing, organogenesis, and cancer progression [84, 164, 165]. Therefore, deciphering how these phenotypic traits relate to the dynamic behaviour of individual cells is crucial for understanding cellular functions and responses in various biological contexts.

To address the challenges discussed, a recently introduced dumbbell-shaped micropattern is employed to study the cell dynamics and invasiveness of various different motile cell lines [24]. The focus of this study is to investigate whether cellular dynamics can be used to quantitatively describe and identify phenotypic character-

istics in distinct cell types. To achieve this, we utilise cell lines with an epithelial or a mesenchymal phenotype and induce perturbations targeting specific phenotypic characteristics for further analysis. This approach allows us to examine how changes in cellular behaviour correlate with distinct phenotypes and how perturbations affect these dynamics. Specifically, we will focus on the influence of the epithelial-to-mesenchymal transition (EMT) on single cell dynamics.
The majority of the results presented in this chapter are published in Publication [P2]. The influence of EMT, specifically the miRNA200c, on cell invasiveness and dynamics is described in Publication [P1] [166].

4.1 Dependency on Phenotype

The different cell lines are cultured and seeded on the dumbbell pattern. Once the cells adhere to the patterns, they establish a front-rear polarisation and begin to form elongated protrusions that span over the bridge between the squares. In order to transition over the bridge, the cells assemble long stress fibers and the protrusions grow into a fan like shape as visible in Fig. 4.1A. The branched actin polymerisation at the tip of the protrusion pushes the plasma membrane forward, ultimately resulting in a transition of the cell from one island across the bridge onto the opposite island. During that transition over the bridge, the nucleus is deforming and adapts an elongated shape. The cell is capable to extend its size across the whole pattern with extending membrane ruffles reaching the corners of the islands as shown in Fig. 4.1B.

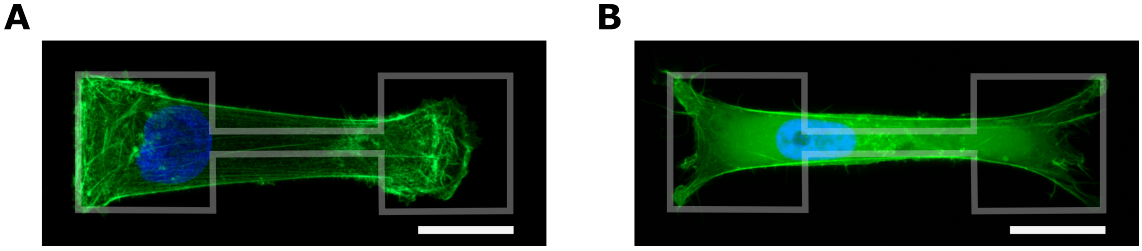

Figure 4.1: Actin distribution in different cell lines in confinement. F-actin fibers (green) in A) a MCF10A cell or B) a MDAMB231 cell confined on a dumbbell pattern. Scale bar is 25 μm and the nucleus is stained in blue.

In order to explore the variations in single cell dynamics on a dumbbell pattern, a range of various motile cell lines across human tissue have been measured.
The triple negative breast cancer (TNBC) cell lines MDAMB231 and MDAMB436 (or short MDA231, MDA436) lack the receptors for the hormones oestrogen and progesterone, as well as the Human Epidermal Growth Factor Receptor 2 (HER2) commonly found in breast cancer. This form of cancer is challenging to treat since hormone therapy does not work on these types of cancer. Additionally, TNBCs are highly metastatic and aggressive. The cells are characterised by a spindle like morphology and they rarely form adhesive bonds between each other. This is partly due

to the fact that they do not express the adhesion protein E-Cadherin, MDAMB231 cells also do not express N-Cadherin (Fig. 4.2B).
The fibrosarcoma cancer cells HT1080 are also characterised by a lack of E-Cadherin expression. While some adhesive bonds between the cells are present, it is not enough to build stable monolayers (Fig. 4.2A). This form of cancer has a high metastatic potential and is often used in migration studies.
The lung cancer cells A549 express both Cadherins and show a more round morphology with the ability to form stable adhesions and therefore maintain and grow as a monolayer. The metastatic potential of these cells is low.
The non cancerous human breast cell line MCF10A expresses high level of E-Cadherin and forms stable monolayers (Fig. 4.2). All cell lines express the type

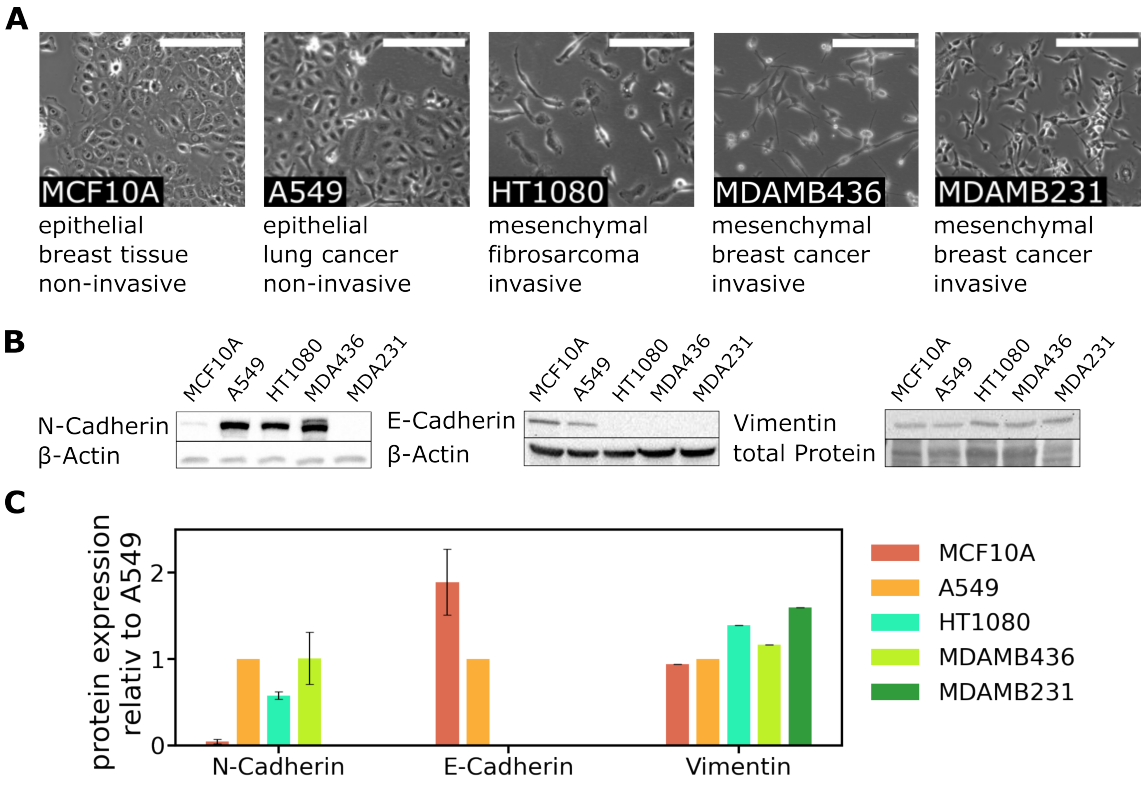

Figure 4.2: Phenotypic characteristics in various cell lines. A) Brightfield images of the different cell lines growing in culture. B) Exemplary western blots for the proteins E-Cadherin, N-Cadherin and Vimentin. For loading control the housekeeping protein β-Actin was employed and for Vimentin a ponceau staining to determine total protein concentration was used. C) Western blot analysis of protein expression levels N-Cadherin, E-Cadherin and Vimentin of the different cell lines normalised to the expression in A549 cells. Three independent replicates were conducted for the Cadherins and one for Vimentin. Error bars indicate mean ± SD of triplicate measurements.

III intermediate filament (IF) protein Vimentin (Fig. 4.2B & C).
The TNBC cell lines and HT1080 cells are traditionally classified as *mesenchymal* due to their absence of E-Cadherin, high motility, and inability to form stable

adhesions. A549 and MCF10A cells are characterised as *epithelial* by their high expression of E-Cadherin and the ability to form stable adhesions. However, it is noteworthy that A549 also express high levels of N-Cadherin, which is often associated with a mesenchymal phenotype. In table 4.1 the characteristics of the cell lines and their EMT protein expressions are listed.

Cell line	origin	phenotype	invasive potential	E-Cadherin	N-Cadherin	Vimentin
MCF10A	breast tissue	E	low	+++	+	+
A549	lung cancer	E	low	++	+++	+
HT1080	fibrosarcoma	M	high	-	++	++
MDAMB436	breast cancer	M	high	-	+++	++
MDAMB231	breast cancer	M	very high	-	-	+++

Table 4.1: Summary of the cell line characteristics.

To analyse the single cell dynamics and the invasive potential of these cell lines, the cell nucleus is tracked for up to 48h. The array of dumbbell patterns allows for high-throughput data collection, yielding hundreds of trajectories for a detailed analysis of the cell dynamics. Exemplary time-lapse series for each of the cell lines are shown in Fig. 4.3A.
The epithelial cell lines MCF10A and A549, exhibit a lower frequency of transitions between the islands and typically require more time to cross the bridge compared to the mesenchymal cell lines. This observation is also visible in the one dimensional trajectories shown in Fig. 4.3B. In Fig. 4.3C the two dimensional trajectory is plotted inside a dumbbell outline. This depiction clearly visualises the differences between the cell lines: mesenchymal cells frequently move back and forth across the bridge, while epithelial cells primarily navigate within the islands.

We now employ the theoretical framework developed by Brückner *et al.* to quantitatively describe the cell migration behaviour of our cell lines [24].
When examining the occupation probabilities, cell lines show an equal distribution across both islands (Fig. 4.4A). The mesenchymal cell lines (MDAMB231, MDAMB436, HT1080) frequently transition over the narrow bridge, while the epithelial cell lines (A549, MCF10A) stay longer on one island before transitioning. This is quantified with the dwell time τ, defined as the time spend on one island between two subsequent transitions (Fig. 4.4B, filled bars). The frequency of the hopping events varies not only between different cell types, but also shows a large variability between cells from the same cell line due to cell-to-cell variations. Thus, this cellular hopping behaviour was found to be a stochastic process and the resulting pattern appeared to be cell-line-specific and characteristic.

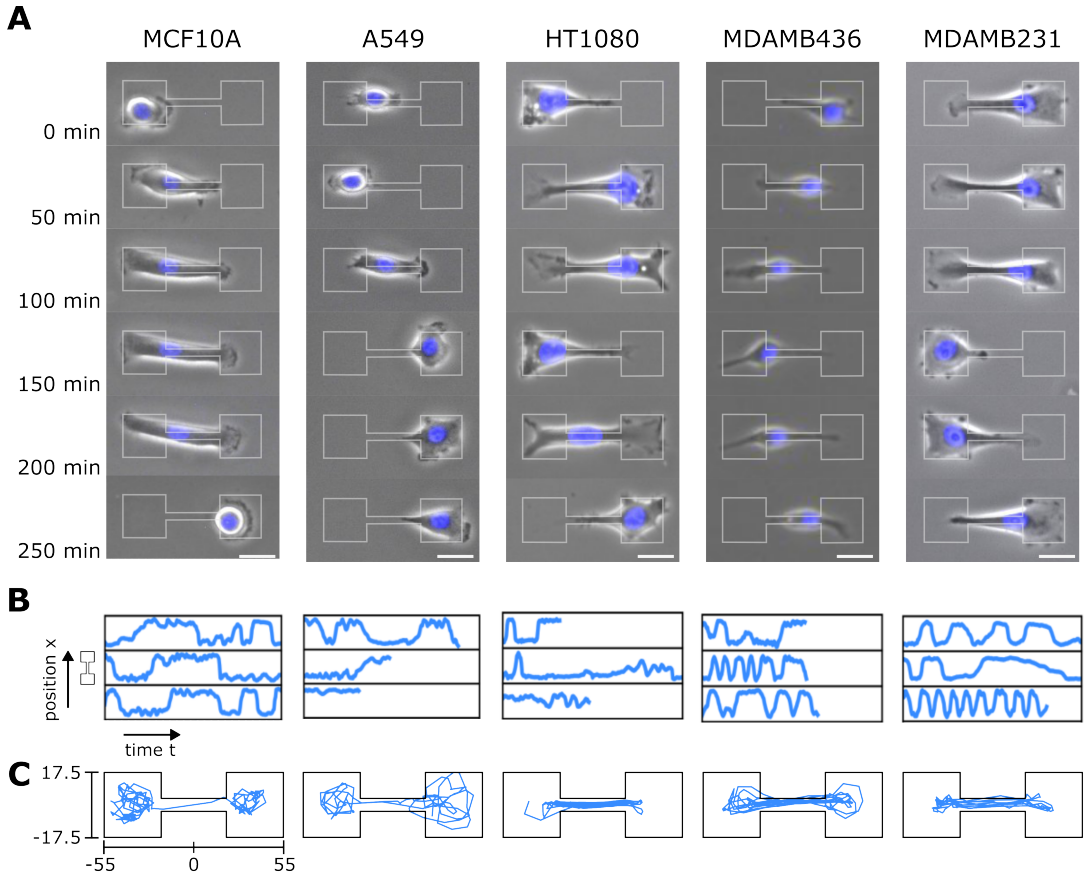

Figure 4.3: Tracking single cell dynamics on dumbbell patterns. A) Time-lapse series of five distinct cell lines on the dumbbell spanning a 250 min time frame. The nucleus is depicted in blue, and the pattern is outlined for better clarity. The scale bar is 25 μm. B) Three trajectories in 1D for each cell line. C) One exemplary trajectory of each cell line shown in 2D inside the dumbbell pattern.

To quantify the transition dynamics, the survival probability *S(t)* that a cell has not completed a transition after a given time, is computed for each single cell and all different cell lines. The survival probability decreases monotonically with time, however there is a discrepancy between the epithelial and mesenchymal cell lines (Fig. 4.4C). The epithelial cells show lower probability to transition, which points at a lower invasive potential in those cells.

Brückner *et al.* established a quantitative theoretical model for stochastic cell migration within the dumbbell structure. A stochastic equation of motion is utilised, which subdivides the dynamics into deterministic and stochastic contributions in the position–velocity phase space [24]:

$$\frac{dv}{dt} = F(x,v) + \sigma(x,v)\eta(t). \tag{4.1}$$

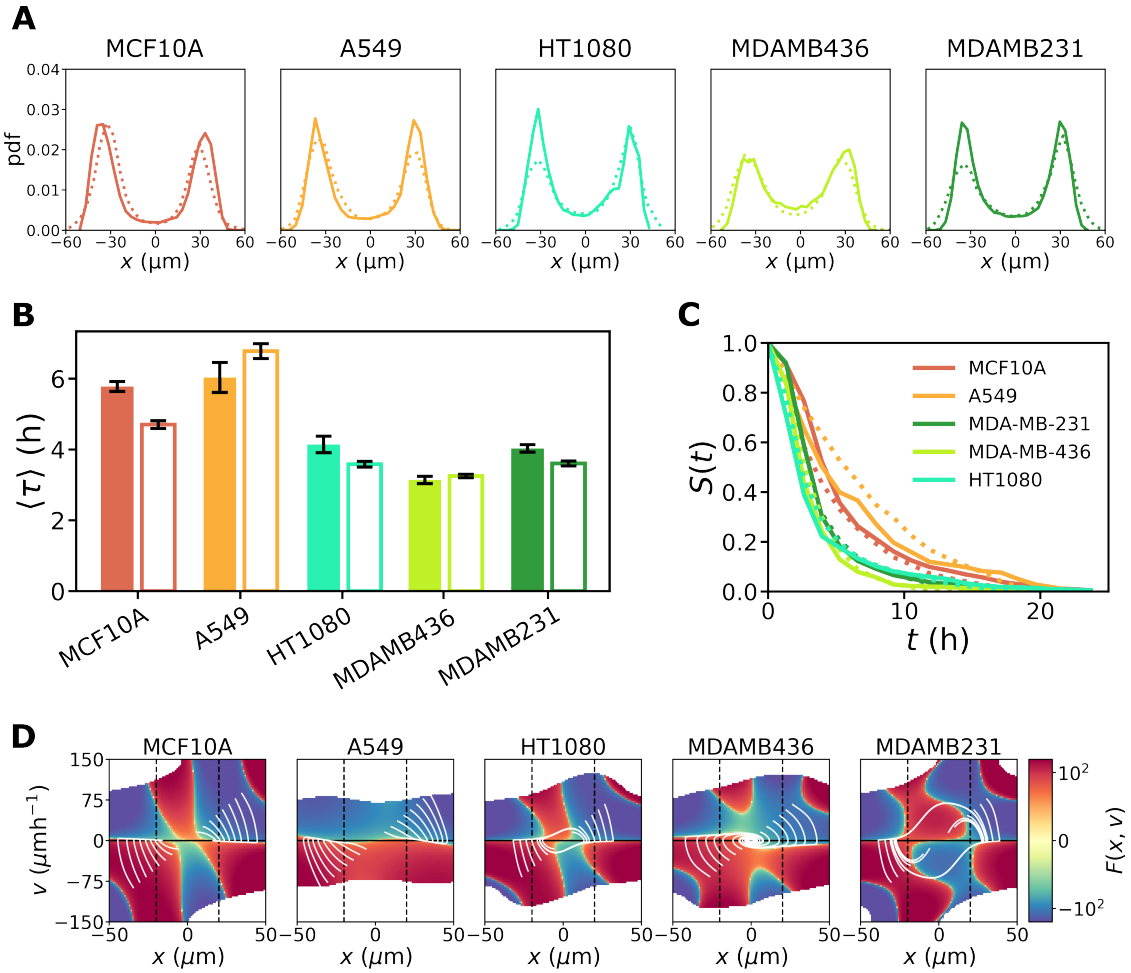

Figure 4.4: Single cell dynamics on the dumbbell. A) Probability distribution of the nucleus position inside the dumbbell over time for the different cell types. Solid lines show experimental data and dotted lines show the prediction of the inferred underdamped description. B) Average dwell times for the different cell lines, filled bars are experimental data and empty bars model data. Error bars show the error of the mean (s.e.m) obtained from bootstrapping. C) Survival probability of all considered cell lines, that describes how likely it is that a cell has not made a transition after time t. Again, solid lines show experimental data and dotted lines the prediction of the inferred underdamped description. D) Inferred effective force $F(x,v)$ for all five cell lines. $F(x,v)$ describes the average acceleration of a cell nucleus given at a certain position x and velocity v. Positive values indicate positive accelerations. The white lines display trajectories of the deterministic dynamics and black dashed lines mark the area of the bridge.

The deterministic term $F(x,v)$ describes the prototypical behaviour of a cell and the stochastic term $\sigma(x,v)\eta(t)$ describes the cell-cell variability and the intrinsic stochasticity of cell movement in the dumbbell pattern.
In order to assess whether this model effectively captures the system-level dynamics of the five phenotypically different cell lines employed in this study, the terms of the

equation are directly inferred from the experimental trajectories [24]. For this, 50% of the experimental data is used in the inference process to "train" the model and then compared to the remaining 50% of the data. By simulating trajectories using the inferred equation of motion, the predictive capability is tested. The model is in good agreement with the experimental data of the dwell time, the survival probability distributions and the occupation probability distribution (Fig. 4.4B empty bars and Fig. 4.4C dotted lines).
The effective force *F(x,v)* describes the deterministic contribution of the the nucleus acceleration in the micropattern at any given position and velocity. A closer look at the phase-space maps of *F(x,v)* (Fig. 4.4D) and the deterministic trajactories (white lines) show the differences in the dynamics of the five cell lines. The cells (except A549 cells) drive themselves deterministically into the bridge indicated by the positive acceleration (red region) around $x=0$ at positive velocities. The epithelial cell lines MCF10A and A549 exhibit two stable fix points on either side of the bridge, indicating excitable bistable dynamics. In other words, the cells only randomly hop between the islands, with the hopping events initiated through stochastic noise. The mesenchymal cell lines, exhibit deterministic oscillatory motion on the pattern, indicating limit cycle dynamics. Here, limit cycle oscillations describe how cells repeatedly and deterministically hop between the two islands as also visible in their trajectories (Fig. 4.3B).

In summary, a notable difference in dynamics between epithelial and mesenchymal cells on the dumbbells is observed. The dwell times of the mesenchymal cells are significantly lower than for the epithelial cells, which is also reflected in the survival probabilities. The phenotypic differences are further highlighted by analysing the inferred single-cell behaviour in phase-space. Epithelial cells show two stable fixed points and primarily exhibit a bistable hopping behaviour, remaining largely within their island and only occasionally escaping the fixed points due to noise. In contrast, mesenchymal cells frequently transition back and forth and display limit cycle oscillations.

4.2 Influence of EMT

To investigate whether the distinct dynamics observed between epithelial and mesenchymal phenotypes are inherent traits, we will explore the relationship between phenotypic shifts and changes in cellular dynamics. Specifically, we aim to determine if a switch in phenotype correlates with a switch in dynamic behaviour. To achieve this, we study the effect of EMT on the cell dynamics.
EMT is a reversible biological process in which epithelial cells transform into mesenchymal cells. During EMT, there is activation or silencing of various genes, leading to a loss of adhesion properties, cell polarity, and an enhanced migratory capacity [164, 167]. It has been shown that EMT changes the coordinated interaction behaviour of epithelial cells to that of more individually migrating cells [164]. One of the key features of EMT is the downregulation or complete loss of the epithelial marker E-Cadherin. E-Cadherin is responsible for calcium-dependent cell adhesion,

and its loss is associated with breast cancer progression [83].
As quantified by western blot (Fig. 4.2B-C) the epithelial cell lines MCF10A and A549 express E-Cadherin, while it is absent in the mesenchymal cells. Interestingly, these cell lines also exhibit different single cell dynamics, raising the question to what extend E-Cadherin is involved in regulating the single cell dynamics.
Therefore, the influence of E-Cadherin on single cell dynamics is analysed by blocking the protein with an antibody in MCF10A cells. In contrast, in MDAMB231 cells, lacking E-Cadherin, expression is re-introduced through mRNA transfection with mRNA encoding for E-Cadherin. E-Cadherin expression is visualised in Fig. 4.5A-B in MCF10A and MDAMB231 mRNA-ECadherin (MDAMB231 +ECad) cells *in vitro* without a micropattern. When transfecting MDAMB231 cells with E-Cadherin-GFP mRNA, the cells express the protein and are able to build cell-cell adhesions. This is further underlined by the observation of protein clustering at cell contact sides.

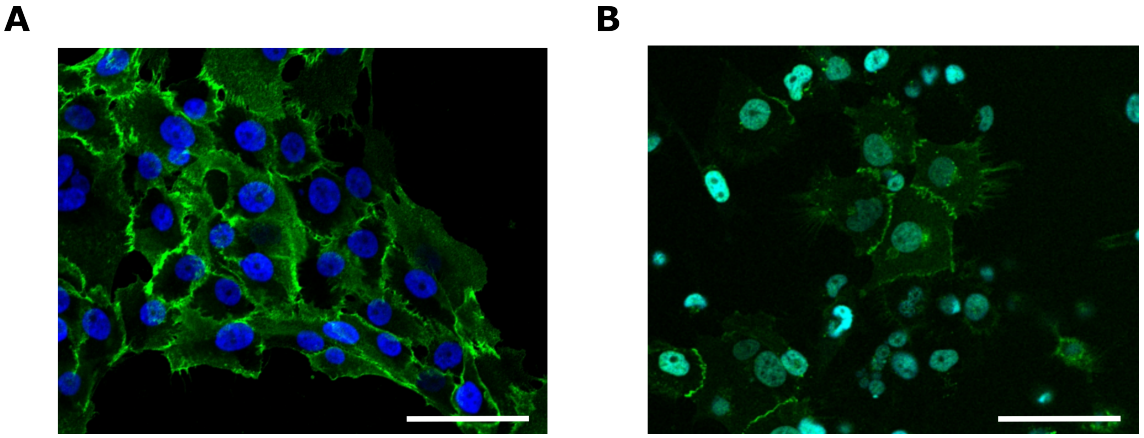

Figure 4.5: E-Cadherin expression. A) Fluorescence images of E-Cadherin (green) distribution in MCF10A cells. B) MDAMB231 cells after transfection with GFP tagged E-Cadherin mRNA. Nuclei are stained in blue. Scalebar is 200μm.

To analyse the impact on E-Cadherin on the cell dynamics, the perturbed cells are placed on the micropattern. Interestingly, the MCF10A cells with blocked E-Cadherin (MCF10A +ECad-AB) seem to behave similarly to the MCF10A cells. The statistical analysis of cell trajectories revealed subtle changes in cell behaviour, particularly a slight increase in average dwell times, indicating that cells take longer before transitioning between states. This behaviour is further supported by a small increase in survival probability (Fig. 4.6A-B). The deterministic dynamics of the MCF10A +ECad-AB cells still show a excitable bistable hopping behaviour (Fig. 4.6C). This indicates that the loss of E-Cadherin does not impact the single cell behaviour in MCF10A cells.

Since E-Cadherin is a known tumour suppressor, we want to analyse its impact on the invasive behaviour of MDAMB231 cells as indicated by the repeated hopping behaviour. In the transfected MDAMB231 cells (MDAMB231 +ECad) a slight decrease in the dwell times is observed (Fig. 4.6A). The survival probability however is

nearly identical with the unperturbed MDAMB231 cells (Fig. 4.6B). Interestingly, the dynamics of the cells as determined by the inferred single cell term *F(x,v)* does change (Fig. 4.6C). Instead of limit cycle oscillations, the MDAMB231 +ECad cells now exhibit an excitable bistable behaviour similar to the MCF10A cells.
However, there is a notable discrepancy between the model results and the experimental data, particularly evident in the dwell times and survival probabilities. This discrepancy may arise from the relatively limited experimental data available for the MDAMB231 +ECad cells compared to the other perturbations (40% less trajectories). To address this issue and draw more robust conclusions, additional experiments need to be conducted.

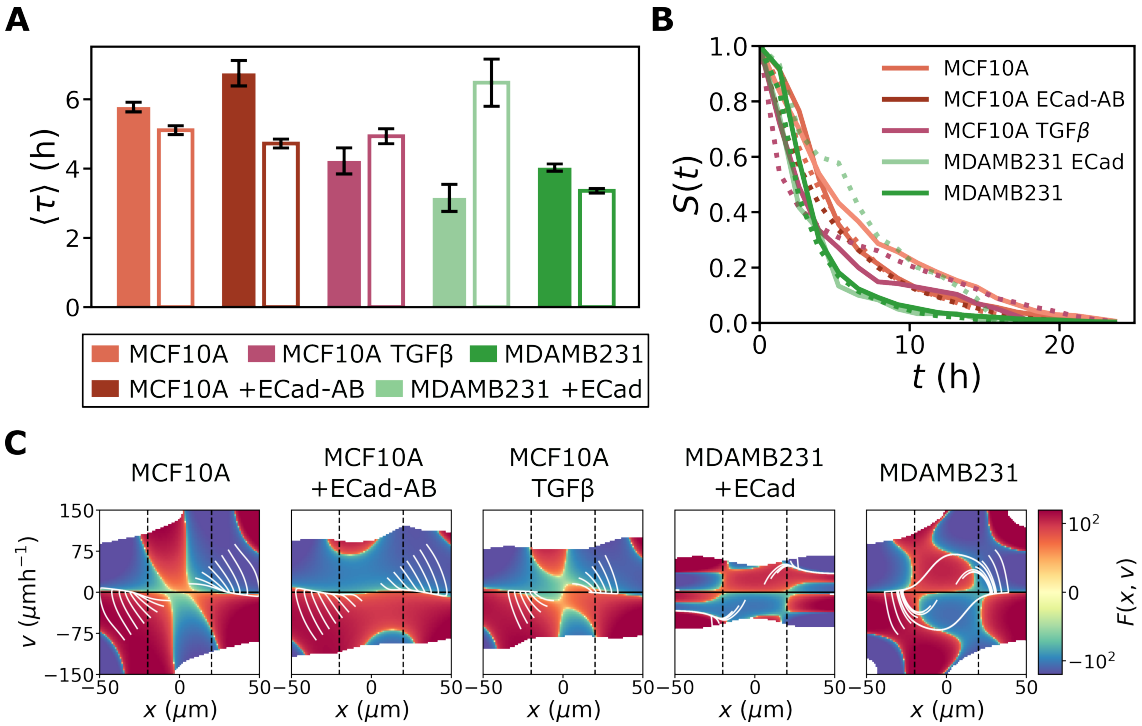

Figure 4.6: Influence of EMT on single cell dynamics. A) Average dwell times derived from the different perturbations, filled bars are experimental data and empty bars model data. Error bars show the error of the mean (s.e.m) obtained from bootstrapping. B) Survival probability of the different perturbations, that describes how likely it is that a cell has not made a transition after time t. Solid lines show experimental data and dotted lines the prediction of the inferred underdamped description. The colour code for the different cell lines and perturbations is shown underneath A) and also applies for B). C) Inferred single cell behaviour in phase space of the cell lines. Heat map indicates the inferred single cell term *F(x,v)* describing the deterministic part of the inferred underdamped Langevin equation. The white lines display trajectories of the deterministic dynamics and black dashed lines mark the area of the bridge.

Furthermore, it is essential to exclude any potential effect of the transfection process itself on confined cell motility, as the transfection reagent can be toxic to cells

and could impact cell behaviour. Therefore, we conducted a control experiment to test the effect of the transfection on the cells using GFP-mRNA. We employed the same ratio between mRNA and transfection reagent in order to achieve comparable conditions. The analysis of the MDAMB231-GFP cells revealed no relevant deviation from the wildtype MDAMB231 experiments, indicating that the effects of the transfection are negligible.

In summary, we discovered that E-Cadherin might have in impact in decreasing the invasive behaviour observed in MDAMB231 cells, while its loss does not induce an invasive behaviour in MCF10A cells. Those findings might seem contradictory, however, it is important to note that the loss of E-Cadherin alone is not sufficient to induce EMT and a phenotypic shift in the cells. Consequently, our next step aims at inducing such a phenotypic shift in MCF10A cells to investigate how this complex transition impacts the single cell dynamics.

In MCF10A cells, the EMT program can be initiated by TGFβ. This leads to a decrease in the epithelial marker protein E-Cadherin and in an increase in mesenchymal marker protein N-Cadherin (Fig. 4.7A). Furthermore, the cells change their morphologies to a more spindle-like shape (Fig. 4.7B).

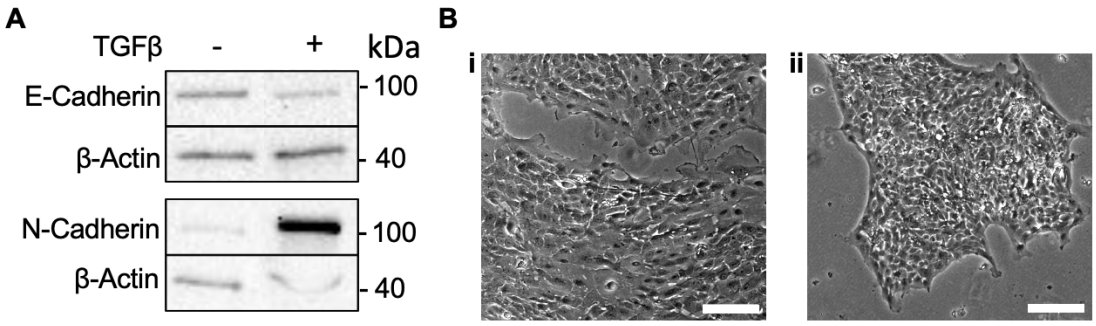

Figure 4.7: A) Western Blot of the proteins E-Cadherin and N-Cadherin in MCF10A cells with and without TGFβ treatment. A decrease in E-Cadherin and an increase in N-Cadherin is observed. B) i) Brightfield image of confluent MCF10A cells after 7days of TGFβ treatment. ii) Brightfield image of confluent MCF10A cells after 7 days in culture without treatment. Morphological changes in the treated cells are observed. Scalebar is 200 μm. Figure adapted from [P2].

The TGFβ treated MCF10A cells show a decrease in average dwell time as well as a higher probability to make a transition (Fig. 4.6A-B). Nonetheless, induction of EMT in MCF10A cells does not switch the cellular dynamics from a bi-stable hopping behaviour to limit cycle oscillations similar to MDAMB231 cells (Fig. 4.6C). This outcome may be attributed to the presence of E-Cadherin on the MCF10A cells, because despite morphological changes, cells still form adhesion between neighbours in confluent cell layers (Fig. 4.7). It is plausible that the cells did not fully transition into the mesenchymal state. Numerous studies have highlighted that, contrary to the classic view of EMT as a binary process with distinct epithelial or mesenchy-

mal states, the transition involves epithelial cells traversing through a spectrum of intermediate states with varied functions and properties [168–170].

4.3 Influence of the MiRNA200c

A critical regulator of EMT is the intricate double negative feedback loop involving several miRNAs such as the miRNA200 family or miRNA34 family, and transcription factors (e.g., Zeb1/2, SNAIL, Slug) (Fig. 2.4B). These small non-coding RNAs can bind to multiple mRNAs, leading to their degradation or inhibition of translation, while the transcription factors control transcription rates by binding to specific DNA sequences, thereby regulating gene expression.
Now, our goal is to investigate the impact of miRNAs on cell dynamics to provide insights into the molecular mechanisms underlying cell behaviour changes associated with cancer metastasis and other pathological processes. Specifically, the miRNA200c, which has been thoroughly investigated, is known to play a pivotal role in various tumorigenesis processes, particularly in EMT [138, 171, 172]. To unravel the underlying mechanisms of the negative feedback loop regulation, we investigate the miRNA / ZEB axis shown in Fig. 2.4 and its effect on cell motility in two cell lines on the dumbell pattern.
The MDAMB231 cells were genetically modified with a TRIPZ-construct to selectively induce miRNA200c expression upon treatment with doxycycline (DOX). Notably, the construct is labeled with a fluorophore (RFP), and its intensity is directly linked to miRNA200c expression levels (Fig. 4.8A-B). To account for potential side effects of the construct and the antibiotic treatment, an empty sequence has been stably introduced into the MDAMB231 cells, creating the control cell line MDAMB231 TRIPZ Ctrl. Further experimental details can be found in [138]. The second system used to study the influence of miRNA200c on invasive properties, is the breast cancer cell line MCF7. Those cells are non metastatic with a low invasive potential. However, due to epigenetic modifications the ZEB / E-Cadherin axis is dormant in those cells, although they express the miRNA200c. A genomic knockout (KO) for miRNA200c was performed in the cells to create the MCF7 miRNA200c KO cell line.

On the dumbbells, the uninduced MDAMB231 miRNA200c cells (-DOX) still frequently transition between the islands, also evident in their trajectories (Fig. 4.8C). The induced MDAMB231 miRNA200c cells (+DOX) fluoresce with RFP and tend to transition less. They also need longer times to cross the bridge (Fig. 4.8C).
The MCF7 cells are not motile on the micropattern. As visible in Fig. 4.8 the cells stay on one side of the micropattern and do not transition, as evident in the straight line marking the trajectories. Interestingly, the knockout of miRNA200c in these cells did not increase the motility (Fig. 4.8D) in the dumbbells. However, other assays performed in [P1], such as scratch assays, showed a significant difference in the average motility between MCF7 and MCF7 miRNA200c KO, especially at low confluence [166]. Additionally, the quantitative analysis of a transwell assay revealed that the relative migration of MCF7 miRNA200c KO cells significantly increased by

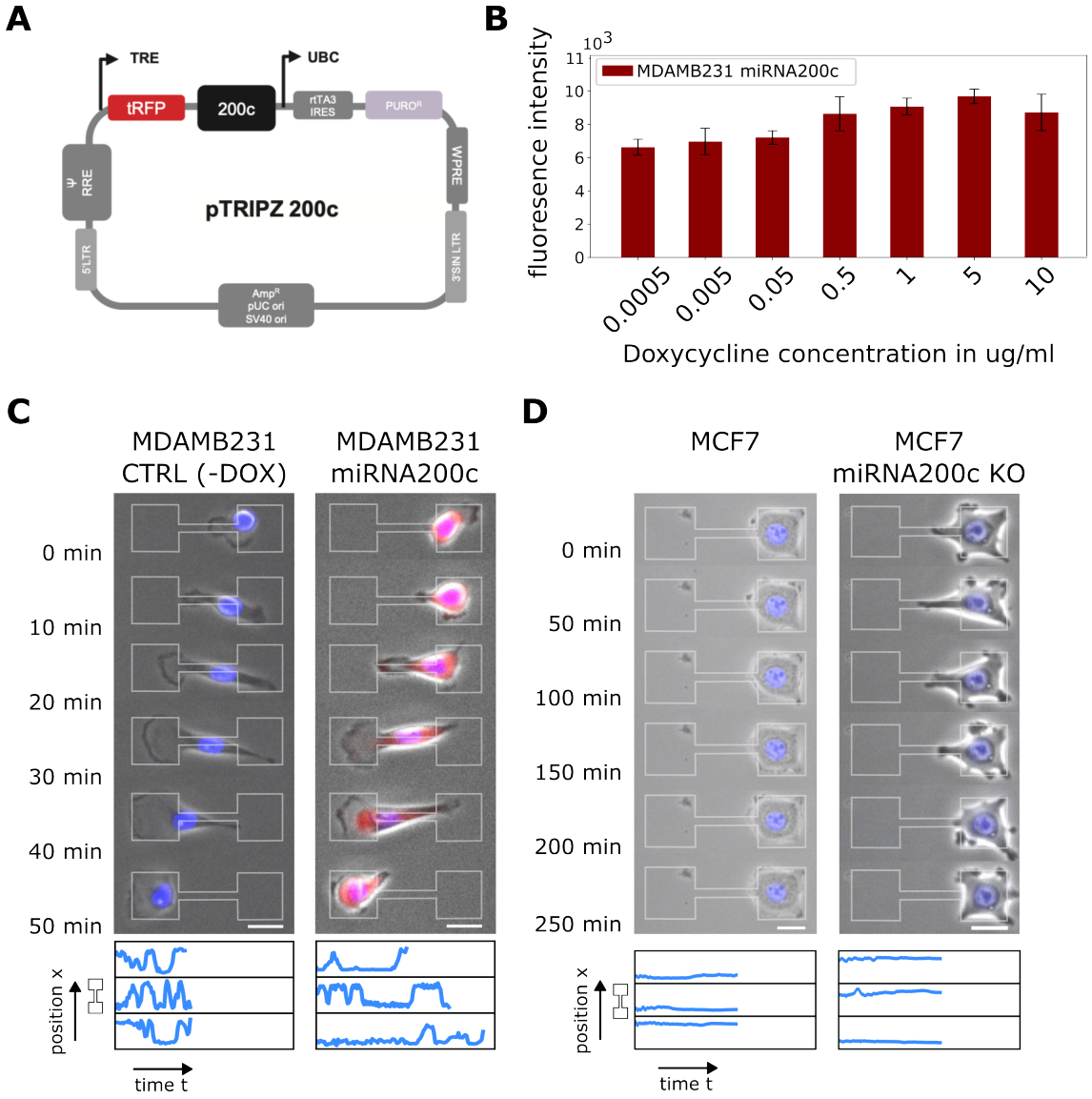

Figure 4.8: Modification of miRNA200c expression in two cell lines. A) TRIPZ miRNA200c construct in MDAMB231 cells, reprinted from [138] with permission. B) Fluorescent expression in MDAMB231 miRNA200c cells after induction with various doxycycline concentrations for 72h. At 5 μg/ml saturation is reached. C) Time-series and exemplary trajectories of MDAMB231 cells without induction of miRNA and with miRNA (indicated with red staining). D) Timeseries and exemplary trajectories of MCF7 cells and MCF7 miRNA200c KO cells. Scalebar is 25 μm. Adapted from [P1].

1.5-fold compared to the wildtype [166]. These results are contrary to the findings of the dumbbell assay, where the lack of miRNA200c in MCF7 cells did not affect the invasive ability of those cells. This discrepancy might indicate to an inability of MCF7 cells to move in a micropatterned confinement. To verify this, both MCF7 cell lines where placed in rectangular patterns (110 μm x 35 μm) with varying pro-

tein coatings (fibronectin, laminin or collagen). However, the cells did not show an increase in motility and predominantly remained in a resting state. Therefore, the stochastic analysis of cell dynamics was only conducted in the motile MDAMB231 miRNA200c cells.

The quantitative analysis of the cellular dynamics of the MDAMB231 construct cells confirmed the differences already observed in the time-series and trajectories of the cells. MDAMB231 (+Dox) cells showed an approximately two-times lower probability to make a transitions after a time t as indicated by the survival probability in Fig. 4.9A.

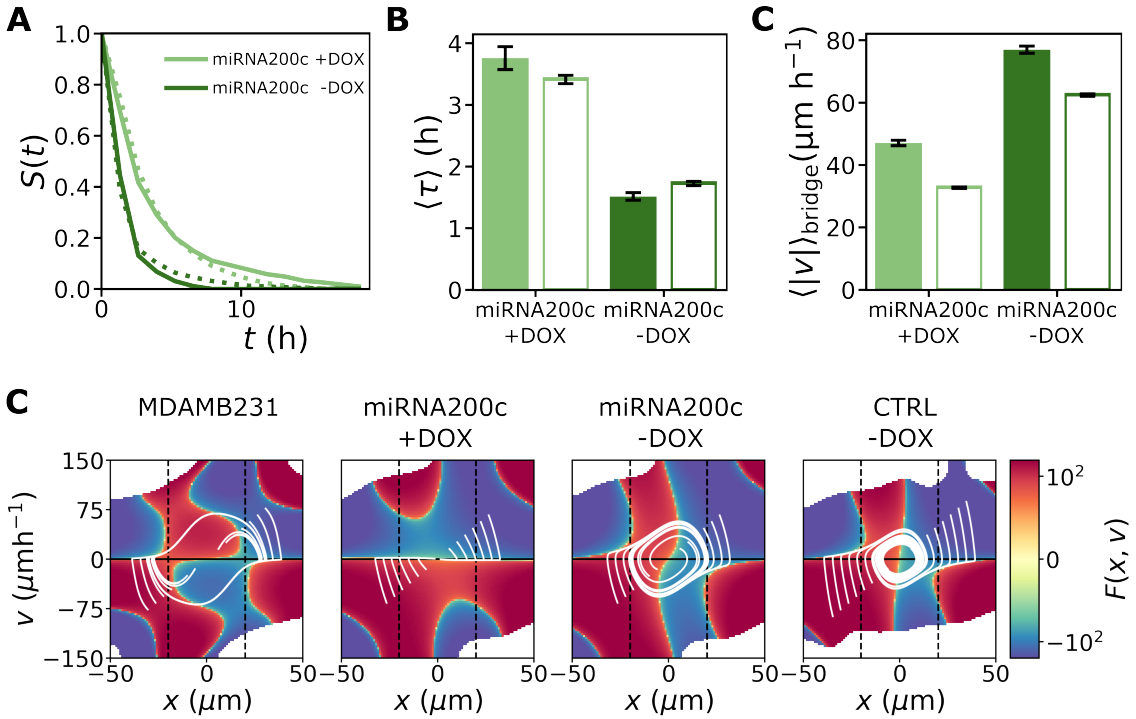

Figure 4.9: Influence of miRNA200c on single cell dynamics. A) Survival probability of the MDAMB231 construct cells, that describes how likely it is that a cell has not made a transition after time t. Solid lines show experimental data and dotted lines the prediction of the inferred underdamped description. B) Average dwell times for the induced cells (+DOX) and uninduced cells (-DOX). Both in B) and C) the filled bars are experimental data and empty bars model data. Error bars show the error of the mean (s.e.m) obtained from bootstrapping. C) Average speed of the induced cells (+DOX) and uninduced cells (-DOX) while making a transition on the bridge. D) Inferred single cell behaviour in phase space of the cell lines. Heat map indicates the inferred single cell term *F(x,v)* describing the deterministic part of the inferred underdamped Langevin equation. The white lines show deterministic trajectories and black dashed lines mark the area of the bridge.

Furthermore, the dwell time of the MDAMB231 (+Dox) cells showed an approximately 2-fold increase (4.9B). This correlates with less frequent transitions after induction of the miRNA200c. Therefore indicating that the miRNA200c lowers

the invasive potential in MDAMB231 cells. Additionally, we quantified the average speed of a cell during a transition on the bridge. We found an approximately two-fold decrease of the transition speeds upon induction of miRNA200c (Fig. 4.9C). Moreover, the model can accurately predict the different survival probabilities (Fig. 4.9A, dotted lines), the dwell times and the average transition speeds of the cells (Fig. 4.9b, empty bars). To have a closer look at the dynamics in the cells, the inferred deterministic force *F(x,v)* is plotted (Fig. 4.9C). From the deterministic trajectories (white lines) a clear difference in the dynamics of MDAMB231 cells depending on miRNA200c expression is observed. The MDAMB231 cells with miRNA200c change to a bistable hopping behaviour similar to the non cancerous cell line MCF10A, which endogenously expresses high levels of miRNA200c. This shift in cellular dynamics demonstrates the capacity of miRNA200c to change the phenotypic migratory behaviour in a confining environment.

To exclude an effect of the miRNA200c-inducer DOX, the induced MDAMB231 control cells (TRIPZ Ctrl) were analysed under similar conditions. As expected, we found that the behaviour of the induced control cells (TRIPZ Ctrl +DOX) is comparable with the behaviour of uninduced MDAMB231 miRNA200c cells (-DOX) which is well described by limit cycle oscillations and is additionally comparable with wildtype MDAMB231 cells. Thus, the treatment with DOX has in general no influence on the migratory behaviour of MDAMB231 cells.

In summary, these results show that both transition frequency and transition speed of migrating MDAMB231 cells decrease due to miRNA200c expression, indicating that miRNA200c negatively affects the efficiency of confined cell migration, as well as the invasive potential. The dynamics are now similar to that of the non-invasive epithelial cell lines (Fig. 4.4).

4.4 Discussion

In this chapter, we investigated the migratory behaviour of single cells from diverse motile cell lines confined within a micropatterned environment. These cell lines can be broadly categorised into two clusters: epithelial and mesenchymal. The differences in molecular composition, morphology and ability to form adhesions observed in these cell lines, reflect the essential cellular diversity required in multicellular organisms. Cells exhibit specialised functions and morphologies driven by intricate genetic programs governing cell fate and differentiation, resulting in a multitude of cell types with unique properties [173, 174].
Despite this diversity, when placed on the micropatterned dumbbells, the distinct morphological differences between cell types become less apparent. Interestingly, we observed that regardless of cell type, cells exhibited similar structural behaviour when traversing the dumbbell. There was a consistent pattern of establishing a front-rear polarity followed by the formation of protrusions at the entrance of the bridge. These protrusions extended into a fan-like shape, reaching toward the unoccupied island, which frequently resulted in a transition of the cell across the bridge. This observed migration mechanism is not unique to our experiment, but appears to

be widely universal across diverse cell types [12, 175]. However, upon closer examination of the dynamics and transition statistics of the distinct cell lines, a notable discrepancy emerged between cells exhibiting an epithelial-like phenotype and those with a mesenchymal-like phenotype. Epithelial cells tended to spend longer periods on the island in a *rest state*, whereas mesenchymal cells frequently transitioned back and forth between the islands, primarily in a *motile state*.

To quantitatively analyse this behaviour, we employed a data-driven approach and a theoretical framework capable to describe the stochastic migration of cells [24]. We confirmed the robustness of this framework across various cell lines, demonstrating its ability to accurately capture the distinct dynamical features of cell locomotion. Furthermore, we discovered that almost all tested cell lines are deterministically driven into the thin bridges. This deterministic driving facilitates a velocity amplification, ensuring a swift transition to the opposite side of the micropattern. Moreover, the dynamics of the cell lines revealed either limit-cycle oscillations for the mesenchymal cells and excitable bistable dynamics for the epithelial cells.
Interestingly, cell lines exhibiting limit-cycle oscillations are known to display high invasiveness in several studies, whereas the non-invasive cell lines exhibit stable fix points on the islands. This suggests the potential of the dumbbell system to measure and evaluate invasiveness in several cell lines. Additionally, the dumbbell assay offers advantages over traditional *in vitro* invasion assays such as the transwell assay or a Boyden chamber. For instance, the dumbbell assay has live-imaging capabilities that allow for the direct detection and analysis of cellular dynamics.
Nonetheless, an intrinsic motility of the cell is a prerequisite for an accurate analysis with the dumbbell assay. Several cell lines tested in this thesis, such as MDCK (dog kidney cells), BEAS2B (non-cancerous lung cells), and MCF7 (non-metastatic breast cancer cells), did not exhibit movement on the dumbbell and had to be excluded from the single cell analysis.

Furthermore, the dumbbell assays provides an optimal platform for studying cellular locomotion at the molecular level by employing strategic molecular perturbations. Surprisingly, we found that the loss of E-Cadherin in MCF10A cells did not affect single-cell behaviour and dynamics, despite E-Cadherin being widely considered as a suppressor of invasion and often found inactive in tumour progression [176, 177]. The cadherin adhesion complex plays a critical role in cellular functions by directly interacting with the cytoskeleton, facilitating mechanosensing, force transmission, and the regulation of microtubule stability. Loss of E-Cadherin disrupts these interactions, leading to disturbances in cell polarisation and should subsequently alter cell dynamics [178]. However, in isolated single cells such complexes cannot form, which could explain the lack of observed changes in dynamics following the blocking of E-Cadherin.
Furthermore, studies have reported that decreased expression of E-cadherin does not always correlate with invasion in breast cancer cells [101]. Instead, N-cadherin is implicated in increasing invasion and motility in breast cancer cells [179]. Therefore, it would be of great interest to investigate the influence of N-Cadherin on single cell dynamics.

In order to transform the phenotype of MCF10A cells into a more mesenchymal like state, we induced EMT via TGFβ treatment. The TGFβ treated MCF10A cells showed an increased expression in N-Cadherin and a reduction in dwell times on the island. However, despite the TGFβ induction aiming to transition MCF10A cells from epithelial to mesenchymal states, we did not observe the oscillatory motion previously detected in other mesenchymal cell lines. A plausible explanation could be that EMT is a dynamic process rather than a bi-stable switch [168, 170] and our treated cells may be in an intermediate state rather than having fully transitioned to a mesenchymal phenotype.

Lastly, we induced the miRNA200c in the invasive MDAMB231 and discovered a shift from limit cycle oscillations towards a bistable hopping behaviour similar to the non-invasive cell lines. This suggests that miRNA200c plays a pivotal role in regulating confined cell migration and invasiveness. One possible explanation is that miRNA200c induces changes in the cytoskeleton, resulting in reduced cellular protrusions on the bridge and decreased intracellular forces that would enable the nucleus to follow these protrusions onto the bridge. Filamin A is regulated by the miRNA200c and its loss could lead to morphological changes and reduced cellular motility [138]. Furthermore, the lack of miRNA200c increases the expression level of Vimentin, which is associated with a promotion of cell migration [180, 181]. To disentangle the role of miRNA200c further research is needed due to the fact that miRNA is involved in a variety of complex molecular pathways. Nonetheless, it can be concluded, that miRNA200c negatively affects the invasive capabilities of MDAMB231 cells.

In summary, the study of single-cell migration in a dumbbell-shaped micropattern revealed different dynamical patterns for distinct phenotypes. Moreover, the dumbbell assay and the theoretical framework developed by Brückner *et al.* proved robust for a variety of distinct motile cells and can be effectively combined with molecular perturbations to uncover fundamental principles governing cell migration dynamics, such as the influence of specific molecular components on cell behaviour and the underlying mechanisms of cell movement.

5. Dynamics of Cell-Cell Interactions

As a next step in unveiling the physical mechanisms behind cellular dynamics and behaviour in confinement, we utilise the dumbbell system to study the interaction behaviour of two cells. The shape of the micropattern enforces repeated head-to-head collision, leading to a large data set of cell-cell interactions.
Cellular interactions are an essential part in various aspects of the body and influence a multitude of physiological processes [4, 6, 77]. Impairments or dysfunctions in these interactions can lead to a variety of diseases and are often observed in the progression of cancer [182, 183]. Upon contact, a multitude of signals are converged between the cells, enabling a coupling of the two migratory machineries. Such intercellular processes are mediated by a wide range of different surface proteins. For instance, the adhesion protein E-Cadherin enables force transmission between the cytoskeletons, while the Eph-ephrin systems is involved in cell recognition during contact inhibition of locomotion (CIL) [81, 101]. Furthermore, the regulation and alteration of cell polarity during cell-cell interactions depend on a complex network of surface proteins that signal downstream to the cytoskeleton. The diversity of surface proteins and active signalling pathways present on various cell types contributes significantly to the variability in cell-cell interactions. However, it appears that the fundamental migration mechanisms employed by many cells is largely universal [12]. This universality in cell migration mechanisms raises the questions of whether there are also universal cell-cell interaction mechanisms that account for the diverse range of behaviours observed among distinct motile cells. Understanding these mechanisms could reveal common principles that dictate how cells interact in various physiological and pathological contexts.
In previous work, Brückner *et al.* investigated two distinct cell lines in the 'cell collider' to analyse cell-cell interactions. They developed a theoretical framework for inferring cell dynamics directly from experimental data (detailed description in section 2.3.1) [25]. In this chapter, we will extend this investigation by utilising a diverse array of cell lines with distinct phenotypes, varying in morphology, adhesion capabilities, and surface protein expression, as illustrated in Fig. 4.2.
Most of the results presented in this chapter are content of Publication [P2].

5.1 Cell-Cell Interactions Across Various Cell Types

To explore the cell-cell interaction behaviours of several motile cell lines, we employ the previously used dumbbell shaped micropattern as a minimal cell collider. (Fig. 5.1A). Cells are seeded on the pattern and after cell division, the nuclei of the mother-daughter cells are tracked over 48h. This process generates a substantial dataset of one-dimensional trajectories, with examples depicted in Fig. 5.1B. Analysis of these trajectories allows us to identify three distinct types of interaction events: reversal, sliding, and following. During reversal events, also known as contact in-

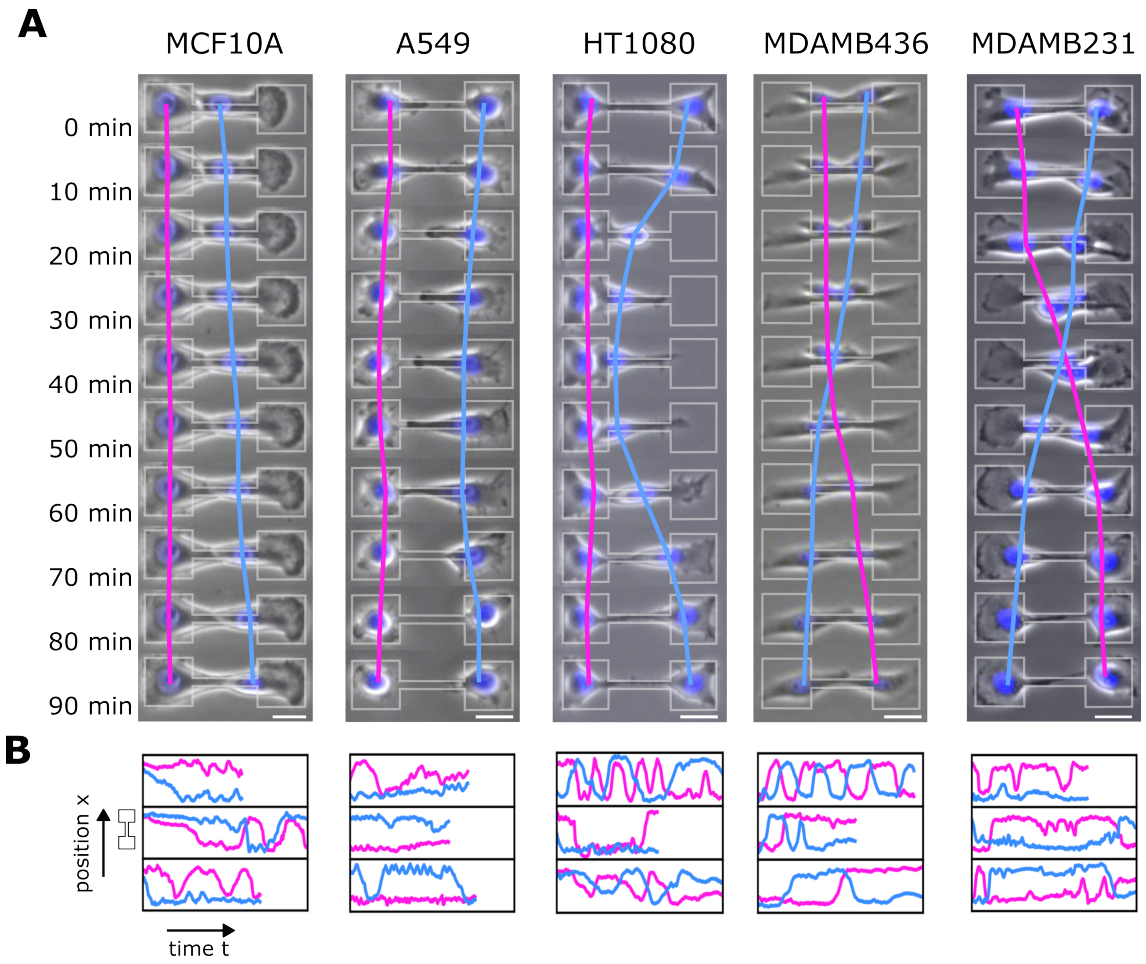

Figure 5.1: Tracking of cell-cell interactions on the dumbbell pattern. A) Time-lapse series of the five distinct cell lines on the dumbbell pattern, spanning a 100 min time frame. The nuclei are depicted in blue, and the pattern is only outlined for better clarity. Scale bar is 25 μm. B) Three exemplary trajectories in 1D for each cell line.

hibition of locomotion, cells come into close contact before reversing and polarising away from each other. For instance, in Fig. 5.1A the HT1080 cells are performing a reversal event. The other prominent interaction mechanism observed in the cell types is the sliding of cells past each other. The cells come into contact and swap

places while maintaining their direction of velocity, as observed in MDAMB231 and MDAMB436 cells (Fig. 5.1A). Lastly, cells could also follow each other, where they come into contact and move in tandem across the pattern. However, this behaviour is not commonly observed across the cell types.

To identify the cytoskeletal structures during cell-cell interaction, we use immunofluorescence confocal microscopy for visualisation of the F-actin fibers in the cells. In Fig. 5.2A-B the F-actin fibers are visualised in MCF10A and MDAMB231 cells, respectively. In MCF10A cells the F-actin filaments are mostly straight and form highly oriented bundle-like structures similar to a single cell on the pattern. In contrast, the actin fibers inside the MDAMB231 cell are thin and randomly distributed at the edges of the pattern (top row in B). During a sliding event (bottom row in B), both cells establish long and straight stress fibers to perform a transition. No clear outlines of the two cells are detectable, since they overlap on the bridge. Interestingly, the cells show frayed edges on the island with short and thin actin fibers curving outwards, contrasting to the straight and thick fibers observed in the MCF10A cells (top row in A).

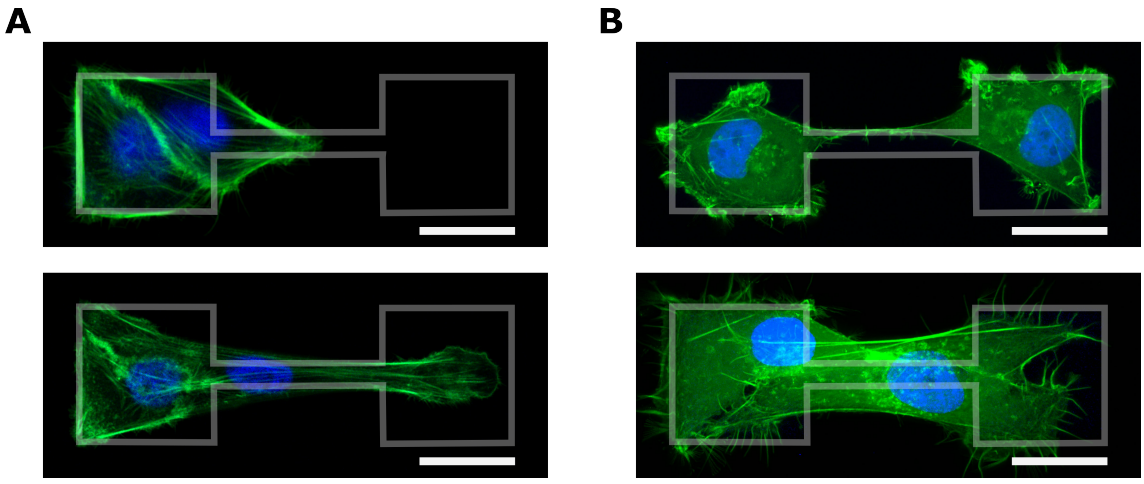

Figure 5.2: Actin distribution in two cells in confinement. A) F-actin fibers (green) in A) MCF10A cells and B) MDAMB231 cells confined to a dumbbell pattern. Scale bar is 25 μm and the nuclei are stained in blue.

As an initial step in understanding how cell pairs interact when confined on a dumbbell pattern, we analyse the positions of the cells over time. Typically, the cells prefer to occupy opposite ends of the pattern. This preference is evident in their trajectories, which frequently show only brief periods of overlap before the cells separate again. In order to characterise the cell-cell interaction behaviours, we employ the theoretical framework developed by Brückner *et al.* to calculate various statistics [25]. To quantify this observation, we calculate the position cross correlation function:

$$\langle x_1(t)x_2(t')\rangle := \frac{1}{2\sum_{j=1}^{N_{pairs}} T_j} \sum_{j=1}^{N_{pairs}} \sum_{t'=1}^{T_j} x_1(t)x_2(t'). \tag{5.1}$$

Here, N_{pairs} is the number of tracked cell pairs and T_j denotes the total number of time points in the trajectory of cell pair j.
This reveals a strong correlation in the positions of the two cells. In Fig. 5.3A the position cross correlation function exhibits a negative long-timescale correlation for all cell lines. This results indicates that, independent of cell type, there is a mutual exclusion behaviour where cells prefer to occupy opposite islands on the micropattern.

Next, we investigate how the cells coordinate their behaviour, when they are in close proximity to each other, while they occupy the same island on the dumbbell pattern. To this end, we calculate the velocity cross-correlation of the two cells:

$$C(|t-t'|) = \langle v_1(t)v_2(t')\rangle := \frac{1}{2\sum_{j=1}^{N_{pairs}} T_j^{same}} \sum_{j=1}^{N_{pairs}} \sum_{\Theta_{same}} v_1(t)v_2(t'). \tag{5.2}$$

Here, Θ_{same} denotes the set of time-point combinations (t, t'), when cell pairs are on the same island on the dumbbell pattern at time t and t'. T_j^{same} is the total number of those time-point combination of a cell pair j. Here, positive values mark correlated cell motion and negative values indicate an anti-correlation of cell motion.
The epithelial cell lines MCF10A and A549 exhibit positive velocity correlations, while the mesenchymal like cell lines MDAMB231 and MDAMB436 show negative velocity correlation (Fig. 5.3B). The mesenchymal HT1080 cells only show weak velocity correlation.
The instantaneous velocity correlations for $C(|t-t'|=0)$ in Fig. 5.3C highlight the differences between the cell lines. There is a shift from negative to positive velocity cross correlation, which coincides with the phenotype of the cells.
In order to gain insight into how cells navigate each other during collisions on longer time scales, we now quantify the distribution of collision events in the different cell lines. MCF10A, A549 and also HT1080 cells show a strong preference in reversing upon contact, while the two triple negative breast cancer (TNBC) cell lines predominantly slide past each other (Fig. 5.3D). Although all cell lines show a mutual exclusion behaviour as indicated by the negative position correlation, they still exhibit different coupled collision behaviour.

To identify the dynamical processes leading to the distinct interaction behaviour across cell types, we employ a previously introduced data-driven inference approach [25]. Specifically, we infer an equation of motion from the experimental trajectory data, which captures the effective dynamics of cell-cell interactions:

$$\frac{dv}{dt} = F(x,v) + f(|\Delta x|)\Delta x + \gamma(|\Delta x|)\Delta v + \sigma(x,v)\eta(t). \tag{5.3}$$

The interacting equation of motion for the observed stochastic two-cell dynamics consists of a effective deterministic force term $F(x,v)$ describing the deterministic acceleration of the cell nucleus due to single cell motility and interactions with the environment. A noise term $\sigma(x,v)\eta(t)$ is added to capture the inherent stochasticity of cell migration. The cell-cell interactions are incorporated in the effective positional interaction term $f(|\Delta x|)\Delta x$ and the directional interaction term $\gamma(|\Delta x|)\Delta v$. Both

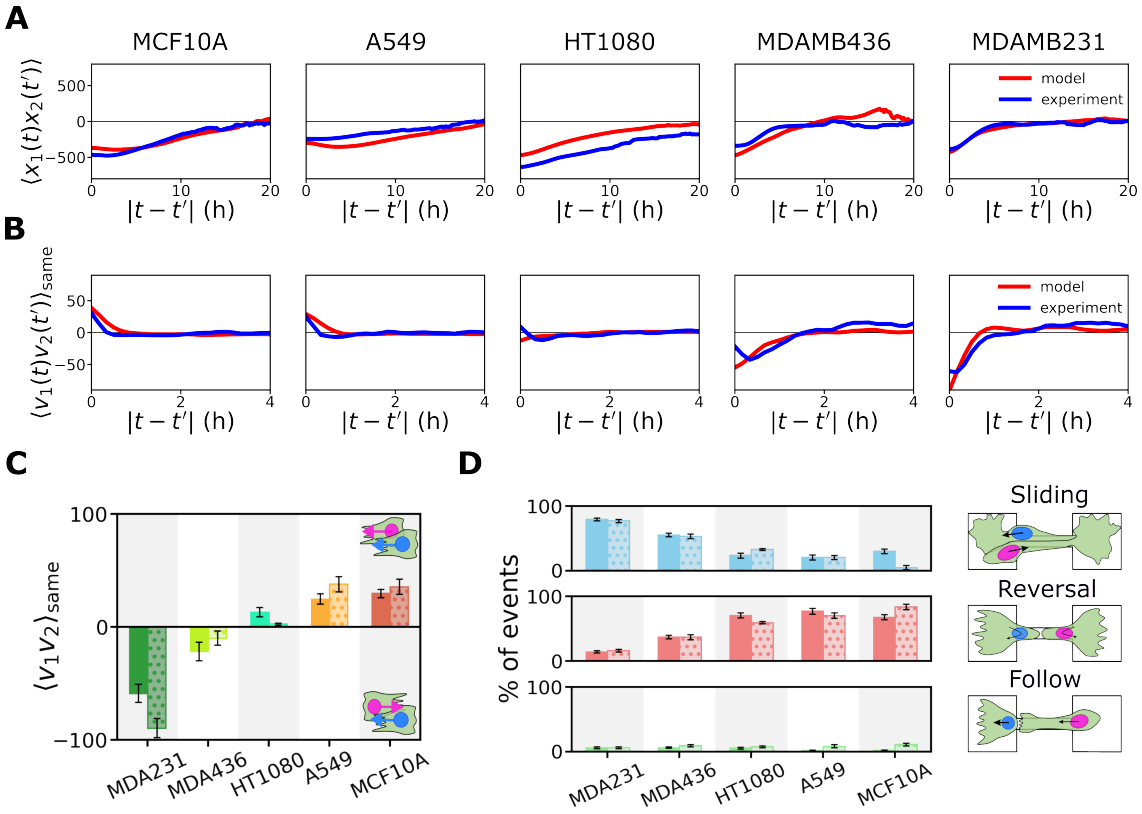

Figure 5.3: Quantification of cell-cell collision behaviour. A) Position cross correlation function for all cell lines. B) Velocity cross correlation function for all cell lines. C) Instantaneous velocity cross-correlation between cell pairs occupying the same island. Solid bars show experimental results, dotted bars show the prediction of the inferred underdamped model. Error bars show the error of the mean (s.e.m) obtained from bootstrapping. D) Behaviour distribution of the different cell lines showing percentages of the observed three different collision events. Again solid bars show experimental results, dotted bars show the prediction of the inferred underdamped description and error bars show the error of the mean (s.e.m) obtained from bootstrapping. Figure adapted from [P2].

terms describe the average acceleration of the cell nuclei influenced by their relative separation Δx and relative velocity Δv [25]. Negative values of $f(|\Delta x|)\Delta x$ imply attraction between cell nuclei, while positive values indicate repulsion. Therefore, this term can be understood to capture the effective cohesion between the nuclei of the cells. If the directional interaction term $\gamma(|\Delta x|)\Delta v$ is negative, cells would decelerate when sliding past each other, indicating effective cell-cell friction. Positive values would correspond to an acceleration of cells when sliding past each other, indicating effective cell-cell anti-friction [25].
In order to determine these effective cell-cell interactions in our cell lines, we employ a theoretical learning framework called Underdamped Langevin Inference (ULI) to infer the functions $f(\Delta x)$ and $\gamma(\Delta x)$ from the coupled trajectories [25].
The simulated trajectories show a good agreement with the experimental data, which

we observe in the analysed statistics. The model correctly predicts the cross correlation for position and velocity as illustrated by the red line in Fig. 5.3A and B, and indicates a robust compliance to the observed behaviour distribution (Fig. 5.3D dotted bars).

The different coupled collision behaviour is also reflected by the inferred effective friction and cohesion interaction terms (Fig. 5.4A). The dynamics of cell-cell interactions in MCF10A and A549 cells are well described by a combination of repulsion interactions and friction interactions. In contrast, the TNBC cell lines are well described by a combination of short-range attraction coupled with long-range repulsion and pronounced anti-friction interactions. The HT1080 cells show similar repulsion interactions as MCF10A and A549 cells, but exhibit no detectable friction interactions (Fig. 5.4A). Although the inferred effective interactions vary strongly between the different cell types, they still capture the variety of different cell-cell collision behaviour.

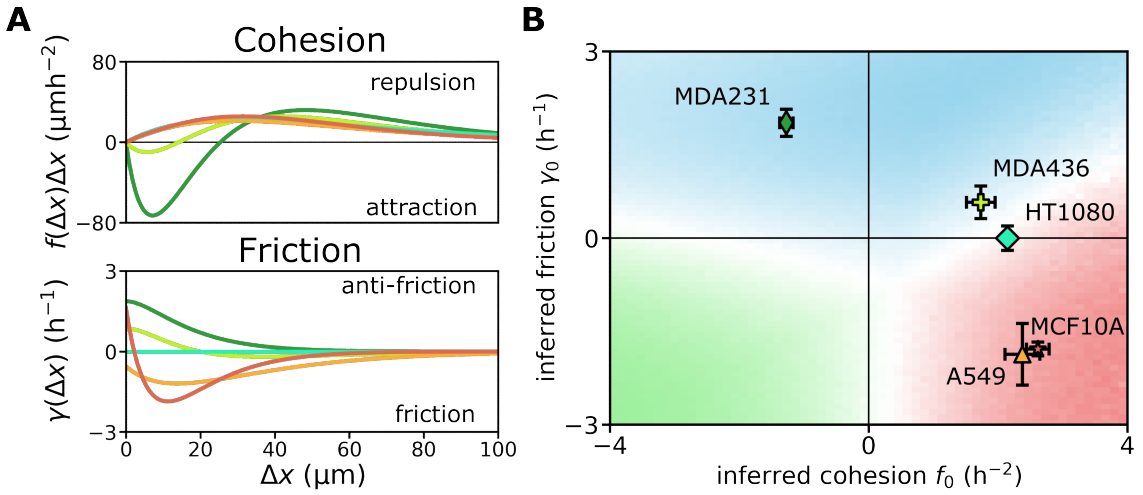

Figure 5.4: Underdamped Langevin inference reveals cohesion and friction interactions. A) Inferred effective cohesion interactions $f(|\Delta x|)\Delta x$ and inferred effective friction interactions $\gamma(|\Delta x|)\Delta v$ for the five different cell lines (colour code as in Fig. 4.4). B) Interaction behaviour space, which summarises a low dimensional representation of the inferred cohesion and friction interactions in the different cell lines. Colours represent the dominant collision event predicted from the pairs of cohesion and friction interactions. Error bars show the standard error of the mean (s.e.m) obtained from bootstrapping of the experimental data. Figure adapted from [P2].

In addition, the predominant collision behaviour can be identified directly from the interaction behaviour space (IBS), which is delineated by different coloured areas. Red areas indicate a predominant reversal behaviour, blue areas indicate a predominantly gliding behaviour and green areas indicate a predominant following behaviour (Fig. 5.4B). The cell lines are distributed across the space and no clustering according to their traditional phenotype is observed. However, only the E-Cadherin expressing cell lines MCF10A and A549 show pronounced friction interactions and are therefore located in a region, where repulsion and friction in-

teractions are strong, giving rise to mostly reversal behaviour. In contrast, the MDAMB436 and HT1080 cells, lacking E-Cadherin, yet expressing N-Cadherin, are situated in a region where repulsion and weak friction interactions predominate. Interestingly, only the MDAMB231 cells, which lack expression of both E-Cadherin and N-Cadherin, are located in a region where attraction and anti-friction dominate, leading to a prevalence of sliding behaviour.

While the five cell lines are not organised into distinct clusters according to their phenotype within the IBS, they do exhibit a general distribution along a single arc that spans from the lower right corner to the upper left corner of the phase-space. This observation prompts the question of whether there exists a unified underlying mechanistic framework capable of describing the various cell-cell interaction dynamics observed across different cell lines. This will be addressed in the following section.

5.2 Polarity Alignment as a Universal Cell-Cell Interaction Mode

In order to uncover an underlying cell-cell interaction mechanism, we use the inferred interactions from the experimental data to systematically constrain possible interaction mechanisms. This data-driven top down approach enables us to develop a more phenomenological description of the cellular dynamics observed in various motile cells. We adopt a simplified model, focusing on two key positional variables: the nucleus position, x_n and the protrusion position x_p. This minimalistic approach effectively captures the elongated shape of cells observed in our experiments (see Fig. 5.2, bottom row). Moreover, we incorporate an explicit representation of cell polarity, P, which drives an active pushing force to the cell's protrusive regions. Including cell polarisation in our model allows for a more accurate depiction of cell-cell interaction behaviours. The direction and adjustment of a cell's polarisation machinery upon contact are critical in determining the interaction outcome. This aspect is essential as it influences how cells align their movement and interact dynamically with each other. The dynamics of the cell is furthermore defined through a force balance of the friction with the substrate, with all forces acting on the positional degrees of freedom. A schematic of the microscopic model is shown in Fig. 5.5A.
The three overdamped equations have the following form [184]:

$$\dot{x}_n = F_n(x_n, x_p) + G_n(\Delta x_n, \Delta x_p, P, \Delta P) \tag{5.4}$$

$$\dot{x}_p = F_p(x_n, x_p) + P(t) + G_p(\Delta x_n, \Delta x_p, P, \Delta P) + F_{boundary}(x_p) \tag{5.5}$$

$$\dot{P} = F_p(x_p, P) + G_P(\Delta x_n, \Delta x_p, P, \Delta P) + \sigma\eta(t) \tag{5.6}$$

The nucleus and protrusion of the cells are coupled through a linear spring, which is embedded within the terms

$$F_n(x_n, x_p) = -\frac{k_n}{\gamma(x_n)}(x_n - x_p) \tag{5.7}$$

and

$$F_p(x_n, x_p) = k_p(x_n - x_p) \tag{5.8}$$

with the spring constants $k_n = k/\zeta_n$ and $k_p = k/\zeta_p$. Here, ζ_p and ζ_n represent the friction coefficient for the protrusion and nucleus. To accurately model the narrower adhesive areas that a cell encounters while traversing the bridge of the pattern, we introduce a dimensionless rescaling factor, $\gamma(x_n)$, which is dependent on the position of the cell nucleus. This rescaling factor is defined to be minimal when the cell nucleus is positioned on the bridge, reflecting the reduced adhesion in this region. Here, we employ the findings of Brückner *et al.* and set [185]:

$$\gamma(x_n) = \frac{1 - \gamma_{\min}}{2}\left(1 - \cos\left(\frac{x_n \pi}{L_{\text{pattern}}}\right)\right) + \gamma_{\min} \tag{5.9}$$

L_{pattern} denotes the size of the dumbbell pattern and $\gamma_{\min}$ is the minimum rescaling factor when the nucleus is located on the bridge. These force terms encapsulate the single cell dynamics within the microenvironment. P characterises the intracellular actin polymerisation at the front of the cell, a critical process for cell advancement. The boundary force $F_{boundary}(x_p)$ ensures a soft repulsive force at the edges to confine the cellular protrusion in the micropattern. Furthermore, the polarity of a cell in this model is influenced by the geometry of the pattern, as such that the polarity is growing when protrusions enter the bridge and is attenuated when the cell is on one island. We implement this in the function $\alpha(x_p)$, which switches sign dependent on the position of the protrusion x_p [185].

$$\alpha(x_p) = -\frac{\alpha_0 - \alpha_{\min}}{2}\cos\left(\frac{x_p \pi}{L_{\text{pattern}}}\right) + \frac{\alpha_{\min} + \alpha_0}{2} \tag{5.10}$$

On the island, $\alpha(x_p) = \alpha_0$ and on the bridge $\alpha(x_p) = \alpha_{\min} < 0$. To prevent an infinite growth of the polarisation, a higher order term βP^3 is implemented, additionally inducing a preferred polarity when $\alpha(x_p)$ is negative.
This new model cannot be directly inferred from experimental data as our data does not include direct measurements of the polarisation P. Nonetheless, the model features can be constrained on the experimental data, through the inferred single cell dynamics on the dumbbell pattern and the inferred cell-cell interactions [24,25].

The cell-cell interactions implemented in this model G_n, G_p, and G_P are generic interaction terms that couple the three degrees of freedom x_n, x_p and P of the two cells. The candidate cell-cell interaction terms are systematically defined and constrained by proposing several rules:

(i) the interactions should only depend on the four vectorial quantities: $\Delta x_n = x_{n,i} - x_{n,j}$, $\Delta x_p = x_{p,i} - x_{p,j}$, P, $\Delta P = P_i - P_j$
(ii) the interaction terms should only be linear in the four vectorial quantities
(iii) the interactions should decay exponentially on a length scale r to prevent interactions between separated cells

Following these imposed rules leads to five cell-cell interaction terms that depend

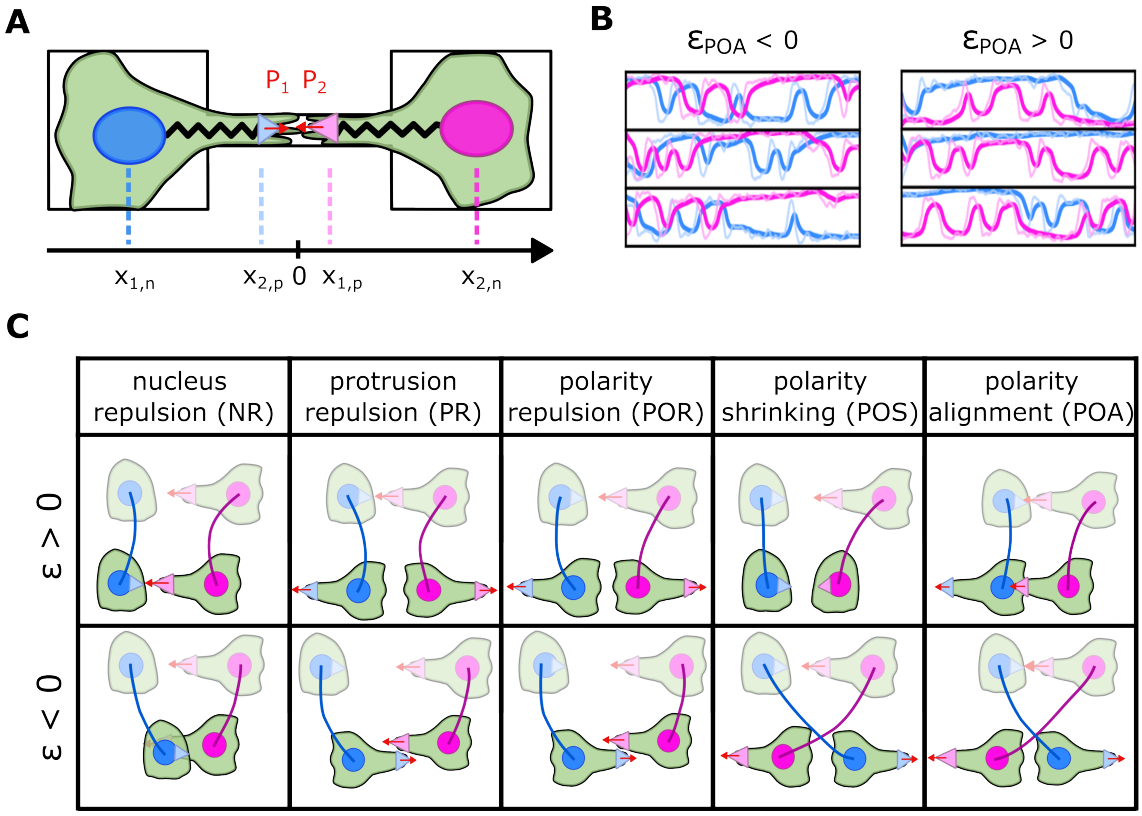

Figure 5.5: Microscopic model reveals candidate cell-cell interactions. A) Schematic of the mechanistic model. The cell nucleus is connected to the protrusion by a spring. The protrusion of the cell is driven by actin polymerisation described as an active pushing force P. B) Exemplary trajectories simulated for polarity alignment interactions with varying interaction strength ϵ_{POA}. C) Schematic of the five candidate cell-cell interactions for positive and negative interaction strength. Figure adapted from [P2].

on the interaction strength ϵ (Fig. 5.5C):
Two of those interactions model excluded volume interactions between the cell nuclei (i) termed nucleus repulsion

$$G_n(\Delta x_n) = \epsilon_{NR} e^{-|\Delta x_n|/r_n} \Delta x_n \tag{5.11}$$

and between the cell protrusions (ii) termed protrusion repulsion

$$G_p(\Delta x_p) = \epsilon_{PR} e^{-|\Delta x_p|/r_p} \Delta x_p. \tag{5.12}$$

The remaining three cell-cell interactions include various polarity interaction mechanisms: (iii) polarity repulsion

$$G_P(\Delta x_p) = \epsilon_{POR} e^{-|\Delta x_p|/r_p} \Delta x_p \tag{5.13}$$

captures how the polarity growth rate is influenced by the distance between cell protrusions and their orientation relative to each other. For positive ϵ_{POR} this

interaction is similar to mechanisms associated with CIL.
(iv) Polarity shrinking or growing (depending on the sign ϵ_{POS}) of

$$G_P(\Delta x_p, P) = \epsilon_{POS} e^{-|\Delta x_p|/r_p} P \tag{5.14}$$

models the decrease or increase in polarity based on the relative separation between cells, regardless of their orientations.
Lastly, (v) polarity alignment

$$G_P(\Delta x_p, \Delta P) = \epsilon_{POA} e^{-|\Delta x_p|/r_p} \Delta P \tag{5.15}$$

models the alignment of the cell's polarisation for $\epsilon_{POA} > 0$ dependent on the relative separation between the protrusions and anti-alignment for $\epsilon_{POA} < 0$. A schematic drawing of the five candidate cell-cell interactions for positive and negative interaction strength can be found in Fig. 5.5C.

As a next step, we test which of the five proposed cell-cell interactions can capture the experimentally observed cell dynamics of the distinct cell lines. Therefore, we simulate trajectories for each interaction (Fig. 5.5B) and predict the nucleus dynamics, the cross correlation functions for velocity and position and the behaviour distribution for each cell line. By varying the interaction strength ϵ, we can predict a mapping from our mechanistic model parameters to the inferred underdamped cohesion and friction parameters f_0 and γ_0. In Fig. 5.6A the five different interaction terms are mapped onto our IBS (dashed curves).
The nucleus repulsion interaction primarily predicts cohesion interactions and can only capture the behaviour observed in HT1080 cells. Polarity repulsion and protrusion repulsion interactions predict effective friction interactions and attraction, corresponding to the lower-left region of the IBS, as well as repulsion and small effective anti-friction interactions. Those two mechanism are able to capture the cell-cell interaction behaviour of HT1080 and MDAMB436 cells, but fail to capture the other three cell lines. Similar to nucleus repulsion, polarity shrinking primarily predicts cohesion interactions, but also predicts repulsion accompanied by effective friction interactions, capable of capturing the behaviour of MCF10A and A549 cells. The only mechanism capable to qualitatively capture the cell-cell interaction behaviour observed in every tested cell line is polarity alignment (dashed blue curve in Fig. 5.6A). For negative interaction strengths, the nucleus exhibits anti-friction combined with attraction, as seen in MDAMB231 and MDAMB436 cells, while positive values entail friction and repulsion between cell nuclei, as seen in MCF10A and A549 cells. However, this mechanism fails to accurately predict the mutual exclusion behaviour observed in all five cell lines.

To achieve a quantitative fit with polarity alignment interactions to the dynamics of all cell lines, we propose combinations of polarity alignment with the four remaining cell-cell interactions. For simplicity reasons, only pairwise combinations are considered, yielding four additional different candidate cell-cell interaction mechanisms summarised in table 5.1. Interestingly, upon plotting the model prediction for each of the four combinations that best fit f_0 and γ_0 in the IBS, it appears that all of the combinations are capable of fitting the dynamics of the

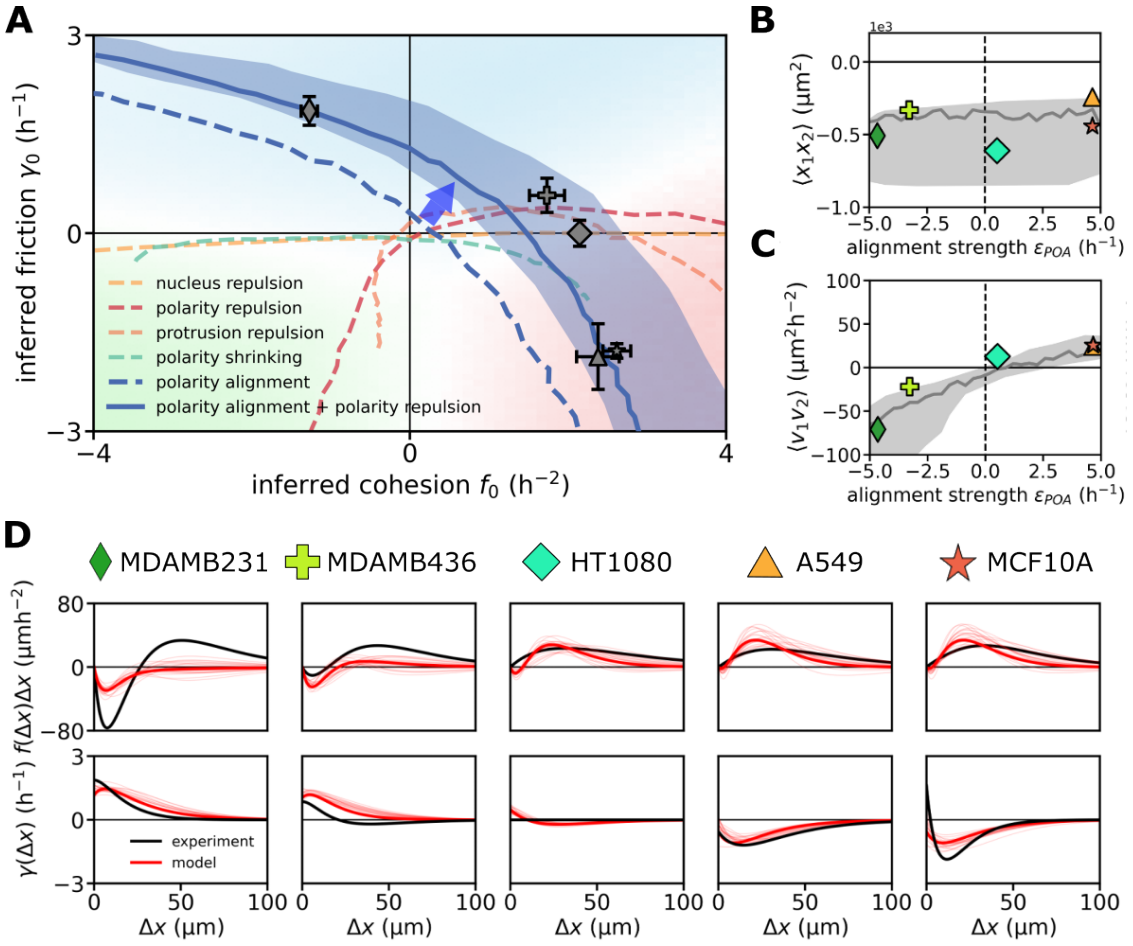

Figure 5.6: Model prediction of the five candidate cell-cell interactions. A) Interaction behaviour space with the model prediction of the five candidate cell-cell interactions (dashed curve). Solid blue curve shows the model prediction for the combination of polarity alignment + polarity repulsion. Blue area indicates the confidence interval of the parameters r_p and ϵ_{NR}. B) Instantaneous position correlation for experimental (symbols) and model (solid line) results. C) Instantaneous velocity correlation for experimental (symbols) and model (solid line) results. Experimental results are fitted at the best fitting polarity alignment strength. D) Inferred underdamped cohesion and friction interactions for experiment (black) and model (red) in all cell lines. Model result is obtained from simulating the best fitting candidate cell-cell interaction POA+POR. Thin red lines indicate model results for 20 best fitting parameter combinations. Error bars indicate the standard error of the mean (s.e.m) obtained from bootstrapping the experimental data. Figure adapted from [P2].

various cell types. Specifically, the combination of polarity-alignment with one of the repulsion mechanisms leads to a shift of the mapping $(f_0(\epsilon_{POA}), \gamma_0(\epsilon_{POA}))$, which is indicated with the blue arrow in Fig. 5.6 A. In the fitting process, only the polarity alignment strength ϵ_{POA} is adjusted, while the interaction strengths of the repulsion mechanism remains constant. This indicates that there is no

candidate interaction	**equation**
nucleus repulsion (NR)	$G_n = \epsilon_{NR} e^{-\lvert\Delta x_n\rvert/r_n} \Delta x_n$
protrusion repulsion (PR)	$G_p = \epsilon_{PR} e^{-\lvert\Delta x_p\rvert/r_p} \Delta x_p$
polarity repulsion (POR)	$G_P = \epsilon_{POR} e^{-\lvert\Delta x_p\rvert/r_p} \Delta x_p$
polarity shrinking (POS)	$G_P = \epsilon_{POS} e^{-\lvert\Delta x_p\rvert/r_p} P$
polarity alignment (POA)	$G_P = \epsilon_{POA} e^{-\lvert\Delta x_p\rvert/r_p} \Delta P$
pol. alignment + nucleus repulsion	$G_P = \epsilon_{POA} e^{-\lvert\Delta x_p\rvert/r_1} \Delta P +$ $G_N = \epsilon_{NR} e^{-\lvert\Delta x_n\rvert/r_2} \Delta x_n$
pol. alignment + polarity shrinking	$G_P = \epsilon_{POA} e^{-\lvert\Delta x_p\rvert/r_1} \Delta P + \epsilon_{POS} e^{-\lvert\Delta x_p\rvert/r_2} P$
pol. alignment + protrusion repulsion	$G_P = \epsilon_{POA} e^{-\lvert\Delta x_p\rvert/r_1} \Delta P +$ $G_P = \epsilon_{PR} e^{-\lvert\Delta x_p\rvert/r_2} \Delta x_p$
pol. alignment + polarity repulsion	$G_P = \epsilon_{POA} e^{-\lvert\Delta x_p\rvert/r_1} \Delta P + \epsilon_{POR} e^{-\lvert\Delta x_p\rvert/r_2} \Delta x_p$

Table 5.1: Summary of the nine different candidate cell-cell interactions. Adapted from [P2]

singular mechanism that comprehensively captures the observed cell-cell interaction behaviour in our cell lines and that polarity alignment interactions coupled with any of the repulsion mechanisms can accurately capture the diversity in cell-cell interaction behaviour. This is also reflected in the interaction statistics, where the combination of polarity alignment with a repulsion mechanism provides a good fit to the experimental behaviour statistics in all cell types (Fig. 5.6B-C). Furthermore, the quantitative fit of the underdamped interactions of all cell types is in good agreement with the experimental observed data (Fig. 5.6C).

5.3 Discussion

In this chapter, we analysed the coupled two-cell behaviour of various distinct cell lines in a dumbbell shaped micropattern. Our aim was to uncover shared mechanisms governing cell-cell interactions, offering deeper insights into the interaction

behaviour of cells on larger scales, such as collective processes. Based on our observations of the single cell migration dynamics, we sought to elucidate potential correlations between cell phenotype and their cell-cell interaction dynamics.
To this end, we analysed the stochastic two-cell dynamics by employing a recently introduced theoretical framework ([25]) and found repulsion and friction interaction in the two epithelial cell lines, contrasting with an attraction and anti-friction dynamic seen in the mesenchymal breast cancer cell lines. Notably, the mesenchymal fibrosarcoma cell line HT1080 displayed a unique behaviour, showing no detectable friction interactions, while exhibiting strong repulsion interaction similar to epithelial cells. This could be attributed to the high expression level of N-Cadherin in HT1080 cells, which has been associated with reversal behaviour and CIL [186–188]. For instance, Scarpa *et al.* demonstrated that neural crest cells acquire CIL through an E- to N-cadherin switch during EMT [188]. However, MDAMB436 cells displayed a preference for sliding behaviour upon contact regardless of their N-Cadherin expression, suggesting the involvement of other mechanisms in guiding their interaction behaviour. These findings indicate that the behaviour of cell-cell interactions exceeds a simple classification into epithelial or mesenchymal phenotypes. Instead, it is likely to be more strongly influenced by complex molecular pathways, including interactions with surface proteins and signalling to the cytoskeleton.

To address this complexity and uncover the underlying mechanisms that determine the cell-cell interaction behaviour, we proposed several candidate cell-cell interactions. This approach was developed to accurately capture the different dynamics observed during cell collisions. Our findings pointed towards alignment interactions between the cell's polarisation machinery as a promising candidate for quantitatively describing the behaviour of different cell types. We achieved this match between theory and experiment by only tuning the strength and sign of polarity alignment. Here, we captured the entire spectrum of polarity alignment interactions. MCF10A and A549 cells demonstrated strong polarity alignment interactions, HT1080 cells exhibited almost no polarity alignment interactions, and MDAMB231 and MDAMB436 cells displayed polarity anti-alignment interactions. Remarkably, we did not need to include information about molecular markers or biochemical signalling pathways as found in several other biophysical models to quantitatively capture the behaviour [34,124,189]. Combined, this suggests that while the specifics of interaction pathways vary among different cells, they influence the interaction strength rather than the fundamental interaction mechanism. This will be challenged in the next chapter by inducing molecular perturbations.

Previous investigations into cell-cell interactions have primarily emphasised repulsive behaviour such as CIL [34, 189–191]. For instance, studies conducted in fibrillar-like environments have shown that CIL-like repulsion results in contact-initiated reversal, while cells that maintain their migration direction exhibit a sliding response [35]. Moreover, many different biophysical models have successfully incorporated repulsive interactions to accurately describe collision behaviour across diverse cell types [124, 190, 192, 193]. In our experimental setup, we introduced CIL-like repulsion interactions to quantitatively capture the dynamics of distinct cell lines,

promoting reversal behaviour and mutual exclusion between cells. However, these interactions alone were insufficient to predict the observed correlation between cell velocities and the sliding behaviour predominantly seen in the invasive breast cancer cell lines. To address this, we introduced polarity (anti-) alignment interactions, which not only created (anti-) correlations between cell velocities, but also promoted sliding behaviour, providing an accurate description of cell dynamics.
Polarity interactions have been found in a variety of complex processes [109,194,195]. In large-scale moving structures, the collective motion of epithelial cells is described by velocity and polarity alignment between cells. This multicellular polarity organisation is essential for the collective migration of cell clusters [194]. Similar, the alignment of cellular polarisation among neighbouring cells promotes a highly coordinated multicellular flow [195]. This alignment of cellular polarities enables efficient communication and coordination between cells during migration and other collective behaviours. Our findings underscore the importance of considering direct interactions between cellular polarities to effectively describe collision behaviour across a diverse range of cell types.

6. Unraveling the Molecular Dynamics of Cell-Cell Interactions

Cell-cell interactions are intricately governed by molecular pathways and the coupling of surface proteins, facilitating signal transduction between neighbouring cells [81,196]. Specifically, cell adhesion and recognition play a pivotal role in cell response upon contact [197]. Interestingly, the cell-cell interaction dynamics observed in the five phenotypically distinct cell lines investigated in this thesis appear to be regulated by a combination of friction and cohesion interactions, reflecting their diverse molecular compositions and signalling pathways upon cell-cell contact. However, the specific molecular pathways through which proteins modulate these interactions remain poorly understood. Moreover, our mechanistic model introduced in Chapter 5 demonstrates that polarity interactions can accurately capture and predict cell-cell interaction dynamics without explicitly accounting for specific signalling pathway or protein interactions. It seems to be sufficient to only vary the interaction strength of the polarity alignment to capture the behaviour of the five different cell lines. This indicates that polarity alignment is an underlying mechanism governing the cell-cell interaction behaviour. However, how molecular markers influence the interaction strength and the dynamics of the cells remains elusive. Consequently, the robustness of the model against perturbations inducing different cellular responses needs to be investigated. Furthermore, the region depicting friction and attractive interactions, where following interactions would dominate, appears vacant in the IBS illustrated in Fig. 5.6. This region is also not captured by our mechanistic model. It is intriguing to investigate whether specific perturbations can shift the cell-cell interaction behaviour into that unoccupied region.

To address the challenges discussed, we employ molecular perturbations to specifically disrupt several cell-cell interaction pathways, aiming to elucidate the influence of targeted proteins on cell-cell dynamics, particularly with respect to the effective friction and cohesion interactions of the nucleus. Furthermore, we assess whether our mechanistic model can accurately capture the manipulated behaviour of the cells in response to these perturbations.

6.1 Contact-Mediated Adhesion Impacts Polarity Alignment

The calcium-dependent transmembrane protein E-Cadherin is involved in intercellular interactions, mainly in the formation and maintenance of adherens junctions. Upon cell-cell contact, E-Cadherin proteins form homotypic dimers between neighboring cells, facilitating both signal and force transduction across cell membranes [31, 186]. E-Cadherin is essential in maintaining the epithelial phenotype and its loss is associated with EMT [164]. In cancer cells, E-Cadherin is often downregulated, which results in decreased adhesive properties and metastatic dissemination [82, 83, 164].
In our experiments, we observed that only the E-Cadherin expressing cell lines (MCF10A, A549) show strong repulsive interactions combined with effective friction between cell nuclei. Furthermore, the mechanistic model revealed pronounced polarity alignment between those cell lines. This raises the question what role E-Cadherin has in establishing repulsive forces between cells and its broader involvement in shaping cell-cell interaction dynamics, especially its influence on the polarity alignment strength.
While MCF10A cells express high levels of E-Cadherin, MDAMB231 cells do not express E-Cadherin and additionally show strong polarity anti-alignment (table 4.1). Given that both cell lines originate from breast tissue, they serve as ideal model systems for conducting perturbation experiments to further uncover the influence of E-Cadherin on cell-cell interactions. Although MCF10A cells are known to establish stable adherens junctions mediated by E-Cadherin in monolayers (Fig. 4.5B), it is important to note that this does not necessarily imply the formation of such bonds on shorter timescales when cells are confined in the dumbbell. However, an immunostaining analysis conducted on the MCF10A cells within the dumbbells revealed clustering of E-Cadherin at sites of cell contact (Fig. 6.1A).

To inhibit the function of E-Cadherin, we utilise an E-Cadherin blocking antibody, which is added to the cells. This antibody binds specifically to the extracellular binding domain of the protein, effectively inhibiting the formation of E-Cadherin dimers. Following this treatment, the behaviour of the E-Cadherin blocked MCF10A cells shifts towards more sliding and less reversal interactions (Fig. 6.2A). Moreover, they lose the positive velocity correlation previously observed in the untreated cells. The analysis of the inferred dynamics of cell-cell interactions reveals a reduction in repulsion interactions at intermediate intercellular nucleus distances, along with weaker friction interactions and slightly non-zero anti-friction at very short nucleus distances (Fig. 6.2B). In the IBS, the E-Cadherin blocked MCF10A cells are shifted diagonally towards the origin (square in Fig. 6.2D).
Furthermore, the mechanistic model reveals a reduction of polarity alignment interactions with an interaction strength ϵ_{POA} close to zero (square in Fig. 6.2C). This suggests that while E-Cadherin is essential for establishing the repulsive response observed in alignment interactions among MCF10A cells, its absence alone is insufficient to induce anti-alignment between the cells.

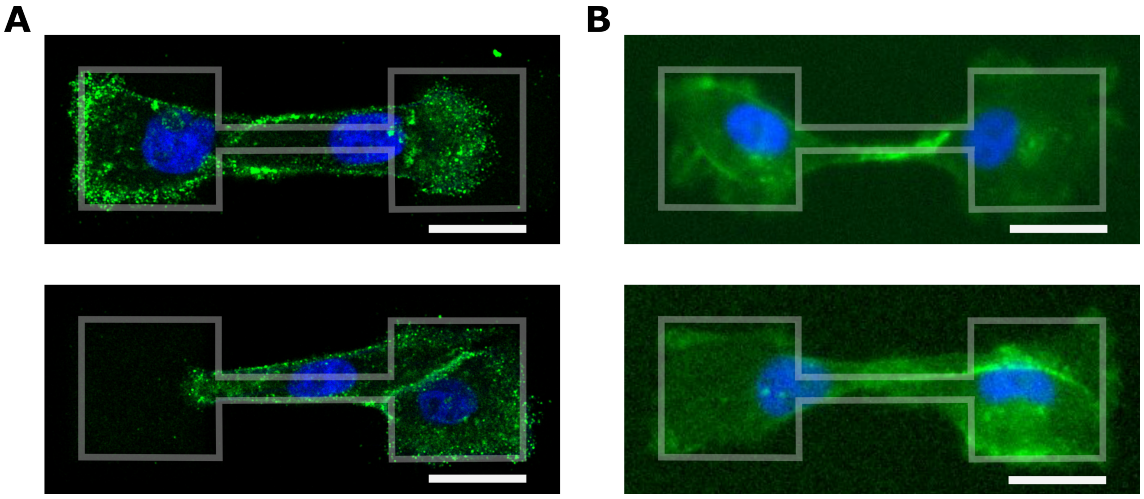

Figure 6.1: E-Cadherin expression on two interacting cells. A) Immunostaining of E-Cadherin (green) in MCF10A cells on the micropattern. At the cell contact area a clustering of E-Cadherin is visible. B) Fluorescence image of MDAMB231 cells transfected with E-Cadherin mRNA. E-Cadherin expression is tagged with GFP and visible in green. Scale bar is 25 μm and the nuclei are stained in blue.

However, the precise mechanism by which E-Cadherin regulates polarity alignment interactions remains unclear. E-Cadherin is known to facilitate mechanotransduction processes such as stress-polarity coupling, which have been observed in epithelial collective cell migration [198–200]. Alternatively, E-Cadherin bonds are implicated in numerous signalling pathways [201–203]. Of particular interest are the downstream signalling pathways to the cytoskeleton involving various small Rho GTPases, including Cdc42, RhoA, and Rac1, which can profoundly influence cell-cell interaction behaviour [60, 88].

To shed light on this, we introduce a E-Cadherin knockout MCF10A cell line, referred to as MCF10A KO. This cell line has a zinc finger (ZNF) modulation resulting in the deletion of four base pairs on exon 11 of the gene, effectively inhibiting the function of the protein. Immunostaining for E-Cadherin revealed that part of the protein is still expressed on the surface. However, the frameshift mutation is induced in exon 11, resulting in a truncated form of E-Cadherin, in which only the extracellular domain and part of the transmembrane domain are present.
As a result, the MCF10A KO cells are still able to form E-Cadherin bonds upon cell contact, but they lack downstream signalling due to the absence of the intracellular tail of the protein.
Consistently, the behaviour of the MCF10A KO cells changes similarly to the E-Cadherin blocked MCF10A cells. An increase in sliding behaviour is observed, although less pronounced compared to the antibody blocking (Fig. 6.2A). The inferred dynamics show weak attraction at short distances, weaker friction interactions at intermediate distances and strong anti-friction at very short nucleus distances (Fig. 6.2B). The positive velocity correlation is lost and a small negative correlation is observed (pentagon in Fig. 6.2C). Furthermore, in agreement with the E-cadherin

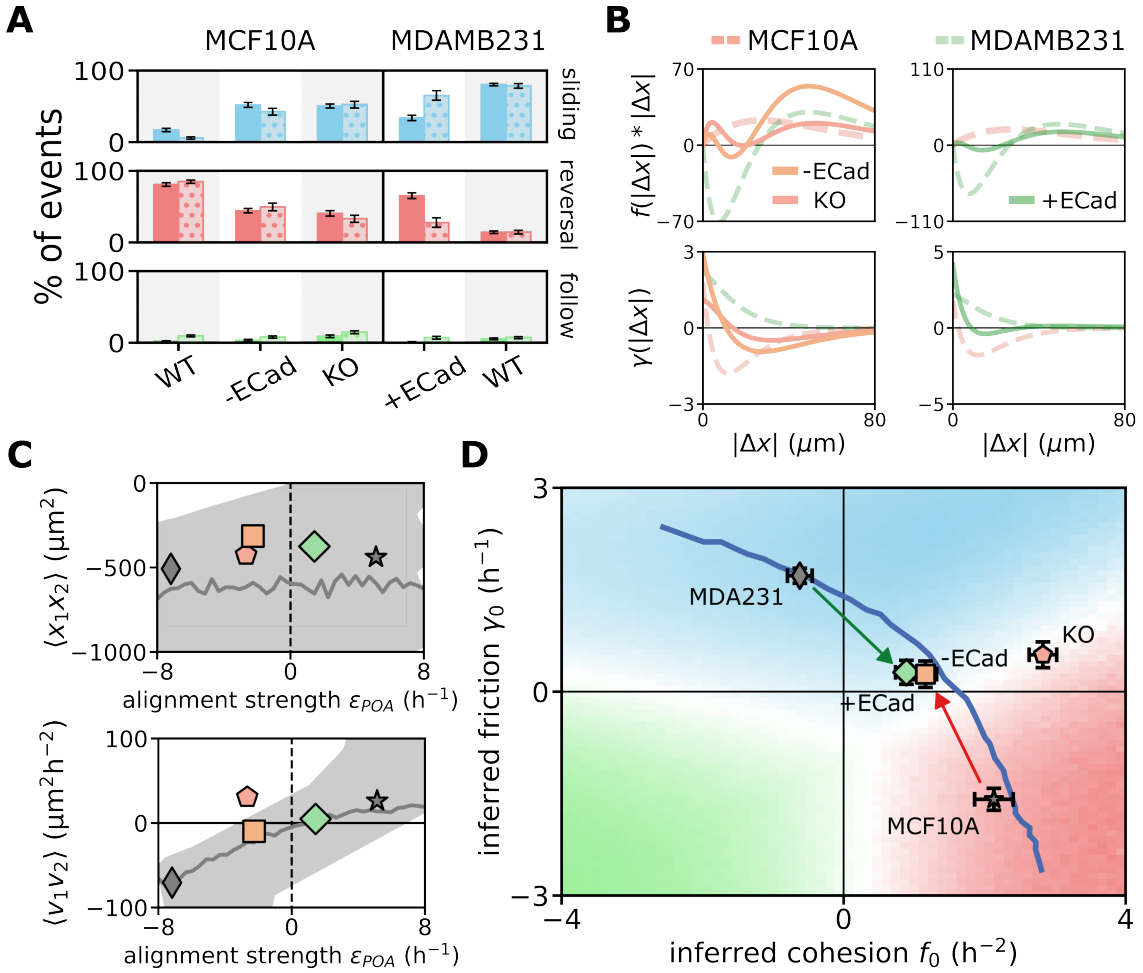

Figure 6.2: A) Behaviour distribution of manipulated MCF10A cells (left) and MDAMB231 cells (right) showing percentages of the observed three different collision events. Solid bars show experimental results, dotted bars show the prediction of the inferred underdamped description. Error bars show the standard error of the mean (s.e.m) obtained from bootstrapping. B) Inferred effective cohesion interactions $f(|\Delta x|)\Delta x$ and inferred effective friction interactions $\gamma(|\Delta x|)\Delta v$ of manipulated MCF10A cell and MDAMB231 cells. C) Instantaneous position (top) and velocity (bottom) cross-correlation between two cells, when they occupy the same island. Symbols show experimental results, solid line indicates our model result obtained from a global fit of the mechanistic model. D) IBS shows the change of the dynamics of the MCF10A and MDAMB231 cell lines due to various molecular perturbations. Solid blue line indicates the model result for the best fitting inferred underdamped cohesion and friction coefficients.

blocking, the mechanistic model shows a reduction of polarity alignment interactions with an interaction strength ϵ_{POA} close to zero (pentagon in Fig. 6.2C-D).
Although E-cadherin blocking and E-Cadherin KO results in qualitatively similar cell-cell interactions, it is important to stretch the differences of the two approaches here. While blocking E-Cadherin with antibodies effectively inhibits all interac-

tions, including mechanical coupling between E-Cadherins, the MCF10A KO cells still possess truncated E-Cadherins capable of mechanical coupling between cells. Despite this, we observe similar effects with both perturbations, suggesting that the influence of E-Cadherin on cell-cell interactions is primarily mediated through signalling pathways. However, further experiments have to be conducted to strengthen this claim.

To further analyse the influence of E-Cadherin on cell-cell interaction dynamics, we transiently transfect the E-Cadherin deficient cell line MDAMB231 with E-Cadherin-mRNA (MDAMB231-ECad). The cells express E-Cadherin during the duration of the experiment as confirmed by the presence of the GFP-tag encoded in the E-Cadherin-mRNA. Similar to the endogenous E-Cadherin expression in MCF10A cells, a clustering of the protein is now observed at cell contact sites (Fig. 6.1B). Consequently, the dynamics of the MDAMB231-ECad cells changes towards fewer sliding events and more reversal events (Fig. 6.2A). Notably, the cells lose their negative velocity correlation and now exhibit a small positive correlation (rhombus in Fig. 6.2C). The inferred dynamics of the cell-cell interactions show a reduction of attractive interaction at short distances, with the cohesion term approaching zero (Fig. 6.2B). While the wildtype MDAMB231 exhibit anti-friction, the MDAMB231-ECad cells now display small friction interactions (Fig. 6.2B - right panel). The location of the MDAMB231-ECad cells now coincides with the E-Cadherin blocked MCF10A cells (rhombus in Fig. 6.2D). Additionally, the presence of E-Cadherin alters the polarity interactions in MDAMB231 cells, with the polarity anti-alignment reduced to almost no detectable polarity interactions (rhombus in Fig. 6.2C).

Overall, these results highlight the significance of E-Cadherin in regulating cell-cell interaction dynamics and provide insights into its role in mediating repulsive responses, as well as in influencing friction and cohesion interactions. Moreover, the presence of E-Cadherin seems to contribute towards the establishment of polarity alignment interactions as observed in MCF10A cells, while it inhibits the polarity anti-alignment in MDAMB231 cells. However, despite the manipulation of E-Cadherin expression in both MCF10A and MDAMB231 cells resulting in observable shifts in cell behaviour, neither the loss nor gain of E-Cadherin was sufficient to invert polarity alignment to anti-alignment, or vice versa.

6.2 EMT Insufficient for Polarity Alignment Switch

To explore whether polarity interactions can effectively capture the behavioural changes associated with EMT, we treat MCF10A cells with TGFβ to induce the transition. Upon induction of EMT, the cells increase their sliding behaviour accompanied by a decrease in reversal events (Fig. 6.3A). The cells show weak positive velocity correlation close to zero and the inferred interactions reveal a reduced repulsive response approaching zero and weak friction interaction between the cells (Fig. 6.3B). The position of TGFβ treated MCF10A cells in the interaction behaviour

space is shifted diagonally towards the center (pentagon in Fig. 6.3D). The dynam-

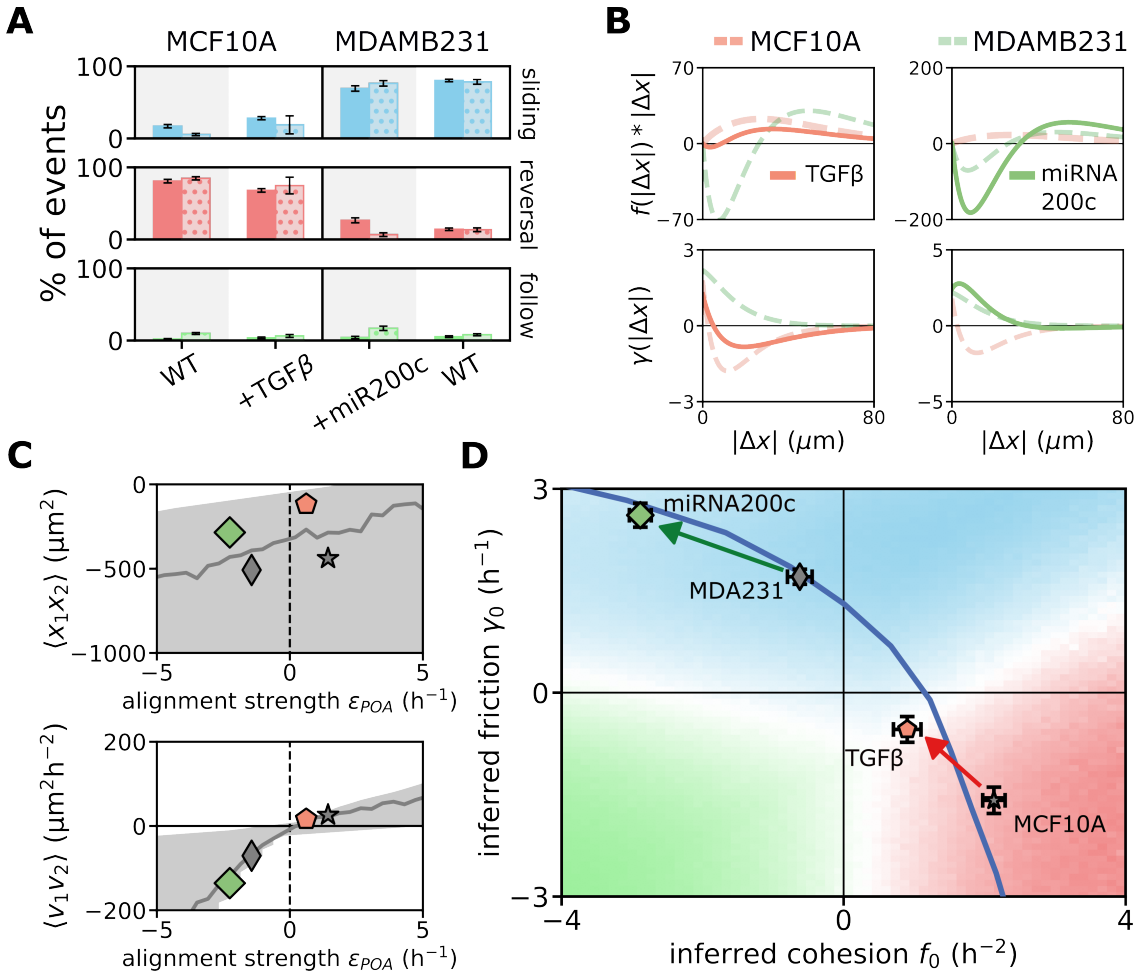

Figure 6.3: A) Behaviour distribution of the manipulated MCF10A cells and MDAMB231 cells showing percentages of the observed three different collision events. Solid bars show experimental results, dotted bars show the prediction of the inferred underdamped description. Error bars show the standard error of the mean (s.e.m) obtained from bootstrapping. B) Inferred effective cohesion interactions $f(|\Delta x|)\Delta x$ and inferred effective friction interactions $\gamma(|\Delta x|)\Delta v$ of the manipulated MCF10A cells and MDAMB231 cells. C) Instantaneous position (top) and velocity (bottom) cross-correlation between two cells, when they occupy the same island. Symbols show experimental results, solid line indicates our model result obtained from a global fit of the mechanistic model. D) IBS shows the change of the dynamics of the MCF10A and MDAMB231 cell lines due to various molecular perturbations. Solid blue line indicates the model result for the best fitting inferred underdamped cohesion and friction coefficients.

ics of the treated cells can be captured by weaker polarity interactions compared to the wildtype cells as indicated by a lower alignment interaction strength ϵ_{POA} (pentagon in Fig. 6.3C). The polarity alignment interactions between the treated cells are almost lost. Interestingly, initiating EMT in MCF10A cells has an overall

similar effect on collision behaviour and polarity interactions as blocking E-Cadherin in MCF10A.
This observation is striking, considering that the loss of E-Cadherin alone is insufficient to induce the mesenchymal phenotype, whereas TGFβ treatment triggers this transition effectively. The similar effects of E-Cadherin blocking and TGFβ treatment on cell behaviour and polarity interactions imply that the transition from epithelial to mesenchymal phenotypes does not necessarily entail a switch from strong alignment to strong anti-alignment interactions.

To further verify this finding, our objective was to induce mesenchymal-to-epithelial transition (MET) in MDAMB231 cells by expressing the miRNA200c using a previously described inducible construct. In single cells on the dumbbell pattern, this led to a change in the dynamics from limit cycle oscillations to a bistable hopping behaviour similar to the dynamics of MCF10A cells. As schematically de-

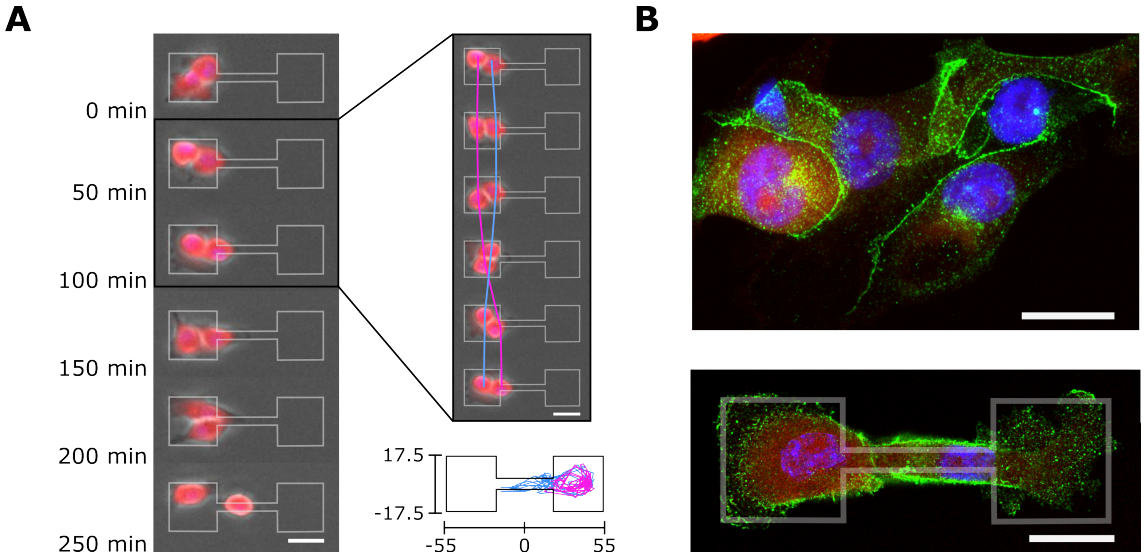

Figure 6.4: Rotational movement in MDAMB231 with miRNA200c. A) Time-lapse series of MDAMB231 cells with miRNA200c expression. Red staining indicates the RFP expression upon doxycycline induction. Inset shows the rotational movement of the two cells. One exemplary track are shown underneath. B) Immunostaining of E-Cadherin (green) in miRNA200c induced MDAMB231 cells *in vitro* (top) and on the micropattern (bottom). Scale bars are 25 μm and the nuclei are stained in blue.

picted in Fig. 2.4B, we expect the miRNA200c-MDAMB231 cells to re-express E-Cadherin, since the miRNA200c should inhibit ZEB1/2 leading to an upregulation in epithelial markers. An immunostaining on fixed miRNA200c-MDAMB231 cells reveals the presence of E-Cadherin on the cell surface (Fig. 6.4B). Intuitively, we expect a shift in the miRNA200c-MDAMB231 similar to the MDAMB231 cells transfected with the E-Cadherin mRNA. Surprisingly an opposite effect is observed. The miRNA200c-MDAMB231 cells increase their sliding behaviour compared to the control cells as quantified by the behaviour distribution (Fig. 6.3A). Furthermore,

the inferred interactions show a more pronounced attraction and anti-friction between the cell nuclei and polarity anti-alignment is still strong in these cells (rhombus in Fig. 6.6B-D). This finding appears contradictory to the results obtained from the MDAMB231-ECad cells, where the adhesion protein was identified as a mediator in establishing polarity alignment interactions. However, in the time-lapse movies and the corresponding trajectories a rotational motion of the two cells in one island is frequently observed (Fig. 6.4A). This rotational behaviour is hardly observed in the wildtype MDAMB231 cells or the control construct cells and might hint at a fourth interaction modus. The cells appear to build strong adhesion between each other, while maintaining their motility resulting in a 2D rotational movement in one island. With the tools at hand, it might be challenging to correctly analyse the cell-cell interaction behaviour of these cells. Additionally, the miRNA-200c is known to be involved in a complex network of signalling pathways by upregulating or downregulating several proteins, including E-Cadherin, Vimentin, Zeb1/2, and N-Cadherin. This adds to the challenge of disentangling the involvement of E-Cadherin in the observed change of dynamics. The effects of miRNA-200c induction on cell behaviour may involve multiple pathways and molecular interactions beyond the direct regulation of E-Cadherin expression.

6.3 Cell Recognition System Mediates Polarity Anti-Alignment

Another system implicated in establishing cell polarity is the Eph-ephrin receptor-ligand system, which is activated upon cell-cell contact [30]. These receptor-ligand interactions regulate cell polarity through downstream regulation of Rho GTPases and thus are crucial for the migratory machinery in cells during cell-cell contacts [92]. EphB receptors have been observed to stimulate Cdc42 expression, which may promote attractive migration [204]. In contrast, when ephrinA2 ligands interact with EphA2 and EphA4 receptors, activation of RhoA at sites of cell-cell adhesion is triggered. This in turn leads to a reduction in forward migration, which is primarily driven by actomyosin contraction regulated by Rho-GTPases [30]. Additionally, Astin *et al.* demonstrated that CIL is mediated through EphA-Rho-ROCK signalling, dependent on the Eph-receptor profile on the cell surface [81]. This places members of the Eph-ephrin family as prime targets to investigate their role in coupled two-cell behaviour.
Since there is no drug or inhibitor to target a large set of ephrin ligands or receptors, we chose to study the influence of the ephrinA2 ligand on cell-cell interactions in MCF10A cells. EphrinA2 is frequently overexpressed in cancer cells [96] and involved in tumorigenesis and invasiveness of breast cancer [97]. Moreover, it was found that ephrinA2 alters EMT-related markers to promote cancer metastasis [205] and up or downregulates several RhoGTPases, such as RhoA [30, 96].
To this end, we chose to inhibit ephrinA2 with specific antibodies in MCF10A cells. This ligand is broadly expressed over the whole surface of MCF10A cells as visualised in Fig. 6.5A. Upon blocking ephrinA2 with an antibody, the MCF10A cells lose their

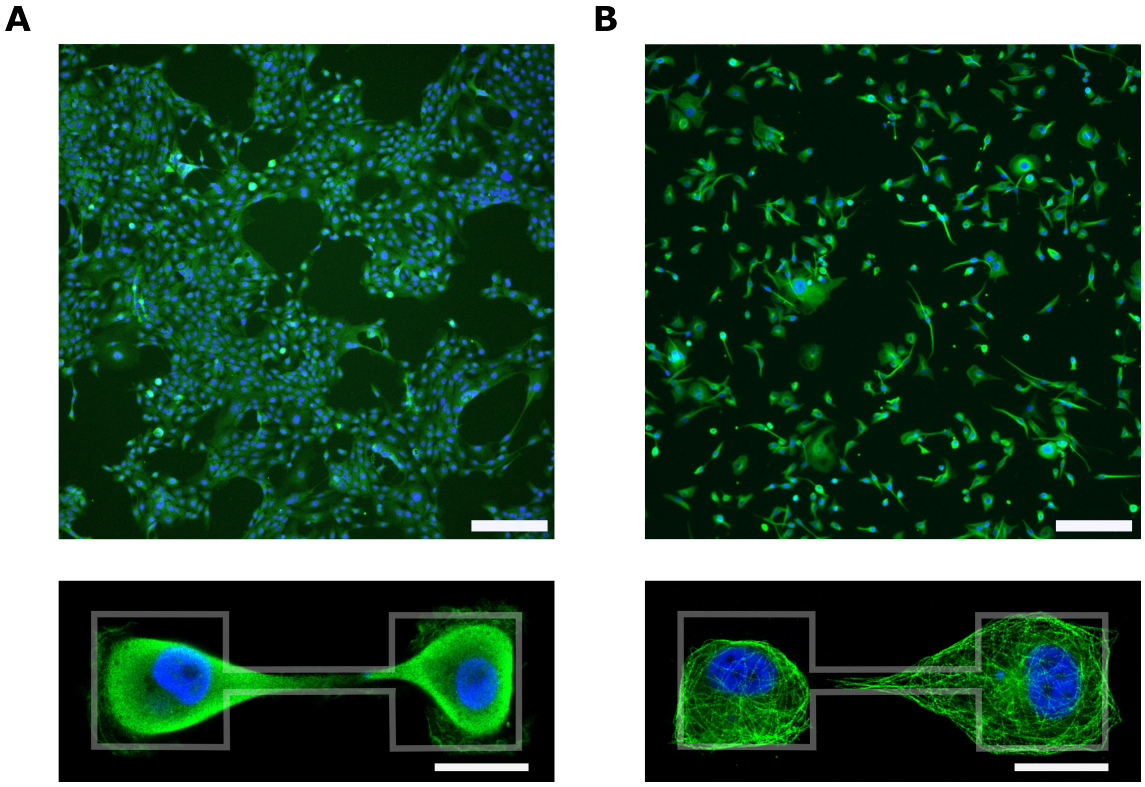

Figure 6.5: Ephrin ligand expression in confluence and confinement. A) Immunostaining of ephrinA2 (green) in MCF10A cells in vitro (top) and on the micropattern (bottom). B) Immunostaining of ephrinB2 (green) in MDAMB231 cells in vitro (top) and on the micropattern (bottom). The Scale bar is 200 μm (top) and 25 μm (bottom). The nuclei are stained in blue.

repulsive behaviour and start to slide past each other (Fig. 6.6A). Remarkably, the inferred interactions are now qualitatively similar to those of the MDAMB231 cells. The cells are well described by a combination of short-range attraction coupled with long-range repulsion and pronounced anti-friction interactions (Fig. 6.6B). Additionally, we observe a switch in velocity correlation from positive to negative and most importantly a switch from polarity alignment interactions to anti-alignment (circle in Fig. 6.6C-D). This indicates, that cells regulate their polarity machinery through Eph-ephrin mediated cell contacts.

To further verify this, we block the ligand ephrinB2 in MDAMB231 cells with an antibody that recognises the extracellular domain of the protein. EphrinB2 was found to be the driver in glioma invasion [204] and ligand-activated EphB receptors regulate several proteins involved in the polarisation machinery of the cells. Therefore, we expect a shift in the behaviour towards more repulsive interactions upon impairing the function of ephrinB2 in the MDAMB231 cells. The expression of the ligand in MDAMB231 cells with and without micropattern is visualised in Fig. 6.5B and an intricate network of the ephrinB2 ligand is observed at higher resolution.
Interestingly, the cell-cell interaction behaviour does not shift significantly upon

ephrinB2 blocking (Fig. 6.6A). A small decrease in sliding events is observed with a slightly lower anti-correlation of the velocity (rhombus in Fig. 6.6C). The inferred interactions are qualitatively similar to the untreated MDAMB231 cells with only a small decrease in anti-friction interaction on short distances (Fig. 6.6B). The ephrinB2-blocked MDAMB231 still exhibit polarity anti-alignment interactions indicated by a negative alignment strength ϵ_{POA} (rhombus in Fig. 6.6C).
However, when comparing these results with the control experiment involving unperturbed MDAMB231 cells under the same conditions, it becomes evident that the observed changes upon ephrinB2 blocking might be caused by biological noise. Both experiments yield quantitatively similar results, suggesting that the effects observed in the ephrinB2 blocking experiment may not be solely attributable to the perturbation. Instead they could be within the range of normal variability due to differences in e.g. cell age.
In summary, our findings indicate that blocking ephrinB2 does not significantly alter the cell-cell interaction behaviour of MDAMB231 cells. However, it is important to note that our approach of using antibodies to inhibit ephrinB2 function lacks a direct means of confirming the effective inhibition of ephrinB2. Thus, further investigations utilising knock-out or silencing techniques, such as siRNA, may offer additional insights into the role of ephrinB2 in mediating cell-cell interactions.

6.4 Collision Behaviour Is Influenced by the Polarisation Machinery

The perturbations on E-Cadherin and the ephrins showed a potential link of the Rho-GTPases guiding polarity involvement. Specifically the small Rho-GTPase RhoA was found to be activated downstream of EphA-ephrinA interactions to stimulate stress fiber formation leading to a loss of cell-cell contacts and consequently an increase in the invasive potential of the cells [206–209]. Additionally, RhoA and actomyosin contractility are activated upon cell-cell contacts through various signalling pathways often mediated through Cadherin bonds [60]. To test the impact of RhoA on guiding cell-cell interactions, we directly perturb the polarity machinery of the cells. We use the drug Y-27632, which is a selective inhibitor of the Rho-associated protein kinase (ROCK). ROCK is a key regulator of the actin cytoskeleton and cell contractility. By inhibiting its activity, Y-27632 disrupts downstream signalling pathways involved in actin cytoskeleton organisation, leading to reduced cell contractility. Furthermore, the inhibition of ROCK directly impairs the downstream signalling and activation of RhoA. The impact of the inhibitor is directly visible in the changed morphology of the cells and on the actin fibers as visualised in Fig. 6.7A through immunostaining. The treated MCF10A cells are unable to form long and stable actin fibers and no clear boarder is observed anymore as in the untreated cells (Fig. 5.2A).
Treatment with Y-27632 changes the behaviour of the cells from a repulsive behaviour, characterised by frequent reversal events, to a behaviour in which the cells attract each other on short distances and predominantly slide upon collisions (Fig.

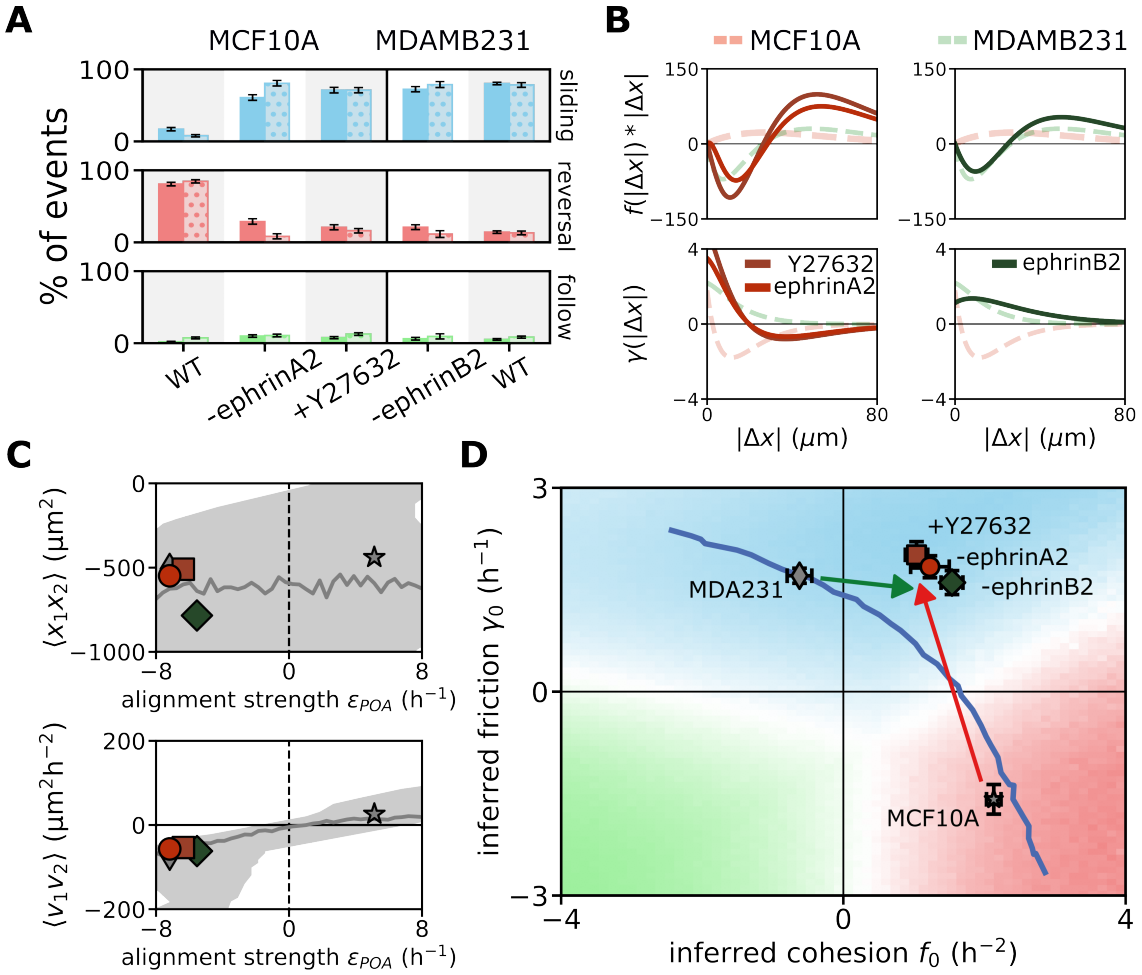

Figure 6.6: A) Behaviour distribution of the manipulated MCF10A cells and MDAMB231 cells showing percentages of the observed three different collision events. Solid bars show experimental results, dotted bars show the prediction of the inferred underdamped description. Error bars show the standard error of the mean (s.e.m) obtained from bootstrapping. B) Inferred effective cohesion interactions $f(|\Delta x|)\Delta x$ and inferred effective friction interactions $\gamma(|\Delta x|)\Delta v$ of the manipulated MCF10A cells and MDAMB231 cells. C) Instantaneous position (top) and velocity (bottom) cross-correlation between two cells, when they occupy the same island. Symbols show experimental results, solid line indicates our model result obtained from a global fit of the mechanistic model. D) IBS shows the change of the dynamics of the MCF10A and MDAMB231 cell lines due to various molecular perturbations. Solid blue line indicates the model result for the best fitting inferred underdamped cohesion and friction coefficients.

6.6A). Additionally, the ROCK-inhibited cells show pronounced anti-friction and the velocity correlation switches from positive to a negative correlation (square in Fig. 6.6B-C). Furthermore, ROCK inhibition is sufficient to shift the polarity alignment interactions in untreated MCF10A cells to anti-alignment interactions. The cell-cell interaction behaviour of the ROCK inhibited MCF10A cells now qualitatively re-

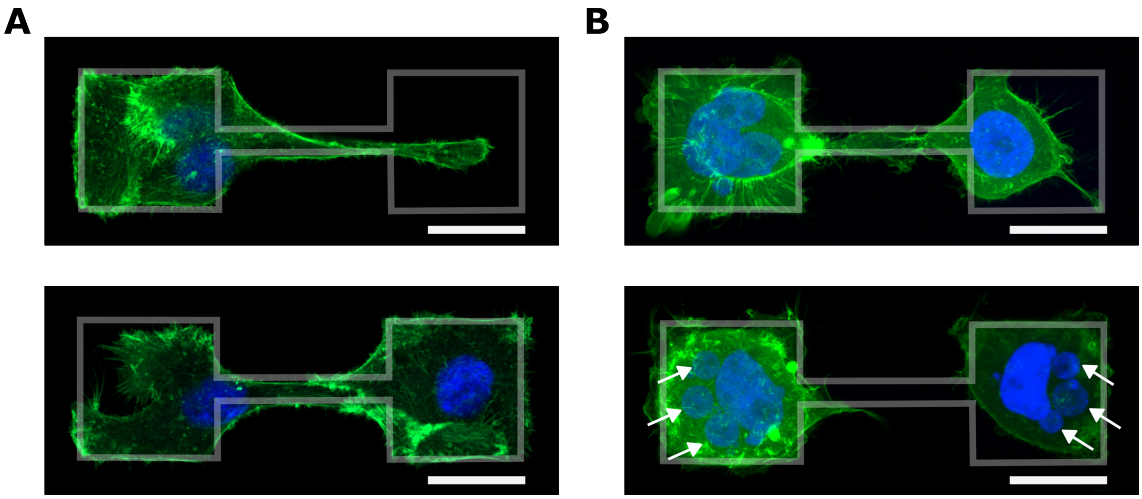

Figure 6.7: Disruption of actin fibers upon drug treatment. A) Immunostaining of F-actin fibers (green) in Y-27632 treated MCF10A cells in the micropattern. B) Confocal images of F-actin fibers (green) in nocodazol treated Life-Act MDAMB231 cells. White arrows indicate the blebbing of the nucleus after nocodazol treatment. Scale bar 25 μm. The nuclei are stained in blue.

sembles that of the MDAMB231 cells. However, their position in the IBS does not coincide with the MDAMB231 cells, as the attraction between the cell pair is not as pronounced, leading to the observed shift (square in Fig. 6.6D). Nevertheless, the interactions are still well described by polarity interactions. Interestingly, the cells with inhibited ROCK activity co-localise with the ephrinA2-blocked MCF10A cells on the IBS, suggesting similar effects induced by both perturbations. This might indicate, that the effect of ephrinA2-blocking stems from disrupting the polarisation machinery by downregulation of RhoA.

In addition to a functional Rho/ROCK signalling [10], the integrity of the microtubule cytoskeleton is essential for maintaining and regulating the polarity in various cell types [210]. Specifically, microtubule stabilisation is associated with strongly polarised cells and contributes to increased migratory persistence. This stabilisation process is regulated through Rho signalling via the Rho effector mDia1 and inhibition of the Rho–ROCK pathway causes a microtubule stabilisation and a corresponding failure of a polarity switch upon cell-cell collision [67, 68, 211, 212].
To investigate the role of microtubule stabilisation on cell-cell interactions and its influence on polarity alignment, we treat MDAMB231 cells with a low dose of the drug nocodazol to destabilise the microtubule network. Nocodazol binds to β-tubulin and disrupts the microtubule assembly/disassembly dynamics leading to its destabilisation. The F-actin network in nocodazol treated cells is shown in Fig. 6.7B.
Again, a change in the morphologies of the cells is observed and the ability to form long stable actin fibers is lost. Furthermore, blebbing at cell boundaries is observed and the actin fibers are short, disordered and often curved.
The nocodazole treatment not only disrupts microtubule stability but also seems to impair cell division. Observations from time-lapse movies reveal that cells attempt-

ing division experience difficulties in separating, resulting in the fragmentation of the nucleus into multiple pieces. The destabilised microtubules might not be able to form the mitotic spindle that is necessary to segregate chromosomes during cell division. Moreover, impaired formation of the cleavage furrow during cytokinesis may further contribute to the flawed separation of the cell into mother and daughter pairs. The fragmentation of the nucleus is often observed upon nocodazol treatment and is shown in Fig. 6.7B as indicated by the white arrows. The nocodazole-treated cells exhibit significant alterations in their cell-cell interactions.
Due to the criteria of only considering cells with intact nuclei, the statistical analysis of this perturbation is limited. However, it is evident that the treatment severely impedes cell mobility and movement, as observed in single cells on the micropattern. In contrast to untreated MDAMB231 cells, which frequently transition between islands, the treated cells only rarely undergo transitions. The destabilised microtubules render the cells nearly incapable of pulling or pushing themselves over the bridges. Consequently, this impedes the accurate analysis of cell pair interactions; if cells cannot transition due to cytoskeletal impairments, their interactions with neighbouring cells are also compromised. Therefore, we chose not to quantitatively analyse the interaction behaviour. Lower doses of nocodazol should be tried in order to avoid stalling the cells completely.

6.5 Discussion

In this chapter, we explored the impact of specific molecular pathways on cell-cell interactions, particularly focusing on cell adhesion and cell recognition pathways and their role in establishing polarity interactions. To achieve this, we introduced various molecular perturbations into our system, starting with the adhesion protein E-Cadherin, which is recognised as a tumor suppressor. Reduction in E-Cadherin expression levels is associated with the disruption of epithelial integrity, which facilitates the detachment of cancer cells from primary tumors and their subsequent invasion into surrounding tissues [213, 214]. In line with previous studies [35], our observations confirm that inhibiting E-Cadherin in MCF10A cells results in an increased sliding behaviour. This behaviour indicates at a disruption in cell-cell adhesion, which likely impedes the establishment of cell polarity.
Such changes of dynamics may result from compromised mechanotransduction pathways, particularly the stress-polarity coupling that depends on E-Cadherin [215]. It is well-established that classical cadherins not only enhance cell-cell cohesion and support the development of migratory polarity in epithelial sheets *in vitro* [88, 178], but also engage in mechanosensing. They respond to mechanical forces by undergoing strain stiffening [32, 216], which plays a crucial role in maintaining the balance of forces at cell-cell junctions. This balance is achieved as forces at the interface are counteracted by traction forces exerted in opposite directions [216, 217]. However, when cell-cell adhesion is compromised, there is a notable decrease in the alignment between local stress orientations and the directions of cellular motion [215].
In our experiments, MCF10A KO cells, although still capable of forming homotypic E-Cadherin dimers between cell pairs, exhibited impaired signal transduction to the

cytoskeleton. The response of these cells mirrors the dynamics observed in MCF10A cells with blocked E-Cadherin, where the ability to form E-Cadherin-mediated adhesions is lost. This suggests that E-Cadherin's signalling to the cell polarity machinery, potentially via polarity cues like RhoA, Rac1, or Cdc42, plays a critical role in how cells react upon encountering one another.
For instance, in MDCK cells, Rac1 and Cdc42 are activated through E-cadherin-mediated homophilic interactions [88, 89]. Moreover, Chen *et al.* discovered significant alterations in the cytoskeletal architecture in E-Cadherin deficient MCF10A cells. Unlike in wildtype MCF10A cells, where microtubules are typically organised in a radial pattern emanating from the centrosome, the microtubules in E-Cadherin-deficient cells display a disorganised arrangement. This observation is complemented by findings in MDCK cells, where interactions between adherens junctions and microtubules indicate a potential mechanistic link between epithelial cohesion and polarity [88, 218].
Taken together, this suggests that E-cadherin not only mediates adhesion between cells, but also plays a role in controlling polarity alignment by signaling to the cytoskeleton and possibly through mediating microtubule dynamics.
Additionally, the transfection of E-Cadherin in MDAMB231 cells, which typically lack this adhesion protein, resulted in predominantly repulsive responses upon cell-cell contact and diminished polarity anti-alignment interactions, characterised by a small positive alignment strength ϵ_{POA}.
It was shown that induction of E-Cadherin in MDAMB231 cells leads to a transcriptional modification of over 100 genes including a 2-fold upregulation of Cdc42 and a downregulation of ARHGDIB, which encodes for a regulator of actin cytoskeleton [219]. However, multiple studies indicated that re-expressing E-Cadherin in MDAMB231 cells does not fully revert their mesenchymal traits [219, 220].

Expanding on these findings, we further explored the effects of EMT in MCF10A cells and attempted to induce MET in MDAMB231 cells by modulating miRNA-200c expression levels. In TGFβ treated MCF10A cells, we observed a similar change in dynamics as in E-Cadherin blocked cells. Moreover, we did not observe a shift from polarity alignment to anti-alignment interactions. This may be attributable to the persistently high levels of E-Cadherin in the TGFβ-treated MCF10A cells, as confirmed by western blot analysis. This indicates that the treated cells did not fully adopt a mesenchymal phenotype, but are in an intermediate state.
During the process of EMT, cells undergo several stages of cytoskeletal network remodelling in order to achieve the intracellular reorganisation required for cell state reprogramming [103]. Thus, the several hybrid states can confer distinct functional properties that may influence cellular behaviour in unique ways, potentially affecting cell migration. However, in order to determine the state of transition in our treated cells, further experiments are necessary to assess additional EMT markers such as SNAIL, ZEB1/2, and Twist.

The miRNA200c is a key regulator of these EMT markers and can promote MET by decreasing the expression of ZEB1/2 through direct binding, which subsequently

results in the increased expression of E-cadherin [138, 171]. In MDAMB231 cells, where miRNA-200c expression is naturally inhibited, it was reintroduced in our experiments to study its impact on cell-cell interactions. Remarkably, the cells still exhibited strong polarity anti-alignment interactions despite the presence of E-Cadherin. Although the behaviour and dynamical statistics of the modified cells closely resemble those of the wildtype MDAMB231 cells, we observed a rotational movement of the two cells on one of the islands.
Those spontaneous rotational movements have been observed in many physiological contexts, as well as in epithelial cells, such as the MDCK cell line [200, 221, 222]. Interestingly, Lu *et al.* reported that during such rotational interactions, the polarity vectors of the two cells pointed in opposite directions [222]. This is consistent with our observation of strong polarity anti-alignment interactions in the rotating MDAMB231 cells after reintroduction of miRNA200c. Furthermore, their study indicated significant myosin accumulation at the cell-cell interface, suggesting that the rotation is driven by myosin-generated gradients of active tension, which are influenced by the interacting polarity axes of the cells [222].
Given these insights, it would be highly beneficial to compare the distribution of myosin during cell-cell interactions in wildtype MDAMB231 cells, which do not exhibit this rotational behaviour, to that in the miRNA200c-modified MDAMB231 cells.

Another system implicated in the regulation of cell-cell interaction behaviour, such as CIL, is the vast network of Ephrin receptors and ligands (Eph-ephrin system) [30, 81, 92]. Astin *et al.* demonstrated that CIL is mediated through EphA-Rho-ROCK signalling, depending on the Eph-receptor profile on the cell surface [81]. To this end, we investigated the effects of blocking the ligand ephrinA2 in MCF10A cells, observing a notable reduction in the repulsive response and a switch from polarity alignment to anti-alignment interactions.
A similar result is achieved by treating MCF10A cells with the ROCK inhibitor Y-27632, which directly disrupt the downstream signalling pathway involved in actin cytoskeleton organisation leading to reduced cell contractility. These changes are consistent with observations in various cellular models where ROCK inhibition led to altered cell-cell interaction behaviours.
In neural crest cells, for instance, this inhibition led to a significant increase in following behaviour on micropatterned lanes, and even resulted in a complete loss of contact inhibition of locomotion [27, 77]. Similar observations were made in chick embryonic heart fibroblasts, where ROCK inhibition removed the typical repulsive response, causing cells to instead exhibit pronounced sliding behaviours upon collision [211]. This change was linked to a hyper-stabilisation of microtubules induced by Y-27632 treatment. Kadir *et al.* suggested that microtubule dynamics are influenced by cell-cell contact, and that a specific increase in these dynamics is necessary for cells to repolarise upon such contact [211].
Combined with our findings, this suggests a complex interplay where cell-cell contacts and microtubule stability are critical for the re-polarisation and directional decisions of cells.
Collectively, our findings suggest a potential link between molecular signalling

pathways modulated by ephrins and ROCK, as well as microtubule dynamics, in the establishment of polarity interactions.

7. Conclusion and Outlook

In this thesis, I utilised a micropatterned two-site array to examine the dynamics of single cells and their cell-cell interaction behaviour across a range of phenotypically different cell lines derived from human tissues. This setup enabled the collection of an extensive dataset of cell trajectories, allowing for a quantitative analysis of cell behaviour within a controlled and standardised environment. The geometry of the array is designed to mimic physiological challenges faced by cells, making it a valuable tool for correlating cellular dynamics with phenotype and invasive potential. It also serves as an effective "cell-cell collider" for precisely studying head-to-head collisions between cells.

Our findings indicate that while the motility mechanisms of single cells within the dumbbell pattern appear to be consistent across the tested cell lines, there are distinct differences in the dynamics between epithelial and mesenchymal cells. Almost all cell types are driven deterministically into the constriction, yet epithelial cells exhibit excitable bi-stable hopping dynamics, whereas mesenchymal cells demonstrate limit cycle oscillations. We hypothesise that these dynamic fingerprints are not only indicative of the cells' phenotypes but also reflective of their invasive capabilities. In experiments involving MDAMB231 cells with and without miRNA200c, a known tumour suppressor, the behaviour observed on the dumbbell mirrored results from traditional invasion assays [166, 171]. This correlation suggests that further comparative studies of single-cell dynamics, alongside established invasion assays, could be instrumental in uncovering links between dynamic migration properties and the metastatic potential of cancer cells. Understanding these connections could have significant implications for cancer therapies, potentially leading to the development of targeted treatments that inhibit cancer progression by disrupting specific migration mechanisms.

Furthermore, the dumbbell assay provides a robust platform for investigating fundamental cellular processes involved in migration within confined environments. While we found that E-Cadherin does not change the dynamical pattern of cells, it would be of interest to test other EMT associated proteins such as N-Cadherin or Vimentin. Additionally, visualising cytoskeletal components like F-actin or microtubules during live imaging could reveal the general motility mechanisms employed by cells. This could be accomplished by either transiently transfecting cells with GFP-tagged mRNA specific to these proteins or by creating stable cell lines using methods like lentiviral transfection. Such approaches would provide more detailed observations of cell shape, cell viability, and the dynamics of cytoskeletal rearrangements, enhanc-

ing our understanding of how cells navigate and adapt to their microenvironment. Moreover, by employing targeted pharmacological interventions to actively perturb the cellular migration machinery, such as using latrunculin to disrupt F-actin polymerisation, blebbistatin to inhibit myosin II, or taxol to interfere with microtubule dynamics, we could further dissect the key components that define the dynamic fingerprint of cells. These studies would not only help in identifying the critical molecular players involved in cell motility but also in understanding how modifications in these elements influence cellular behaviour in restricted spaces.

One significant aspect not explored in this thesis is the role of focal adhesions and their interactions with the substrate, which are crucial in mediating cell migration [69, 86]. It is well-documented that the migratory properties of cells vary depending on the stiffness of the substrate they are adhered to [223,224]. This variance in migration is partially due to the mechanosensitive nature of focal adhesions; these structures dynamically adjust their composition and behaviour in response to the mechanical properties of the surrounding environment. Additionally, different types of cells exhibit preferences for various ECM proteins, which facilitate adhesion to the substrate [225–227]. These preferences can influence not only the strength and stability of the adhesions formed but also the signalling pathways activated during cell-substrate interactions. Therefore, it would be of interest to analyse the dynamics of single cells on dumbbells coated with different types of ECM proteins, such as Collagen IV, Collagen I or Laminin.

Building on the findings from the single cell behaviours, we extended our analysis to coupled two-cell interactions within the same micropatterns. Our research aimed to uncover shared biophysical mechanisms that govern cell-cell interactions, offering deeper insights into the 'social behaviour' of cells on larger scales. Unlike in the single cell study where we could directly correlate the cells phenotype with cell dynamics, the two-cell interactions did not show such a straightforward correlation with phenotypic traits. On the contrary, the cell lines exhibited a diverse spectrum of cohesion and friction interactions, ranging from attraction and anti-friction to strong repulsion and friction between the cell nuclei.
Throughout our experiments, we were able to confirm the robustness of the theoretical framework developed by Brückner *et al.* and validated its predictive potential. However, this framework does not provide information on the underlying mechanisms cells employ upon cell collision. To address this, we proposed a simple mechanistic model that includes the polarisation of the cells to describe the cell-cell interaction behaviour in a phenomenological way. We discovered that polarity alignment interactions, when combined with a repulsion mechanism such as Contact Inhibition of Locomotion (CIL), provided a quantitative description of the coupled cell behaviour for several phenotypically distinct cells on our micropattern. Remarkably, the interaction behaviour of the cells was captured by only tuning the interaction strength and sign of polarity alignment. Thus, we hypothesise that polarity alignment interactions might be a general mechanism cells employ to navigate transient cell-cell contacts.
Polarity alignment interactions are well-documented in various cell migration stud-

ies [109, 194, 195]; however, polarity anti-alignment interactions have been less frequently reported. In our analysis, while repulsion interactions like CIL were essential to quantitatively capture the dynamics of all our cell types, only the implementation of polarity anti-alignment could accurately predict the sliding behaviour observed in the breast cancer cell lines. This novel insight suggests that polarity anti-alignment, alongside CIL, plays a critical role in the interaction dynamics of cancer cells.
To deepen our understanding of the polarity alignment interactions observed in our cell lines, accurately measuring cell polarity would be essential. Tracking polarity in real-time presents a considerable challenge, as it requires precise identification and monitoring of polarity markers. One feasible yet less precise method involves analysing the cell's outline to infer the direction of polarisation based on cell shape. This approach, however, may be less effective since the differentiation between two closely positioned cells is challenging due to overlap of protrusions. To address this issue, sophisticated image segmentation algorithms that can accurately separate individual cells in close proximity, such as the deep learning-based segmentation method *CellPose* should be employed [228]. A more reliable method would involve tracking specific cell organelles or the distribution of key polarity cues. For instance, monitoring the position of the centrosome can provide insights into the cell's orientation since the centrosome typically precedes the nucleus in the direction of movement, especially during migration [229]. Similarly, visualising the distribution of polarity proteins such as RhoA or Rac1, which are critical in defining front-rear polarity in motile cells, could offer more definitive information on the state of cell polarisation.

To date, our analysis has focused exclusively on the homotypic interaction behaviour of various cell lines. Moving forward, it would be intriguing to also investigate the collision dynamics between two different types of cells. It is well-documented that in many cell lines, particularly cancerous ones, homotypic CIL remains intact while heterotypic CIL is often impaired [230, 231]. This impairment allows cancer cells to navigate through different types of tissues without being repelled, facilitating their invasive and metastatic behaviour. Therefore, an interesting area of study would be to explore what occurs when cells that exhibit polarity anti-alignment interactions in homotypic collisions encounter cells that demonstrate the opposite polarity alignment. This scenario is especially pertinent considering that disruptions in the mutual antagonism between Rac1 and RhoA have been shown to result in defective heterotypic CIL [230]. Understanding these dynamics could provide deeper insights into the mechanisms through which cancer cells override normal cellular repulsion cues to advance their spread through tissues.

Further, we explored the impact of specific molecular pathways on cell-cell interactions, particularly focusing on cell adhesion and cell recognition pathways and their roles in defining the amplitude of the interaction strength. Specifically, we challenged our model by implementing molecular perturbations targeting the polarisation machinery. We found that while almost every molecular perturbation induced a shift in the cell-cell interaction behaviour, it was still well captured by using polarity (anti-) alignment interactions. One notable discovery was the role of E-Cadherin in facil-

itating polarity alignment interactions within MCF10A cells. E-Cadherin, known for its involvement in contact-mediated adhesion and force transduction, seemed to orchestrate these polarity dynamics effectively. However, contrasting behaviour was observed in MDCK cells, which, despite expressing E-Cadherin, exhibited polarity anti-alignment interactions [222]. This divergence suggests that the presence of E-Cadherin is not a definitive indicator of polarity alignment interactions among epithelial cells, which prompts further investigation into this phenomenon.
Given that E-Cadherin-mediated bonds were observed between cells in our dumbbell pattern, further explorations into how adherens junctions influence cell behaviour could provide deeper insights. One promising approach would be the use of a functional DNA-E-cadherin hybrid, which allows tuning of adhesion strength based on DNA sequence and length [232]. Employing techniques such as force spectroscopy could enable direct measurements of the binding strength exerted by E-Cadherins between cell pairs. This method could also illuminate the strength dependency of adherens junctions and enhance our understanding of their mechanosensing capabilities. Such investigations could lead to a more comprehensive understanding of how cellular adhesion mechanisms contribute to the complex dynamics of cell-cell interactions.

Additionally, our studies indicated that the EphA-RhoA-ROCK signalling axis may be a critical determinant in whether cell types exhibit polarity alignment or anti-alignment interactions. Blocking of ephrinA2 as well as ROCK inhibition through Y-27632 resulted in a switch from polarity alignment to anti-alignment interactions in MCF10A cells. This signalling pathway is tightly intertwined with the cytoskeletal dynamics, involving a vast network of proteins, proving a challenge in determining the exact mechanisms by which the cells regulate their interaction behaviour. We hypothesise that microtubule dynamics are crucial in determining the outcomes of cell-cell collisions. Particularly, the stability of microtubules may play a critical role; highly stable microtubules could be indicative of the pronounced sliding behaviours observed in some cell lines. To explore this hypothesis further, the use of specific pharmacological agents, such as destabilising agents like nocodazol or stabilising agents like taxol could yield insights into this topic.

While the specific geometry of the dumbbells was chosen to mimic a physiological-like environment, there are inherent limitations to this setup. One significant limitation is that the cells were not confined in the Z-direction, and despite strong passivation outside the dumbbell pattern, cells were still able to traverse passivated areas if part of the cell remained attached to the fibronectin-coated pattern. Additionally, results from 2D environments do not always accurately reflect behaviours in more complex 3D environments, where cells interact within a three-dimensional matrix and experience different mechanical and biochemical cues. To gain deeper physiological insights into cell-cell interactions and the mechanisms by which cells navigate through narrow constrictions, transitioning to a 3D experimental setup would be highly beneficial. Such a setup could involve the use of specific hydrogels that can be engineered to mimic the extracellular matrix. These hydrogels can be designed with tuneable stiffness, allowing for precise control over the mechanical

properties of the environment [128]. This feature is particularly advantageous for studying how cells respond to mechanical cues and for measuring the forces exerted by cells as they navigate through these structures.

As a future incentive, it would be fascinating to explore whether these alignment interactions not only capture two-cell interaction behaviour but also provide insights into the collective dynamics of tissues. Furthermore, it would be interesting to investigate if the alignment strength determined in the two-cell setup also applies to a multicellular system. For instance, polarity alignment interactions have already been used to describe the flocking behaviour of epithelial cell lines in 1D tracks as well as in collective sheet migration [194, 195]. Therefore, a simple setup that constrains multiple cells within a short lane could provide valuable insights. By adjusting the lane geometry, we could precisely control the number of cells in the system and systematically study their collective dynamics. Expanding this study to a larger set of cells in a controlled environment could enable testing whether polarity (anti-) alignment interactions translate to the different collective migration behaviours observed in epithelial versus mesenchymal cells. This exploration would be particularly relevant in contexts such as wound healing, where cells need to coordinate their movements to close gaps, or in cancer metastasis, where a breakdown in these coordinated behaviours can lead to invasive cell dynamics. The proposed future directions, building upon the findings of this study, are summarised in Fig. 7.1.

In summary, I employed a strategically designed two-state array to systematically unravel the underlying mechanisms of migration and cell-cell interaction across a diverse range of motile cells. Initially, we focused on single-cell behaviour and discovered that migration dynamics within our micropattern varied significantly depending on cellular phenotype and characteristics, potentially also serving as an indicator of the invasive potential of these cells. Expanding on this, we examined the behaviour of pairs of cells and identified diverse cell-cell interaction behaviours across different cell lines. Through this investigation, we discovered an underlying mechanism of polarity (anti-) alignment interactions that accurately quantified the observed interaction behaviour across all cell lines. Moreover, it proved robust against a diverse set of molecular perturbations induced to impact the cell-cell interaction behaviour. These insights could be used in future studies aiming to bridge the gap between individual cell migration and collective cell movements.

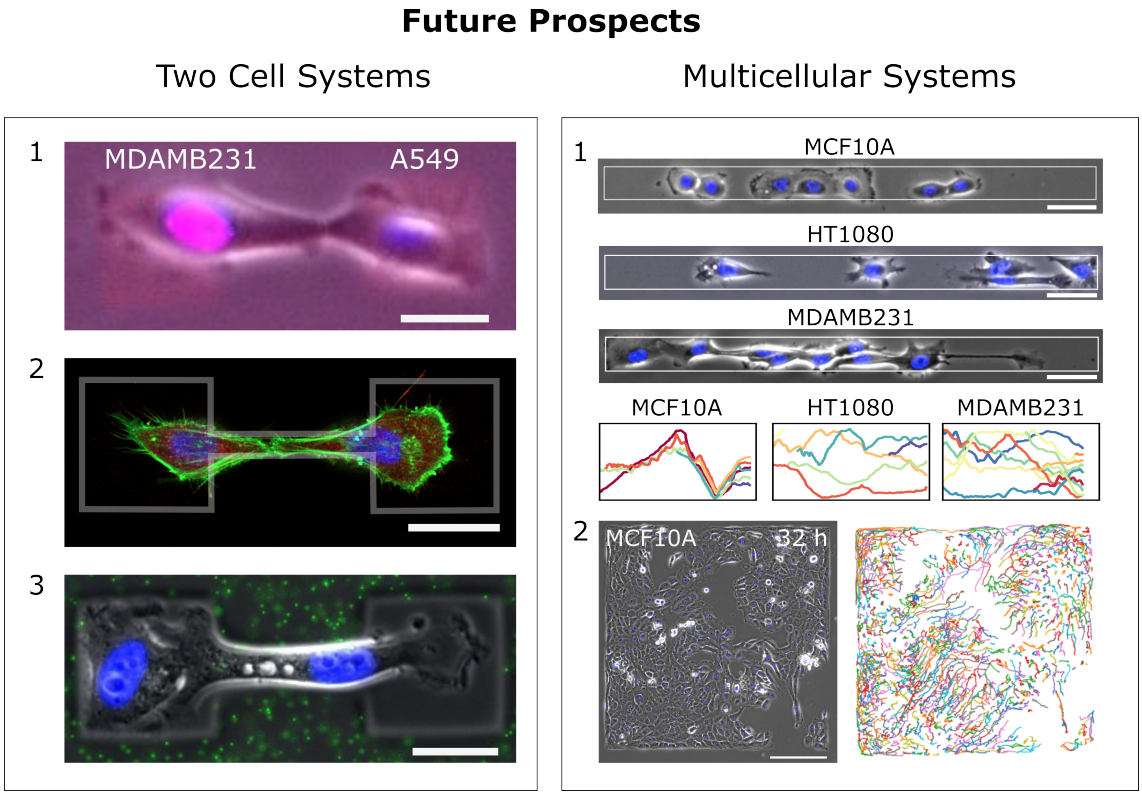

Figure 7.1: Future directions. Two cell systems: 1) Heterogeneous cell-cell interactions, MDAMB231 with nuclear mCherry stain and A549 with Hoechst stain to distinguish cell lines. Scale bar = 25 μm. 2) Focal adhesion visualisation, integrin is stained in red and F-actin network in green. Scale bar = 25 μm. 3) Cell-cell interactions in 3D hydrogel dumbbells. Scale bar = 25 μm. Image courtesy of Stefan Stöberl. Multicellular systems: 1) Multiple cells of various cell lines and their corresponding trajectories on a micropatterned lane. Scale bar = 50 μm. 2) Collective cell migration of MCF10A confined to a square pattern and corresponding trajectories. Scale bar = 250 μm.

A. Materials and Methods

A.1 Microfabrication of Dumbbell Pattern

To prepare the surface of the ibiTreat μ-dish (ibidi) for micropatterning, a small drop of 0.01% (w/v) poly-L-lysine (PLL, Sigma-Aldrich) was applied to passivate the dish. This PLL coating was left to incubate at room temperature for 30 minutes to ensure full coverage and adhesion to the surface. Following incubation, the dish was thoroughly rinsed with HEPES buffer (pH=8.3, Thermo Scientific) to remove any excess PLL. Subsequently, a solution of 100 mg/ml mPEG-SVA (5000 M molecular weight, Laysan Bio) dissolved in 0.1 M HEPES was evenly distributed over the surface of the dish. This layer was incubated at room temperature for at least one hour to allow complete reaction of the PEG molecules with the surface, providing an effective passivation layer. The dish was then rinsed thoroughly with milliQ water to remove any unbound PEG molecules.
For the photopatterning process, the PRIMO module (Alvéole, France), mounted on an automated inverted Nikon Eclipse Ti microscope, was used. After the passivation step, PLPP gel (Alveole) was diluted in 99% ethanol to achieve a uniform distribution across the surface. The dumbbell-shaped pattern was then applied to the dish using the Leonardo software (Alvéole), and the pattern was exposed to UV light at a dose of 15 mJ/mm^2 to initiate photopolymerisation.
Following photopatterning, the dish was washed extensively with milliQ water and rehydrated with PBS for 5 minutes to prepare the surface for protein adhesion. Fibronectin-Alexa647 (labelled, Y-proteins, Thermo Fisher) was then added at a concentration of 20 μg/ml and incubated for 15 minutes at room temperature. This step allows for the specific binding of fibronectin to the exposed areas of the pattern, creating distinct regions of cell adhesion that can be utilised for subsequent cellular studies.

A.2 Cell Culture

The **MCF10A** cells (ATCC) are cultured at 5% CO2 at 37°C in DMEM/F-12 medium including Glutamax (Gibco) supplemented with 5% horse serum, 20 ng/ml human epidermal growth factor, 100 ng/ml cholera toxin, 10 ug/ml insulin and 500ng/ml hydrocortisone. For passaging, cells are being washed and treated with Accutase for 15 min. For experiments the cell solution is centrifuged at 500 r.c.f. for 6 min and the cells are resuspended in Medium. Approximately 15 000 cells

are added into the micropatterned μ-dish and left to adhere for up to 4h in the incubator. After this incubation period, the medium is exchanged and 25nM Hoechst 33342 for staining of cell nuclei is added.

The **MCF10A CDH1 -/-** cells (Merck) are cultured the same way as the MCF10A cells.

The **MDA-MB-231 H2B-mCherry** were kindly provided by Prof. Timo Betz at the University of Göttingen. Cells are cultured at 0% CO2 at 37°C in L-15 medium (Gibco), supplemented with 10% fetal bovine serum. For passaging, cells are being washed and treated with accutase for 5 min. For experiments the cell solution is centrifuged at 800 r.c.f. for 3 min and the cells are resuspended in medium. Approximately 10 000 cells are added into the micropatterned μ-dish and left to adhere for up to 4h in the incubator. After this incubation period, the medium is exchanged for phenol red free L-15 medium.

The **MDA-MB-436** cells (ATCC) are cultured at 0% CO2 at 37°C in L-15 medium (Gibco), supplemented with 10% fetal bovine serum. For passaging, cells are being washed and treated with accutase for 5 min. For experiments the cell solution is centrifuged at 800 r.c.f. for 3 min and the cells are resuspended in medium. Approximately 10 000 cells are added into the micropatterned μ-dish and left to adhere for up to 4h in the incubator. After this incubation period, the medium is exchanged for phenol red free L-15 medium and 25nM Hoechst 33342 for staining of cell nuclei is added.

The **A549** cells (DSMZ) are cultured at 5% CO2 at 37°C in RPMI medium (Gibco) supplemented with 10% fetal bovine serum. For passaging, cells are being washed and treated with accutase for 5 min. For experiments the cell solution is centrifuged at 800 r.c.f. for 3 min and the cells are resuspended in medium. Approximately 10 000 cells are added into the micropatterned μ-dish and left to adhere for up to 4h in the incubator. After this incubation period, the medium is exchanged for phenol red free L-15 medium and 25nM Hoechst 33342 for staining of cell nuclei is added.

The **HT1080** cells (cell line authenticated by CLS) are cultured at 5% CO2 at 37°C in Dulbecco's MEM medium (Gibco) supplemented with 10% fetal bovine serum. For passaging, cells are being washed and treated with accutase for 5 min. For experiments the cell solution is centrifuged at 800 r.c.f. for 3 min and the cells are resuspended in medium. Approximately 10 000 cells are added into the micropatterned μ-dish and left to adhere for up to 4h in the incubator. After this incubation period, the medium is exchanged for phenol red free L-15 medium and 25nM Hoechst 33342 for staining of cell nuclei is added.

The **MDA-MB-231 TRIPZ 200c** cells were kindly provided by Andreas Roidl (reference) and are cultured at 0% CO2 at 37°C in L-15 medium (Gibco),

supplemented with 10% fetal bovine serum. For passaging, cells are being washed and treated with accutase for 5 min. For experiments the cell solution is centrifuged at 800 r.c.f. for 3 min and the cells are resuspended in medium. Stimulation of the cells with doxycycline was performed at a concentration of 5 μg/ml in L-15 72h prior to the start of the experiment. Approximately 10 000 cells are added into the micropatterned μ-dish and left to adhere for up to 4h in the incubator. After this incubation period, the medium is exchanged for phenol red free L-15 medium supplemented with 5 μg/ml doxycycline and 25nM Hoechst 33342 for staining of cell nuclei is added.

The **MCF7** cells were kindly provided by Andreas Roidl and are cultured at 5% CO2 at 37°C in Dulbecco's MEM medium (Gibco) supplemented with 10% fetal bovine serum. For passaging, cells are being washed and treated with accutase for 5 min. For experiments the cell solution is centrifuged at 800 r.c.f. for 3 min and the cells are resuspended in medium. Approximately 10 000 cells are added into the micropatterned μ-dish and left to adhere for up to 4h in the incubator. After this incubation period, the medium is exchanged for phenol red free L-15 medium and 25nM Hoechst 33342 for staining of cell nuclei is added.

The **MCF7 KO-200c** cells were kindly provided by Andreas Roidl and are cultured at 5% CO2 at 37°C in Dulbecco's MEM (Gibco) medium supplemented with 10% fetal bovine serum. The cell line has a miRNA200c knock-out via TALENs reporter. The plasmid compromises a puromycin and RFP reporter. For passaging, cells are being washed and treated with accutase for 5 min. For experiments the cell solution is centrifuged at 800 r.c.f. for 3 min and the cells are resuspended in medium. Approximately 10 000 cells are added into the micropatterned μ-dish and left to adhere for up to 4h in the incubator. After this incubation period, the medium is exchanged for phenol red free L-15 medium and 25nM Hoechst 33342 for staining of cell nuclei is added.

The **MDCK II** cells are cultured at 5% CO2 at 37°C in Dulbecco's MEM medium (Gibco) supplemented with 10% fetal bovine serum. For passaging, cells are being washed and treated with accutase for 15 min. For experiments the cell solution is centrifuged at 800 r.c.f. for 3 min and the cells are resuspended in medium. Approximately 10 000 cells are added into the micropatterned μ-dish and left to adhere for up to 4h in the incubator. After this incubation period, the medium is exchanged for phenol red free L-15 medium and 25nM Hoechst 33342 for staining of cell nuclei is added.

The **BEAS2B** cells are cultured at 5% CO2 at 37°C in Earls's MEM medium (Gibco) supplemented with 10% fetal bovine serum. For passaging, cells are being washed and treated with accutase for 5 min. For experiments the cell solution is centrifuged at 800 r.c.f. for 3 min and the cells are resuspended in medium. Approximately 10 000 cells are added into the micropatterned μ-dish and left to adhere for up to 4h in the incubator. After this incubation period, the medium is

exchanged for phenol red free L-15 medium and 25nM Hoechst 33342 for staining of cell nuclei is added.

A.3 Cellular Perturbations with Antibodies and Drugs

To inhibit the function of E-Cadherin, ephrinA2 and ephrinB2 in our cellular assays, specific blocking antibodies were utilised. Functional grade CD324 antibody (Invitrogen) was employed to disrupt E-Cadherin interactions, while anti-mouse ephrinA2 antibody (OTI3E3, Thermo Fisher) and anti-rat ephrinB2 (Thermofisher) targeted ephrinA2 and ephrinB2 respectively. These antibodies were added to the culture following cell adherence to the micropatterned surfaces. The used concentration are listed in table A.1.
In experiments aimed at perturbing the polarisation machinery of the cells, the ROCK inhibitor Y27632 (Calbiochem, Sigma Aldrich) was introduced after the cells had attached to the pattern. The inhibitor was used at a concentration of 2 mug/ml to effectively interfere with downstream signalling pathways that contribute to cellular polarity and movement. For targeting the microtubules in the cells, a low dose of nocodazol (Merck) was added to the cells after attachement to the pattern.
Following the application of these treatments, the dishes were incubated for one hour to allow the cells to adjust to the stress applied to them. Subsequently, time-lapse imaging was initiated to capture the cellular behaviours in response to these molecular interventions over time.
Additionally, to induce EMT, cells were treated with 10 ng/ml of TGFβ (Thermo Fisher) for up to seven days. The medium with new TGFβ was exchanged every second day. This long-term treatment was designed to provoke significant changes in cell morphology and migratory capabilities, mimicking processes that occur during cancer progression and metastasis.

Blocking antibodies and drugs		
Antibody/Drug	concentration	Reference Number
E-Cadherin	5 μg/ml	16-3249-82 (Thermofisher)
ephrinA2	1 μg/ml	MA5-25187 (Thermofisher)
ephrinB2	2 μg/ml	JM53-21 (Thermofisher)
Y27632	30 μM	SCM075 (Sigma-Aldrich)
Nocodazol	0.5 μM	M1404 (Sigma-Aldrich)
TGF-β	10 nM	rcyc-htgfb1 (InvivoGen)

Table A.1: Drugs and antibodies used in the experiments. Their respective concentrations used to inhibit or block pathways and specific proteins are also listed.

A.4 Western Blots

As a first step in quantifying the expression of specific proteins in the cells, the proteins have to be extracted. Therefore, the cells are harvested in a T-75 flask in advance. Cell medium is aspirated and the cells are washed once with PBS. Cell lysis is achieved by adding 400 μl RIPA (Thermofisher) lysis buffer in the flask. In order to protect the proteins from degradation, 1mM PMSF and a protease inhibitor cocktail (Thermofisher) are added to the lysis buffer. After an incubation period of 20 min on ice, cells are removed from the flask by scraping. The cell solution is centrifuged for 15 min at 14000 xg to remove cell debris. The supernatant is then transferred to a fresh tube. To determine the total protein concentration in the cell lysate, a Bradford assay is utilised. For better isolation of the proteins in SDS-PAGE gel electrophoresis, 35 μg of protein are mixed with 6X laemmli sample buffer (Thermofisher) and heated at 95°C for 5 min. The samples are loaded onto precast gradient 4-20% gel (BioRad) and separated by SDS gel electrophoresis. The transfer is performed on immuno-Blot polyvinylidene difluoride (PVDF) membranes (BioRad) with the Trans-blot turbo transfer system (BioRad) during 7.5 min. For determining total protein amount loaded onto the membrane, a Ponceau staining is conducted. After, the membrane are blocked with 5% non-fat dried milk (ThermoFisher) in PBS 0.1% Tween 20 (Roth) for 1h and then incubated with the primary antibody (see table A.2) at 4°C over night. After three washing steps with PBS 0.1% Tween 20, the membrane is incubated for 1h with the secondary antibody conjugated to the horseradish peroxidase (HRP) enzyme (see table A.3) at room temperature. The enzyme reacts with the HRP substrate luminol emitting light at 428 nm. However, luminol emits light only weakly, so enhancers are added to the reaction to increase the signal. Development was performed using Pierce western enhanced chemiluminescence (ECL) substrate (Thermofisher) using a ChemiDoc MP imaging system (BioRad). The intensity of the band was quantified via densitometry using ImageJ. For quantification, protein amount was normalised to a beta-actin loading control on the same membrane.

A.5 Immunostaining

After the time-lapse experiment cells are fixed in the dish using ice cold 4% paraformaldehyde (PFA) in PBS for 15min. After three washing steps with PBS, cells are permeabilised with 0.02% Triton X-100 (Roth) for 10 min at room temperature to remove some of the cellular membrane lipids to allow large molecules like antibodies to enter the cell. The cells are blocked for 45 min in cold 4% BSA (Thermofisher). Following, the cells were rinsed once with cold 1% BSA. The excess liquid was removed and the cells were subjected to primary antibodies (see table A.2) diluted in 1% BSA at 4°C over night. After three washing steps with 1% BSA, cells are incubated for 1h with the secondary antibody conjugated with a specific fluorophore (see table A.3) for detection at room temperature in the dark. Since the cells are not mounted and sealed on a coverslip, imaging should take place on

the same day.

Primary Antibodies					
Protein target	Host/Isotype	Class	Reference Number	IF conc.	WB conc.
E-Cadherin	Mouse IgG1	Monoclonal	13-1700 (Thermofisher)	1:200	1:1000
N-Cadherin	Rabbit IgG	Polyclonal	PA5-85495 (Thermofisher)		1:2000
beta Actin	Mouse IgG1	Monoclonal	MA1-140 (Thermofisher)		1:10000
EphrinA2	Mouse IgG2b	Monoclonal	13-1700 (Thermofisher)	1:100	
EphrinB2	Rabbit IgG	Monoclonal	JM53-21 (Thermofisher)	1:50	

Table A.2: Primary antibodies and the concentration used for Western Blots or Immunostaining

Secondary Antibodies					
Conjugate	Target species	Class	Reference Number	IF conc.	WB conc.
Alexa Fluor 488	Mouse IgG (H+L)	Polyclonal	(Thermofisher)	1:1000	
Alexa Fluor 647	Mouse IgG (H+L)	Polyclonal	(Thermofisher)	1:1000	
Alexa Fluor 488	Rabbit IgG (H+L)	Polyclonal	(Thermofisher)	1:1000	
Rhodamine	Phalloidin		R415 (Thermofisher)	1:1000	
HRP	Anti-mouse IgG (H+L)	Polyclonal	32430 (Thermofisher)		1:10000
HRP	Anti-rabbit IgG (H+L)	Polyclonal	31458 (Thermofisher)		1:10000

Table A.3: Conjugated secondary antibodies and the concentration used for Western Blots or Immunostaining

A.6 Transfection Procedure

Before transfection, cells were cultured in a non-patterned µ-dish (ibidi) until they reached 90% confluency. For the transfection process, Lipofectamine™ 2000 (In-

vitrogen, Germany) was used to introduce E-Cadherin mRNA into the cells. The transfection mix was prepared by combining 2 μl of Lipofectamine™ 2000 with 398 μl of OptiMEM (Invitrogen), followed by a 5-minute incubation step at room temperature to allow the reagent to form liposomes. Concurrently, 2 μl of E-Cadherin mRNA at a concentration of 1735 ng/μl was diluted in 198 μl of OptiMEM. This mRNA solution was then gently mixed with 200 μl of the prepared Lipofectamine™ 2000 dilution and incubated for an additional 20 minutes at room temperature to form lipoplexes.
After this incubation period, the cells were washed once with OptiMEM to remove any residual media and debris. The newly formed lipoplexes were then added to the cells, ensuring an even distribution across the dish. The cells were incubated with the lipoplexes for at least 1 hour, allowing sufficient time for the lipoplexes to facilitate mRNA entry into the cells. Subsequently, the cells were washed again to remove any unbound lipoplexes and then returned to normal growth medium to recover and express the introduced mRNA.
For control experiments, similar transfections were conducted using GFP-mRNA to analyse the impact of the transfection procedure on cell dynamics. Additionally, some control groups were treated with lipoplexes where milliQ water was used instead of mRNA, serving as a negative control to assess any effects caused by the transfection reagent itself. These controls are essential for validating the specificity and effectiveness of the transfection protocol.

A.6.1 mRNA Construction

To produce in vitro-transcribed mRNA (IVT RNA), the plasmid (Addgene plasmid # 45769) was first linearized downstream of the poly(A) tail using SapI digestion and then purified using the NEB Monarch PCR and DNA Cleanup Kit (NEB, T1030S). One μg of this linearised vector served as the template for the in vitro transcription reaction, conducted with the Biozym MessageMAX™ T7 ARCA-Capped Message Transcription Kit. This kit ensures that 100% of the Anti-Reverse Cap Analog is incorporated in the correct orientation, thereby enhancing the translation efficiency of the IVT RNA. The reaction mixture was incubated at 37°C for 45 minutes, followed by DNA removal using DNaseI for 15 minutes at the same temperature. The RNA was then precipitated using ammonium acetate at a final concentration of 2.5 M and washed twice with 70% ethanol. Finally, the RNA pellet was dissolved in RNase-free water.

A.7 Time-Lapse and Confocal Microscopy

Time-lapse measurements were conducted over a 48-hour period using either an inverted Nikon Eclipse Ti microscope or an inverted Nikon Eclipse Ti2 microscope. For these observations, either a 10x or a 20x objective was utilised, with the latter specifically for MDAMB231 cells transfected with E-Cadherin. The samples were maintained in a heated chamber (either Okolabs or Ibidi) at 37°C, with an atmosphere of 5% CO2 applied exclusively for MCF10A cells. Images were captured

every 10 minutes, alternating between brightfield and fluorescence imaging (using either a DAPI or mCherry filter, based on the cell line) to facilitate cell tracking. To maximise data throughput, the setup was configured to record multiple positions, allowing the microscope to cycle through them within each 10-minute interval. The micropattern was recorded once at the beginning of the time-lapse in the corresponding fluorescence channel (Alexa 488 or Cy5).
For confocal microscopy a ZEISS LSM 980 with Airyscan 2 microscope was utilised. The fixed and immunostained samples were imaged using a 40x water immersion objective and the airyscan mode for better resolution. Z-Stacks of up to 20 μm were acquired. Airyscan images were processed using the ZEISS LSM software.

B. Image and Data Analysis

B.1 Cell Exclusion Criteria

The nucleus of each cell was tracked to analyse the dynamics of different cell lines. Given the extensive dataset, a preliminary selection of cells was performed based on a set of criteria to ensure high comparability between various experiments and cell lines. The eligibility criteria for tracking cells included:

1. The cells must be fully adhered to the pattern. Tracking only commences once cells have flattened out on the pattern, as rounded cells are not fully attached.
2. The cells must be viable, as determined by their morphologies and nuclear shapes. For example, cells exhibiting cytoplasmic bubbles were excluded from analysis.
3. The cells must be free of physiological defects. Any abnormalities such as multiple nuclei or disrupted nuclei result in the exclusion of those tracks.
4. The trajectories must span at least 50 consecutive frames (equivalent to 500 minutes).
5. Cells that are not fully confined within the boundaries of the micropattern are excluded.
6. Cells that undergo apoptosis or any form of cell death during the experiment are also excluded.
7. Experiments displaying any signs of bacterial infection are completely excluded from the analysis.

B.2 Tracking Procedure

The selection of single cells and cell pairs on the micropattern was carried out manually in compliance with the specified cell selection criteria. Once selected, the cells were individually cropped from overview positions that may contain up to 50 dumbbells each. This cropping was performed using ImageJ. Additionally, the original time-lapse movies were adjusted such that the long axis of the micropattern is aligned horizontally. This orientation facilitates easier analysis of cell movements

and interactions across the micropattern. The cells trajectories were determined by tracking the nuclei signals over time. The tracking was done by an in house code using TrackPy (Python Version 3.10.5). The trajectories were inspected manually to correct for tracking mistakes. Lastly, the fluorescence image of the micropatterned was used to determine the coordinate origin of the trajectories. The origin was set at the centre of the bridge. The resulting tracks were then converted from pixel values to micrometers (0.648 μm for measurements done at the Nikon Ti microscope). The resulting trajectory data sets for all single cell experiments and all two-cell experiments with corresponding perturbations are listed in Table B.2 and Table B.1 respectively.

B.3 Error Analysis

The errors of the experimental observables as well as in the model prediction for the dwell times, instantaneous velocity cross-correlation, behaviour distribution statistics and position in the interaction behaviour space, were calculated by a bootstrapping procedure. This procedure is a statistical technique used to estimate characteristics of a population by leveraging the resampling of a dataset. Here, our data consisted either of N cell pair trajectories denoted as x_k, where $k = 1, \ldots, N$, or single cell trajectories represented as $D = X_1, X_2, \ldots, X_N$, each with N entries. We then generated a large number N_{BS} of bootstrap realisations. For each realisation, we randomly sampled entries from the original dataset (either X_N or the N cell pair trajectories) with replacement. Each of these bootstrap samples was the same size as the original dataset, but because sampling was done with replacement, some observations may appear more than once while others may not appear at all. The error associated with an observable Θ_{exp} measured from the experimental dataset, was now determined by calculating Θ for each of the N_{BS} bootstrap realisations. We then used the standard deviation of these Θ values as an estimate for the error in Θ_{exp}. This provides a measure of how much Θ_{exp} might vary due to the inherent variability in the dataset. For providing errors to our model prediction observables, we performed underdamped Langevin inference for all N_{BS} bootstrap realisations and then simulated several trajectories in order to estimate Θ for each set of trajectories. Again, the standard deviation of all Θ was used to estimate the error in Θ_{model} [24, 25].

B.4 Collision Events

To analyse the behaviour distribution of each cell line, we initially categorised the collision events, reversal, sliding, and following, based on the paired trajectories of cell pairs. A collision event was identified when the nuclei of two cells come within a proximity of Δx_c. We set Δx_c=20μm, which is slightly greater than the typical diameter of a cell on one dumbbell-patterned island. To differentiate between reversal and sliding events, it was crucial to determine whether the cells exchanged positions during the collision. If the cells remained in their original positions post-collision,

cell line	perturbation	N	comment
MCF10A	wildtype	251	including data adapted from [25]
MCF10A	E-Cadherin KO	65	
MCF10A	E-Cadherin blocking	89	adapted from Georg Ladurner
MCF10A	Y-27632	72	adapted from Georg Ladurner
MCF10A	ephrinA2 blocking	103	adapted from Georg Ladurner
MCF10A	TGFβ	101	
A549	wildtype	100	
HT1080	wildtype	87	
MDAMB436	wildtype	102	
MDAMB231	wildtype	185	including data adapted from [25]
MDAMB231	ephrinB2 blocking	102	
MDAMB231 TRIPZ 200c	uninduced	58	
MDAMB231 TRIPZ 200c	doxycycline	100	
MDAMB231 TRIPZ CTRL	doxycycline	76	
MDAMB231	ephrinB2 blocking	102	
MDAMB231	E-Cadherin transfection	63	
MDAMB231	GFP transfection	97	
Beas2B	wildtype	87	
MDCKII	wildtype	100	
MCF7	wildtype	80	
MCF7	miRNA200c KO	59	

Table B.1: Overview over the various cell-cell interaction experiments conducted in this thesis. Here, N is the number of trajectories extracted from the experiment and used for analysing cell dynamics.

the event was classified as a reversal; if they switched positions, it was identified as a sliding event. These movements were detectable in the trajectories. We chose a fixed observation window of dT=1h after the collision to accurately identify these events. During this period, a position switch indicated a sliding event, while the absence of such a switch indicated a reversal event. Additionally, to minimise artifacts from cells frequently entering and leaving this proximity threshold, we defined the time-scale between subsequent transitions as longer than dT. Following events were characterised by a head-tail collision that leads to cell adhesion. In the trajectories, a following event was noted when two cells make the same transition across the

cell line	**perturbation**	N	**comment**
MCF10A	wildtype	215	including data adapted from [25]
MCF10A	E-Cadherin KO	100	
MCF10A	E-Cadherin blocking	89	adapted from Georg Ladurner
MCF10A	TGFβ	63	
A549	wildtype	100	
HT1080	wildtype	98	
MDAMB436	wildtype	102	
MDAMB231	wildtype	149	including data adapted from [25]
MDAMB231 TRIPZ 200c	uninduced	85	
MDAMB231 TRIPZ 200c	doxycycline	94	
MDAMB231 TRIPZ CTRL	doxycycline	89	
MDAMB231	E-Cadherin transfection	45	
MDAMB231	GFP transfection	90	
MDCKII	wildtype	91	
MCF7	wildtype	62	
MCF7	miRNA200c KO	44	

Table B.2: Overview over the various single cell experiments conducted in this thesis. Here, N is the number of trajectories extracted from the experiment and used for analysing cell dynamics.

bridge within dT [24, 25].

List of Abbreviations

1D	one dimension(al)
2D	two dimensions/two-dimensional
3D	three dimensions/three-dimensional
AJ	Adherens Junction
ATP	Adenosine Triphosphate
BF	Brightfield
BSA	Bovine Serum Albumin
CIL	Contact Inhibition of Locomotion
CFL	Contact Following of Locomotion
CPM	Cellular Potts Model
CSL	Contact Sliding of Locomotion
DMD	Digital Micromirror Device
ECM	Extracellular Matrix
EMT	Epithelial-to-Mesenchymal Transition
FA	Focal Adhesion
GFP	Green Fluorescent Protein
HER2	Human Epidermal Growth Factor Receptor 2
IBS	Interaction Behaviour Space
miRNA	Micro Ribonucleic Acid
MT	Mesenchymal-to-Epithelial Transition
MLC	Myosin Light Chain

List of Abbreviations

mRNA	Messenger Ribonucleic Acid
MSD	Mean Squared Displacement
MOTC	Microtubule-Organising Center
μCP	Microcontact Printing
μPIPP	Microscale Plasma-Initiated Protein Patterning
OU	Ornstein-Uhlenbeck process
PBS	Phosphate-Buffered Saline
PC	Phase Contrast
PI3K	Phosphoinositide 3-Kinase
PDMS	Polydimethylsiloxane
PEG	Polyethylene Glycol
PMT	Photomultiplier Tube
PLL	Poly-L-Lysine
ROCK	Rho-associated Coiled-coil-containing protein Kinases
TGFβ	Transformation Growth Factor β
TF	Transcription Factors
TJ	Tight Junction
TNBC	Triple Negative Breast Cancer
ULI	Underdamped Langevin Inference
USPC	Universal Coupling between Speed and Persistence
UV	Ultraviolet

List of Figures

List of Tables

Bibliography

[1] Pernille Rørth. Collective cell migration. *Annual Review of Cell and Developmental Biology*, 25(1):407–429, November 2009.

[2] Francisco Merino-Casallo, Maria Jose Gomez-Benito, Silvia Hervas-Raluy, and Jose Manuel Garcia-Aznar. Unravelling cell migration: defining movement from the cell surface. *Cell Adhesion & Migration*, 16(1):25–64, May 2022.

[3] Jessica Stock and Andrea Pauli. Self-organized cell migration across scales – from single cell movement to tissue formation. *Development*, 148(7), April 2021.

[4] Andy Aman and Tatjana Piotrowski. Cell migration during morphogenesis. *Developmental Biology*, 341(1):20–33, May 2010.

[5] Young Min Shin, Hee Seok Yang, and Heung Jae Chun. *Directional Cell Migration Guide for Improved Tissue Regeneration*, page 131–140. Springer Singapore, 2020.

[6] Peter Friedl and Katarina Wolf. Tumour-cell invasion and migration: diversity and escape mechanisms. *Nature Reviews Cancer*, 3(5):362–374, May 2003.

[7] Marianne Lintz, Adam Muñoz, and Cynthia A. Reinhart-King. The mechanics of single cell and collective migration of tumor cells. *Journal of Biomechanical Engineering*, 139(2), January 2017.

[8] Douglas A Lauffenburger and Alan F Horwitz. Cell migration: A physically integrated molecular process. *Cell*, 84(3):359–369, February 1996.

[9] Thomas D Pollard and Gary G Borisy. Cellular motility driven by assembly and disassembly of actin filaments. *Cell*, 112(4):453–465, February 2003.

[10] Anne J. Ridley, Martin A. Schwartz, Keith Burridge, Richard A. Firtel, Mark H. Ginsberg, Gary Borisy, J. Thomas Parsons, and Alan Rick Horwitz. Cell migration: Integrating signals from front to back. *Science*, 302(5651):1704–1709, December 2003.

[11] Satoshi Kurosaka and Anna Kashina. Cell biology of embryonic migration. *Birth Defects Research Part C: Embryo Today: Reviews*, 84(2):102–122, June 2008.

[12] Paolo Maiuri, Jean-François Rupprecht, Stefan Wieser, Verena Ruprecht, Olivier Bénichou, Nicolas Carpi, Mathieu Coppey, Simon De Beco, Nir Gov, Carl-Philipp Heisenberg, Carolina Lage Crespo, Franziska Lautenschlaeger, Maël Le Berre, Ana-Maria Lennon-Dumenil, Matthew Raab, Hawa-Racine Thiam, Matthieu Piel, Michael Sixt, and Raphaël Voituriez. Actin flows mediate a universal coupling between cell speed and cell persistence. *Cell*, 161(2):374–386, April 2015.

[13] Samy Lamouille, Jian Xu, and Rik Derynck. Molecular mechanisms of epithelial–mesenchymal transition. *Nature Reviews Molecular Cell Biology*, 15(3):178–196, February 2014.

[14] Jing Yang, Parker Antin, Geert Berx, Cédric Blanpain, Thomas Brabletz, Marianne Bronner, Kyra Campbell, Amparo Cano, Jordi Casanova, Gerhard Christofori, Shoukat Dedhar, Rik Derynck, Heide L. Ford, Jonas Fuxe, Antonio García de Herreros, Gregory J. Goodall, Anna-Katerina Hadjantonakis, Ruby Y. J. Huang, Chaya Kalcheim, Raghu Kalluri, Yibin Kang, Yeesim Khew-Goodall, Herbert Levine, Jinsong Liu, Gregory D. Longmore, Sendurai A. Mani, Joan Massagué, Roberto Mayor, David McClay, Keith E. Mostov, Donald F. Newgreen, M. Angela Nieto, Alain Puisieux, Raymond Runyan, Pierre Savagner, Ben Stanger, Marc P. Stemmler, Yoshiko Takahashi, Masatoshi Takeichi, Eric Theveneau, Jean Paul Thiery, Erik W. Thompson, Robert A. Weinberg, Elizabeth D. Williams, Jianhua Xing, Binhua P. Zhou, and Guojun Sheng. Guidelines and definitions for research on epithelial–mesenchymal transition. *Nature Reviews Molecular Cell Biology*, 21(6):341–352, April 2020.

[15] Anushka Dongre and Robert A. Weinberg. New insights into the mechanisms of epithelial–mesenchymal transition and implications for cancer. *Nature Reviews Molecular Cell Biology*, 20(2):69–84, November 2018.

[16] Joëlle Roche. The epithelial-to-mesenchymal transition in cancer. *Cancers*, 10(2):52, February 2018.

[17] Xia Liu, Fen Yun, Lin Shi, Zhe-Hai Li, Nian-Rong Luo, and Yong-Feng Jia. Roles of signaling pathways in the epithelial-mesenchymal transition in cancer. *Asian Pacific Journal of Cancer Prevention*, 16(15):6201–6206, October 2015.

[18] Reinhold Fürth. Die brownsche bewegung bei berücksichtigung einer persistenz der bewegungsrichtung. mit anwendungen auf die bewegung lebender infusorien. *Zeitschrift für Physik*, 2(3):244–256, June 1920.

[19] G. E. Uhlenbeck and L. S. Ornstein. On the theory of the brownian motion. *Physical Review*, 36(5):823–841, September 1930.

[20] John L. Tan, Wendy Liu, Celeste M. Nelson, Srivatsan Raghavan, and Christopher S. Chen. Simple approach to micropattern cells on common culture substrates by tuning substrate wettability. *Tissue Engineering*, 10(5–6):865–872, May 2004.

[21] Felix Jakob Segerer, Peter Johan Friedrich Röttgermann, Simon Schuster, Alicia Piera Alberola, Stefan Zahler, and Joachim Oskar Rädler. Versatile method to generate multiple types of micropatterns. *Biointerphases*, 11(1), January 2016.

[22] Jonathan M. Bélisle, Dario Kunik, and Santiago Costantino. Rapid multicomponent optical protein patterning. *Lab on a Chip*, 9(24):3580, 2009.

[23] Pierre-Olivier Strale, Ammar Azioune, Ghislain Bugnicourt, Yohan Lecomte, Makhlad Chahid, and Vincent Studer. Multiprotein printing by light-induced molecular adsorption. *Advanced Materials*, 28(10):2024–2029, December 2015.

[24] David B. Brückner, Alexandra Fink, Christoph Schreiber, Peter J. F. Röttgermann, Joachim O. Rädler, and Chase P. Broedersz. Stochastic nonlinear dynamics of confined cell migration in two-state systems. *Nature Physics*, 15(6):595–601, March 2019.

[25] David B. Brückner, Nicolas Arlt, Alexandra Fink, Pierre Ronceray, Joachim O. Rädler, and Chase P. Broedersz. Learning the dynamics of cell–cell interactions in confined cell migration. *Proceedings of the National Academy of Sciences*, 118(7), February 2021.

[26] M. Abercrombie and Joan E.M. Heaysman. Observations on the social behaviour of cells in tissue culture. *Experimental Cell Research*, 5(1):111–131, 1953.

[27] Carlos Carmona-Fontaine, Helen K. Matthews, Sei Kuriyama, Mauricio Moreno, Graham A. Dunn, Maddy Parsons, Claudio D. Stern, and Roberto Mayor. Contact inhibition of locomotion in vivo controls neural crest directional migration. *Nature*, 456(7224):957–961, December 2008.

[28] John R. Davis, Andrei Luchici, Fuad Mosis, James Thackery, Jesus A. Salazar, Yanlan Mao, Graham A. Dunn, Timo Betz, Mark Miodownik, and Brian M. Stramer. Inter-cellular forces orchestrate contact inhibition of locomotion. *Cell*, 161(2):361–373, April 2015.

[29] Alice Roycroft and Roberto Mayor. Molecular basis of contact inhibition of locomotion. *Cellular and Molecular Life Sciences*, 73(6):1119–1130, November 2015.

[30] Elena B. Pasquale. Eph receptor signalling casts a wide net on cell behaviour. *Nature Reviews Molecular Cell Biology*, 6(6):462–475, June 2005.

[31] F. van Roy and G. Berx. The cell-cell adhesion molecule e-cadherin. *Cellular and Molecular Life Sciences*, 65(23):3756–3788, August 2008.

[32] Quint le Duc, Quanming Shi, Iris Blonk, Arnoud Sonnenberg, Ning Wang, Deborah Leckband, and Johan de Rooij. Vinculin potentiates e-cadherin mechanosensing and is recruited to actin-anchored sites within adherens

junctions in a myosin ii–dependent manner. *Journal of Cell Biology*, 189(7):1107–1115, June 2010.

[33] Peter Coopman and Alexandre Djiane. Adherens junction and e-cadherin complex regulation by epithelial polarity. *Cellular and Molecular Life Sciences*, 73(18):3535–3553, May 2016.

[34] Jugroop Singh, Aldwin Pagulayan, Brian A. Camley, and Amrinder S. Nain. Rules of contact inhibition of locomotion for cells on suspended nanofibers. *Proceedings of the National Academy of Sciences*, 118(12), March 2021.

[35] Daniel F. Milano, Nicholas A. Ngai, Senthil K. Muthuswamy, and Anand R. Asthagiri. Regulators of metastasis modulate the migratory response to cell contact under spatial confinement. *Biophysical Journal*, 110(8):1886–1895, April 2016.

[36] Campbell D Lawson and Keith Burridge. The on-off relationship of rho and rac during integrin-mediated adhesion and cell migration. *Small GTPases*, 5(1):e27958, January 2014.

[37] W. James Nelson. Adaptation of core mechanisms to generate cell polarity. *Nature*, 422(6933):766–774, April 2003.

[38] Lan K. Nguyen, Boris N. Kholodenko, and Alex von Kriegsheim. Rac1 and rhoa: Networks, loops and bistability. *Small GTPases*, 9(4):316–321, September 2016.

[39] Clemens M. Franz, Gareth E. Jones, and Anne J. Ridley. Cell migration in development and disease. *Developmental Cell*, 2(2):153–158, February 2002.

[40] Paolo Maiuri, Emmanuel Terriac, Perrine Paul-Gilloteaux, Timothée Vignaud, Krista McNally, James Onuffer, Kurt Thorn, Phuong A. Nguyen, Nefeli Georgoulia, Daniel Soong, Asier Jayo, Nina Beil, Jürgen Beneke, Joleen Chooi Hong Lim, Chloe Pei-Ying Sim, Yeh-Shiu Chu, Andrea Jiménez-Dalmaroni, Jean-François Joanny, Jean-Paul Thiery, Holger Erfle, Maddy Parsons, Timothy J. Mitchison, Wendell A. Lim, Ana-Maria Lennon-Duménil, Matthieu Piel, and Manuel Théry. The first world cell race. *Current Biology*, 22(17):R673–R675, September 2012.

[41] Pengfei Lu and Yunzhe Lu. Born to run? diverse modes of epithelial migration. *Frontiers in Cell and Developmental Biology*, 9, August 2021.

[42] George S, Martin JAJ, Graziani V, and Sanz-Moreno V. Amoeboid migration in health and disease: Immune responses versus cancer dissemination. *Front Cell Dev Biol.*, 2023.

[43] Lintz M, Muñoz A, and Reinhart-King CA. The mechanics of single cell and collective migration of tumor cells. *J Biomech Eng.*, 139, 2017.

[44] Chiara De Pascalis and Sandrine Etienne-Manneville. Single and collective cell migration: the mechanics of adhesions. *Molecular Biology of the Cell*, 28(14):1833–1846, July 2017.

[45] Eric Theveneau and Roberto Mayor. Collective cell migration of epithelial and mesenchymal cells. *Cellular and Molecular Life Sciences*, 70(19):3481–3492, January 2013.

[46] Wouter-Jan Rappel and Leah Edelstein-Keshet. Mechanisms of cell polarization. *Current Opinion in Systems Biology*, 3:43–53, June 2017.

[47] Sandra Iden and John G. Collard. Crosstalk between small gtpases and polarity proteins in cell polarization. *Nature Reviews Molecular Cell Biology*, 9(11):846–859, November 2008.

[48] Benjamin Woods and Daniel J. Lew. Polarity establishment by cdc42: Key roles for positive feedback and differential mobility. *Small GTPases*, 10(2):130–137, March 2017.

[49] Sudeepa Rajan, Dmitri S. Kudryashov, and Emil Reisler. Actin bundles dynamics and architecture. *Biomolecules*, 13(3):450, February 2023.

[50] A. Mogilner and G. Oster. Cell motility driven by actin polymerization. *Biophysical Journal*, 71(6):3030–3045, December 1996.

[51] C.S. Peskin, G.M. Odell, and G.F. Oster. Cellular motions and thermal fluctuations: the brownian ratchet. *Biophysical Journal*, 65(1):316–324, July 1993.

[52] Vinay Swaminathan, Joseph Mathew Kalappurakkal, Shalin B. Mehta, Pontus Nordenfelt, Travis I. Moore, Nobuyasu Koga, David A. Baker, Rudolf Oldenbourg, Tomomi Tani, Satyajit Mayor, Timothy A. Springer, and Clare M. Waterman. Actin retrograde flow actively aligns and orients ligand-engaged integrins in focal adhesions. *Proceedings of the National Academy of Sciences*, 114(40):10648–10653, October 2017.

[53] Zhongwen Chen, Dongmyung Oh, Kabir H. Biswas, Cheng-Han Yu, Ronen Zaidel-Bar, and Jay T. Groves. Spatially modulated ephrina1:epha2 signaling increases local contractility and global focal adhesion dynamics to promote cell motility. *Proceedings of the National Academy of Sciences*, 115(25), June 2018.

[54] A. Huttenlocher and A. R. Horwitz. Integrins in cell migration. *Cold Spring Harbor Perspectives in Biology*, 3(9):a005074–a005074, September 2011.

[55] Michalina Janiszewska, Marina Candido Primi, and Tina Izard. Cell adhesion in cancer: Beyond the migration of single cells. *Journal of Biological Chemistry*, 295(8):2495–2505, February 2020.

[56] Miguel Vicente-Manzanares, Xuefei Ma, Robert S. Adelstein, and Alan Rick Horwitz. Non-muscle myosin ii takes centre stage in cell adhesion and migration. *Nature Reviews Molecular Cell Biology*, 10(11):778–790, November 2009.

[57] Ehsan Jabbarzadeh. Polarity as a physiological modulator of cell function. *Frontiers in Bioscience*, 24(3):451–462, 2019.

[58] Terry Lechler and Elaine Fuchs. Asymmetric cell divisions promote stratification and differentiation of mammalian skin. *Nature*, 437(7056):275–280, August 2005.

[59] David G Drubin and W.James Nelson. Origins of cell polarity. *Cell*, 84(3):335–344, February 1996.

[60] Soichiro Yamada and W. James Nelson. Localized zones of rho and rac activities drive initiation and expansion of epithelial cell–cell adhesion. *The Journal of Cell Biology*, 178(3):517–527, July 2007.

[61] Joanna L. MacKay and Sanjay Kumar. Simultaneous and independent tuning of rhoa and rac1 activity with orthogonally inducible promoters. *Integrative Biology*, 6(9):885–894, July 2014.

[62] Daniel A. Fletcher and R. Dyche Mullins. Cell mechanics and the cytoskeleton. *Nature*, 463(7280):485–492, January 2010.

[63] Hohmann and Dehghani. The cytoskeleton—a complex interacting meshwork. *Cells*, 8(4):362, April 2019.

[64] Adrian F. Pegoraro, Paul Janmey, and David A. Weitz. Mechanical properties of the cytoskeleton and cells. *Cold Spring Harbor Perspectives in Biology*, 9(11):a022038, November 2017.

[65] Michael F. Olson and Erik Sahai. The actin cytoskeleton in cancer cell motility. *Clinical & Experimental Metastasis*, 26(4), May 2008.

[66] Narendra Thapa, Tianmu Wen, Vincent L. Cryns, and Richard A. Anderson. Regulation of cell adhesion and migration via microtubule cytoskeleton organization, cell polarity, and phosphoinositide signaling. *Biomolecules*, 13(10):1430, September 2023.

[67] J. Victor Small, Benjamin Geiger, Irina Kaverina, and Alexander Bershadsky. How do microtubules guide migrating cells? *Nature Reviews Molecular Cell Biology*, 3(12):957–964, December 2002.

[68] Alexander F. Palazzo, Tiffani A. Cook, Arthur S. Alberts, and Gregg G. Gundersen. mdia mediates rho-regulated formation and orientation of stable microtubules. *Nature Cell Biology*, 3(8):723–729, July 2001.

[69] Keith Burridge and Christophe Guilluy. Focal adhesions, stress fibers and mechanical tension. *Experimental Cell Research*, 343(1):14–20, April 2016.

[70] Sari Tojkander, Gergana Gateva, and Pekka Lappalainen. Actin stress fibers – assembly, dynamics and biological roles. *Journal of Cell Science*, January 2012.

[71] Elena Kassianidou and Sanjay Kumar. A biomechanical perspective on stress fiber structure and function. *Biochimica et Biophysica Acta (BBA) - Molecular Cell Research*, 1853(11):3065–3074, November 2015.

[72] Roberto Mayor and Sandrine Etienne-Manneville. The front and rear of collective cell migration. *Nature Reviews Molecular Cell Biology*, 17(2):97–109, January 2016.

[73] Thuan Beng Saw, Shreyansh Jain, Benoit Ladoux, and Chwee Teck Lim. Mechanobiology of collective cell migration. *Cellular and Molecular Bioengineering*, 8(1):3–13, November 2014.

[74] Lei Qin, Dazhi Yang, Weihong Yi, Huiling Cao, and Guozhi Xiao. Roles of leader and follower cells in collective cell migration. *Molecular Biology of the Cell*, 32(14):1267–1272, July 2021.

[75] Denise J. Montell. Border-cell migration: the race is on. *Nature Reviews Molecular Cell Biology*, 4(1):13–24, January 2003.

[76] Petra Haas and Darren Gilmour. Chemokine signaling mediates self-organizing tissue migration in the zebrafish lateral line. *Developmental Cell*, 10(5):673–680, May 2006.

[77] Elena Scarpa and Roberto Mayor. Collective cell migration in development. *Journal of Cell Biology*, 212(2):143–155, January 2016.

[78] Roberto Mayor and Carlos Carmona-Fontaine. Keeping in touch with contact inhibition of locomotion. *Trends in Cell Biology*, 20(6):319–328, June 2010.

[79] Ricard Alert and Xavier Trepat. Physical models of collective cell migration. *Annual Review of Condensed Matter Physics*, 11(1):77–101, March 2020.

[80] András Szabó, Eric Theveneau, Melissa Turan, and Roberto Mayor. Neural crest streaming as an emergent property of tissue interactions during morphogenesis. *PLOS Computational Biology*, 15(4):e1007002, April 2019.

[81] Jonathan W. Astin, Jennifer Batson, Shereen Kadir, Jessica Charlet, Raj A. Persad, David Gillatt, Jon D. Oxley, and Catherine D. Nobes. Competition amongst eph receptors regulates contact inhibition of locomotion and invasiveness in prostate cancer cells. *Nature Cell Biology*, 12(12):1194–1204, November 2010.

[82] Dmitry V. Ayollo, Irina Y. Zhitnyak, Jury M. Vasiliev, and Natalya A. Gloushankova. Rearrangements of the actin cytoskeleton and e-cadherin–based adherens junctions caused by neoplasic transformation change cell–cell interactions. *PLoS ONE*, 4(11):e8027, November 2009.

[83] ME Bracke, H Depypere, C Labit, V Van Marck, K Vennekens, SJ Vermeulen, I Maelfait, J Philippé, R Serreyn, and MM Mareel. Functional downregulation of the e-cadherin/catenin complex leads to loss of contact inhibition of motility and of mitochondrial activity, but not of growth in confluent epithelial cell cultures. *European journal of cell biology*, 74(4):342—349, December 1997.

[84] Eric Theveneau, Lorena Marchant, Sei Kuriyama, Mazhar Gull, Barbara Moepps, Maddy Parsons, and Roberto Mayor. Collective chemotaxis requires contact-dependent cell polarity. *Developmental Cell*, 19(1):39–53, July 2010.

[85] Benoit Ladoux and Alice Nicolas. Physically based principles of cell adhesion mechanosensitivity in tissues. *Reports on Progress in Physics*, 75(11):116601, October 2012.

[86] Tom Shemesh, Benjamin Geiger, Alexander D. Bershadsky, and Michael M. Kozlov. Focal adhesions as mechanosensors: A physical mechanism. *Proceedings of the National Academy of Sciences*, 102(35):12383–12388, August 2005.

[87] Andrea Hartsock and W. James Nelson. Adherens and tight junctions: Structure, function and connections to the actin cytoskeleton. *Biochimica et Biophysica Acta (BBA) - Biomembranes*, 1778(3):660–669, March 2008.

[88] Ravi A. Desai, Lin Gao, Srivatsan Raghavan, Wendy F. Liu, and Christopher S. Chen. Cell polarity triggered by cell-cell adhesion via e-cadherin. *Journal of Cell Science*, 122(7):905–911, April 2009.

[89] Masato Nakagawa, Masaki Fukata, Masaki Yamaga, Naohiro Itoh, and Kozo Kaibuchi. Recruitment and activation of rac1 by the formation of e-cadherin-mediated cell-cell adhesion sites. *Journal of Cell Science*, 114(10):1829–1838, May 2001.

[90] Luis Glaser. Cell-cell recognition. *Trends in Biochemical Sciences*, 1(2):84–86, 1976.

[91] Dimitar B. Nikolov, Kai Xu, and Juha P. Himanen. Eph/ephrin recognition and the role of eph/ephrin clusters in signaling initiation. *Biochimica et Biophysica Acta (BBA) - Proteins and Proteomics*, 1834(10):2160–2165, October 2013.

[92] Elena B. Pasquale. Eph-ephrin bidirectional signaling in physiology and disease. *Cell*, 133(1):38–52, April 2008.

[93] Thayer K. Darling and Tracey J. Lamb. Emerging roles for eph receptors and ephrin ligands in immunity. *Frontiers in Immunology*, 10, July 2019.

[94] J. Frisen. Ephrins and their eph receptors: multitalented directors of embryonic development. *The EMBO Journal*, 18(19):5159–5165, October 1999.

[95] Uwe Drescher, Friedrich Bonhoeffer, and Bernhard K Müller. The eph family in retinal axon guidance. *Current Opinion in Neurobiology*, 7(1):75–80, February 1997.

[96] Yu-Xiong Feng, Jiang-Sha Zhao, Jing-Jing Li, Tao Wang, Shu-Qun Cheng, Yunfei Yuan, Fudi Wang, Xiao-Fan Wang, and Dong Xie. Liver cancer: Ephrina2 promotes tumorigenicity through rac1/akt/nf-κ b signaling pathway. *Hepatology*, 51(2):535–544, September 2009.

[97] Brian P Fox and Raj P Kandpal. Invasiveness of breast carcinoma cells and transcript profile: Eph receptors and ephrin ligands as molecular markers of potential diagnostic and prognostic application. *Biochemical and Biophysical Research Communications*, 318(4):882–892, June 2004.

[98] Yukiko Nakaya and Guojun Sheng. Epithelial to mesenchymal transition during gastrulation: An embryological view. *Development, Growth & Differentiation*, 50(9):755–766, November 2008.

[99] David M. Gonzalez and Damian Medici. Signaling mechanisms of the epithelial-mesenchymal transition. *Science Signaling*, 7(344), September 2014.

[100] Matjaz Rokavec, Meryem Gülfem Öner, and Heiko Hermeking. lnflammation-induced epigenetic switches in cancer. *Cellular and Molecular Life Sciences*, 73(1):23–39, September 2015.

[101] Augustine Chen, Henry Beetham, Michael A Black, Rashmi Priya, Bryony J Telford, Joanne Guest, George A R Wiggins, Tanis D Godwin, Alpha S Yap, and Parry J Guilford. E-cadherin loss alters cytoskeletal organization and adhesion in non-malignant breast cells but is insufficient to induce an epithelial-mesenchymal transition. *BMC Cancer*, 14(1), July 2014.

[102] Cameron P. Bracken, Philip A. Gregory, Natasha Kolesnikoff, Andrew G. Bert, Jun Wang, M. Frances Shannon, and Gregory J. Goodall. A double-negative feedback loop between zeb1-sip1 and the microrna-200 family regulates epithelial-mesenchymal transition. *Cancer Research*, 68(19):7846–7854, September 2008.

[103] Yoran Margaron, Tomoaki Nagai, Laurent Guyon, Laetitia Kurzawa, Anne-Pierre Morel, Alice Pinheiro, Laurent Blanchoin, Fabien Reyal, Alain Puisieux, and Manuel Théry. Biophysical properties of intermediate states of emt outperform both epithelial and mesenchymal states. October 2019.

[104] Mingyang Lu, Mohit Kumar Jolly, Herbert Levine, José N. Onuchic, and Eshel Ben-Jacob. Microrna-based regulation of epithelial–hybrid–mesenchymal fate determination. *Proceedings of the National Academy of Sciences*, 110(45):18144–18149, October 2013.

[105] Andreas Buttenschön and Leah Edelstein-Keshet. Bridging from single to collective cell migration: A review of models and links to experiments. *PLOS Computational Biology*, 16(12):e1008411, December 2020.

[106] Ulrich S. Schwarz and Samuel A. Safran. Physics of adherent cells. *Reviews of Modern Physics*, 85(3):1327–1381, August 2013.

[107] Gaudenz Danuser, Jun Allard, and Alex Mogilner. Mathematical modeling of eukaryotic cell migration: Insights beyond experiments. *Annual Review of Cell and Developmental Biology*, 29(1):501–528, October 2013.

[108] Athanasius F. M. Marée, Verônica A. Grieneisen, and Paulien Hogeweg. *The Cellular Potts Model and Biophysical Properties of Cells, Tissues and Morphogenesis*, page 107–136. Birkhäuser Basel.

[109] Kaori Sugimura and Hiroshi Kori. A reduced cell-based phase model for tissue polarity alignment through global anisotropic cues. *Scientific Reports*, 7(1), December 2017.

[110] Mitchell H. Gail and Charles W. Boone. The locomotion of mouse fibroblasts in tissue culture. *Biophysical Journal*, 10(10):980–993, October 1970.

[111] Jonathan R. Howse, Richard A. L. Jones, Anthony J. Ryan, Tim Gough, Reza Vafabakhsh, and Ramin Golestanian. Self-motile colloidal particles: From directed propulsion to random walk. *Physical Review Letters*, 99(4), July 2007.

[112] Adele Wright, Yu-Hua Li, and Cheng Zhu. The differential effect of endothelial cell factors on in vitro motility of malignant and non-malignant cells. *Annals of Biomedical Engineering*, 36(6):958–969, April 2008.

[113] Cynthia L. Stokes, Douglas A. Lauffenburger, and Stuart K. Williams. Migration of individual microvessel endothelial cells: stochastic model and parameter measurement. *Journal of Cell Science*, 99(2):419–430, June 1991.

[114] D. Selmeczi, L. Li, L. I.I. Pedersen, S. F. Nrrelykke, P. H. Hagedorn, S. Mosler, N. B. Larsen, E. C. Cox, and H. Flyvbjerg. Cell motility as random motion: A review: Cell motility as random motion. *The European Physical Journal Special Topics*, 157(1):1–15, April 2008.

[115] David Selmeczi, Stephan Mosler, Peter H. Hagedorn, Niels B. Larsen, and Henrik Flyvbjerg. Cell motility as persistent random motion: Theories from experiments. *Biophysical Journal*, 89(2):912–931, August 2005.

[116] Alexander R Sprenger, Lorenzo Caprini, Hartmut Löwen, and René Wittmann. Dynamics of active particles with translational and rotational inertia. *Journal of Physics: Condensed Matter*, 35(30):305101, April 2023.

[117] Ahmed Al Harraq, Mustapha Bello, and Bhuvnesh Bharti. A guide to design the trajectory of active particles: From fundamentals to applications. *Current Opinion in Colloid amp; Interface Science*, 61:101612, October 2022.

[118] François Graner and James A. Glazier. Simulation of biological cell sorting using a two-dimensional extended potts model. *Physical Review Letters*, 69(13):2013–2016, September 1992.

[119] R. Allena, M. Scianna, and L. Preziosi. A cellular potts model of single cell migration in presence of durotaxis. *Mathematical Biosciences*, 275:57–70, May 2016.

[120] Néstor Sepúlveda, Laurence Petitjean, Olivier Cochet, Erwan Grasland-Mongrain, Pascal Silberzan, and Vincent Hakim. Collective cell motion in an epithelial sheet can be quantitatively described by a stochastic interacting particle model. *PLoS Computational Biology*, 9(3):e1002944, March 2013.

[121] Mishel George, Francesco Bullo, and Otger Campàs. Connecting individual to collective cell migration. *Scientific Reports*, 7(1), August 2017.

[122] Markus Basan, Jens Elgeti, Edouard Hannezo, Wouter-Jan Rappel, and Herbert Levine. Alignment of cellular motility forces with tissue flow as a mechanism for efficient wound healing. *Proceedings of the National Academy of Sciences*, 110(7):2452–2459, January 2013.

[123] Guilherme S. Y. Giardini and Gilberto L. Thomas. Velocities of mesenchymal cells may be ill-defined, 10 2023.

[124] Dirk Alexander Kulawiak, Brian A. Camley, and Wouter-Jan Rappel. Modeling contact inhibition of locomotion of colliding cells migrating on micropatterned substrates. *PLOS Computational Biology*, 12(12):e1005239, December 2016.

[125] Johannes C. J. Heyn, Joachim O. Rädler, and Martin Falcke. Mesenchymal cell migration on one-dimensional micropatterns. *Frontiers in Cell and Developmental Biology*, 12, April 2024.

[126] Manuel Théry and Matthieu Piel. *Micropatterning in Cell Biology, Part C*, volume 121. Academic Press, 2014.

[127] Behnam Amiri, Johannes C.J. Heyn, Christoph Schreiber, Joachim O. Rädler, and Martin Falcke. On multistability and constitutive relations of cell motion on fibronectin lanes. *Biophysical Journal*, 122(5):753–766, March 2023.

[128] Stefan Stöberl, Miriam Balles, Thomas Kellerer, and Joachim O. Rädler. Photolithographic microfabrication of hydrogel clefts for cell invasion studies. *Lab on a Chip*, 23(7):1886–1895, 2023.

[129] Elisa D'Arcangelo and Alison P McGuigan. Micropatterning strategies to engineer controlled cell and tissue architecture in vitro. *BioTechniques*, 58(1):13–23, January 2015.

[130] Ammar Azioune, Nicolas Carpi, Qingzong Tseng, Manuel Théry, and Matthieu Piel. *Protein Micropatterns*, page 133–146. Elsevier, 2010.

[131] Eléonore Vercurysse, David B. Brückner, Manuel Gómez-González, Alexandre Remson, Marine Luciano, Yohalie Kalukula, Leone Rossetti, Xavier Trepat, Edouard Hannezo, and Sylvain Gabriele. Geometry-driven migration efficiency of autonomous epithelial cell clusters. July 2022.

[132] Jonathan M. Bélisle, James P. Correia, Paul W. Wiseman, Timothy E. Kennedy, and Santiago Costantino. Patterning protein concentration using laser-assisted adsorption by photobleaching, lapap. *Lab on a Chip*, 8(12):2164, 2008.

[133] Andrew D. Doyle, Matthew L. Kutys, Mary Anne Conti, Kazue Matsumoto, Robert S. Adelstein, and Kenneth M. Yamada. Microenvironmental control of cell migration: Myosin iia is required for efficient migration in fibrillar environments through control of cell adhesion dynamics. *Journal of Cell Science*, January 2012.

[134] Aurélien Pasturel Vincent Studer. Generic method for structuring hydrogels. Patent WO 2020002495 A1, 1 2020. Patent number: WO2020002495A1.

[135] Alexandra Fink, David B. Brückner, Christoph Schreiber, Peter J.F. Röttgermann, Chase P. Broedersz, and Joachim O. Rädler. Area and geometry dependence of cell migration in asymmetric two-state micropatterns. *Biophysical Journal*, 118(3):552–564, February 2020.

[136] Johannes Flommersfeld, Stefan Stöberl, Omar Shah, Joachim O. Rädler, and Chase P. Broedersz. Geometry-sensitive protrusion growth directs confined cell migration, 2023.

[137] Kalpana Mandal, Martial Balland, and Lionel Bureau. Thermoresponsive micropatterned substrates for single cell studies. *PLoS ONE*, 7(5):e37548, May 2012.

[138] Bojan Ljepoja, Christoph Schreiber, Florian A. Gegenfurtner, Jonathan García-Roman, Bianca Köhler, Stefan Zahler, Joachim O. Rädler, Ernst Wagner, and Andreas Roidl. Inducible microrna-200c decreases motility of breast cancer cells and reduces filamin a. *PLOS ONE*, 14(11):e0224314, November 2019.

[139] Christoph Schreiber, Behnam Amiri, Johannes C. J. Heyn, Joachim O. Rädler, and Martin Falcke. On the adhesion–velocity relation and length adaptation of motile cells on stepped fibronectin lanes. *Proceedings of the National Academy of Sciences*, 118(4), January 2021.

[140] Danahe Mohammed, Guillaume Charras, Eléonore Vercruysse, Marie Versaevel, Joséphine Lantoine, Laura Alaimo, Céline Bruyère, Marine Luciano, Karine Glinel, Geoffrey Delhaye, Olivier Théodoly, and Sylvain Gabriele. Substrate area confinement is a key determinant of cell velocity in collective migration. *Nature Physics*, 15(8):858–866, June 2019.

[141] Takehisa Matsuda and Takashi Sugawara. Control of cell adhesion, migration, and orientation on photochemically microprocessed surfaces. *Journal of Biomedical Materials Research*, 32(2):165–173, October 1996.

[142] Charles O'Neill, Peter Jordan, Peter Riddle, and Grenham Ireland. Narrow linear strips of adhesive substratum are powerful inducers of both growth and total focal contact area. *Journal of Cell Science*, 95(4):577–586, April 1990.

[143] Kurt Thorn. A quick guide to light microscopy in cell biology. *Molecular Biology of the Cell*, 27(2):219–222, January 2016.

[144] P.J. Evennett and C. Hammond. *MICROSCOPY — Overview*, page 32–41. Elsevier, 2005.

[145] Javier Ramón-Azcón, Gerardo Lopez-Muñoz, and Artur Rydosz. *Fundamentals*, page 105–135. Elsevier, 2024.

[146] Robert W. Lovitt and Chris J. Wright. *MICROSCOPY — Light Microscopy*, page 1379–1388. Elsevier, 1999.

[147] John D. Bancroft and Alton D. Floyd. *Light microscopy*, page 37–68. Elsevier, 2013.

[148] Jeff W Lichtman and José-Angel Conchello. Fluorescence microscopy. *Nature Methods*, 2(12):910–919, November 2005.

[149] Michael J. Sanderson, Ian Smith, Ian Parker, and Martin D. Bootman. Fluorescence microscopy. *Cold Spring Harbor Protocols*, 2014(10):pdb.top071795, October 2014.

[150] Joerg Schnitzbauer, Maximilian T Strauss, Thomas Schlichthaerle, Florian Schueder, and Ralf Jungmann. Super-resolution microscopy with dna-paint. *Nature Protocols*, 12(6):1198–1228, May 2017.

[151] Giuseppe Vicidomini, Paolo Bianchini, and Alberto Diaspro. Sted super-resolved microscopy. *Nature Methods*, 15(3):173–182, January 2018.

[152] Michael Weber, Marcel Leutenegger, Stefan Stoldt, Stefan Jakobs, Tiberiu S. Mihaila, Alexey N. Butkevich, and Stefan W. Hell. Minsted fluorescence localization and nanoscopy. *Nature Photonics*, 15(5):361–366, March 2021.

[153] Lynn M. Ostersehlt, Daniel C. Jans, Anna Wittek, Jan Keller-Findeisen, Kaushik Inamdar, Steffen J. Sahl, Stefan W. Hell, and Stefan Jakobs. Dna-paint minflux nanoscopy. *Nature Methods*, 19(9):1072–1075, September 2022.

[154] Amicia D. Elliott. Confocal microscopy: Principles and modern practices. *Current Protocols in Cytometry*, 92(1), December 2019.

[155] James Jonkman, Claire M. Brown, Graham D. Wright, Kurt I. Anderson, and Alison J. North. Tutorial: guidance for quantitative confocal microscopy. *Nature Protocols*, 15(5):1585–1611, March 2020.

[156] D.A. Peterson. *Confocal Microscopy*, page 250–252. Elsevier, 2010.

[157] Joseph Huff. The airyscan detector from zeiss: confocal imaging with improved signal-to-noise ratio and super-resolution. *Nature Methods*, 12(12):i–ii, December 2015.

[158] Kseniya Korobchevskaya, B. Lagerholm, Huw Colin-York, and Marco Fritzsche. Exploring the potential of airyscan microscopy for live cell imaging. *Photonics*, 4(4):41, July 2017.

[159] Marcus Prass, Ken Jacobson, Alex Mogilner, and Manfred Radmacher. Direct measurement of the lamellipodial protrusive force in a migrating cell. *The Journal of Cell Biology*, 174(6):767–772, September 2006.

[160] Fabian Heinemann, Holger Doschke, and Manfred Radmacher. Keratocyte lamellipodial protrusion is characterized by a concave force-velocity relation. *Biophysical Journal*, 100(6):1420–1427, March 2011.

[161] Adriana T. Dawes and Leah Edelstein-Keshet. Phosphoinositides and rho proteins spatially regulate actin polymerization to initiate and maintain directed movement in a one-dimensional model of a motile cell. *Biophysical Journal*, 92(3):744–768, February 2007.

[162] Deborah Fanfone, Zhichong Wu, Jade Mammi, Kevin Berthenet, David Neves, Kathrin Weber, Andrea Halaburkova, François Virard, Félix Bunel, Catherine Jamard, Hector Hernandez-Vargas, Stephen WG Tait, Ana Hennino, and Gabriel Ichim. Confined migration promotes cancer metastasis through resistance to anoikis and increased invasiveness. *eLife*, 11, March 2022.

[163] Merino-Casallo F, Gomez-Benito MJ, Hervas-Raluy S, and Garcia-Aznar JM. Unravelling cell migration: defining movement from the cell surface. *Cell Adh Migr.*, 16:25 64, 2022.

[164] Chin-Yap Loh, Jian Chai, Ting Tang, Won Wong, Gautam Sethi, Muthu Shanmugam, Pei Chong, and Chung Looi. The e-cadherin and n-cadherin switch in epithelial-to-mesenchymal transition: Signaling, therapeutic implications, and challenges. *Cells*, 8(10):1118, September 2019.

[165] Hwa-Jin Son and Aree Moon. Epithelial-mesenchymal transition and cell invasion. *Toxicological Research*, 26(4):245–252, December 2010.

[166] Bianca Köhler, Emily Brieger, Tom Brandstätter, Elisa Hörterer, Ulrich Wilk, Jana Pöhmerer, Anna Jötten, Philipp Paulitschke, Chase P Broedersz, Stefan Zahler, Joachim O Rädler, Ernst Wagner, and Andreas Roidl. Unravelling the metastasis-preventing effect of mir-200c in vitro and in vivo. November 2023.

[167] Yuhe Huang, Weiqi Hong, and Xiawei Wei. The molecular mechanisms and therapeutic strategies of emt in tumor progression and metastasis. *Journal of Hematology & Oncology*, 15(1), September 2022.

[168] Yutong Sha, Daniel Haensel, Guadalupe Gutierrez, Huijing Du, Xing Dai, and Qing Nie. Intermediate cell states in epithelial-to-mesenchymal transition. *Physical Biology*, 16(2):021001, January 2019.

[169] Piyush B. Gupta, Ievgenia Pastushenko, Adam Skibinski, Cedric Blanpain, and Charlotte Kuperwasser. Phenotypic plasticity: Driver of cancer initiation, progression, and therapy resistance. *Cell Stem Cell*, 24(1):65–78, January 2019.

[170] Ievgenia Pastushenko and Cédric Blanpain. Emt transition states during tumor progression and metastasis. *Trends in Cell Biology*, 29(3):212–226, March 2019.

[171] Brock Humphries and Chengfeng Yang. The microrna-200 family: small molecules with novel roles in cancer development, progression and therapy. *Oncotarget*, 6(9):6472–6498, January 2015.

[172] Ilan Elson-Schwab, Anna Lorentzen, and Christopher J. Marshall. Microrna-200 family members differentially regulate morphological plasticity and mode of melanoma cell invasion. *PLoS ONE*, 5(10):e13176, October 2010.

[173] Tzachi Hagai, Xi Chen, Ricardo J. Miragaia, Raghd Rostom, Tomás Gomes, Natalia Kunowska, Johan Henriksson, Jong-Eun Park, Valentina Proserpio, Giacomo Donati, Lara Bossini-Castillo, Felipe A. Vieira Braga, Guy Naamati, James Fletcher, Emily Stephenson, Peter Vegh, Gosia Trynka, Ivanela Kondova, Mike Dennis, Muzlifah Haniffa, Armita Nourmohammad, Michael Lässig, and Sarah A. Teichmann. Gene expression variability across cells and species shapes innate immunity. *Nature*, 563(7730):197–202, October 2018.

[174] Dimitra Georgopoulou, Maurizio Callari, Oscar M. Rueda, Abigail Shea, Alistair Martin, Agnese Giovannetti, Fatime Qosaj, Ali Dariush, Suet-Feung Chin, Larissa S. Carnevalli, Elena Provenzano, Wendy Greenwood, Giulia

Lerda, Elham Esmaeilishirazifard, Martin O'Reilly, Violeta Serra, Dario Bressan, H. R. Ali, M. Al Sa'd, S. Alon, S. Aparicio, G. Battistoni, S. Balasubramanian, R. Becker, B. Bodenmiller, E. S. Boyden, D. Bressan, A. Bruna, Marcel Burger, C. Caldas, M. Callari, I. G. Cannell, H. Casbolt, N. Chornay, Y. Cui, A. Dariush, K. Dinh, A. Emenari, Y. Eyal-Lubling, J. Fan, A. Fatemi, E. Fisher, E. A. González-Solares, C. González-Fernández, D. Goodwin, W. Greenwood, F. Grimaldi, G. J. Hannon, O. Harris, S. Harris, C. Jauset, J. A. Joyce, E. D. Karagiannis, T. Kovačević, L. Kuett, R. Kunes, Yoldaş A. Küpcü, D. Lai, E. Laks, H. Lee, M. Lee, G. Lerda, Y. Li, A. McPherson, N. Millar, C. M. Mulvey, F. Nugent, C. H. O'Flanagan, M. Paez-Ribes, I. Pearsall, F. Qosaj, A. J. Roth, O. M. Rueda, T. Ruiz, K. Sawicka, L. A. Sepúlveda, S. P. Shah, A. Shea, A. Sinha, A. Smith, S. Tavaré, S. Tietscher, I. Vázquez-García, S. L. Vogl, N. A. Walton, A. T. Wassie, S. S. Watson, J. Weselak, S. A. Wild, E. Williams, J. Windhager, T. Whitmarsh, C. Xia, P. Zheng, X. Zhuang, Gordon B. Mills, H. Raza Ali, Sabina S. Cosulich, Gregory J. Hannon, Alejandra Bruna, and Carlos Caldas. Landscapes of cellular phenotypic diversity in breast cancer xenografts and their impact on drug response. *Nature Communications*, 12(1), March 2021.

[175] Andrew C Callan-Jones and Raphaël Voituriez. Actin flows in cell migration: from locomotion and polarity to trajectories. *Current Opinion in Cell Biology*, 38:12–17, February 2016.

[176] Jean Paul Thiery, Hervé Acloque, Ruby Y.J. Huang, and M. Angela Nieto. Epithelial-mesenchymal transitions in development and disease. *Cell*, 139(5):871–890, November 2009.

[177] Jürgen Behrens, K. Michael Weidner, Uwe H. Frixen, Jörg H. Schipper, Martin Sachs, Naokatu Arakaki, Yasushi Daikuhara, and Walter Birchmeier. *The role of E-cadherin and scatter factor in tumor invasion and cell motility*, page 109–126. Birkhäuser Basel, 1991.

[178] Christopher T. Capaldo and Ian G. Macara. Depletion of e-cadherin disrupts establishment but not maintenance of cell junctions in madin-darby canine kidney epithelial cells. *Molecular Biology of the Cell*, 18(1):189–200, January 2007.

[179] Marvin T. Nieman, Ryan S. Prudoff, Keith R. Johnson, and Margaret J. Wheelock. N-cadherin promotes motility in human breast cancer cells regardless of their e-cadherin expression. *The Journal of Cell Biology*, 147(3):631–644, November 1999.

[180] Ganesan Arunkumar, Arunagiri Deva Magendhra Rao, Mayakannan Manikandan, Harikrishnan Prasanna Srinivasa Rao, Shanmugam Subbiah, Ramachandran Ilangovan, Avaniyapuram Murugan, and Arasambattu Munirajan. Dysregulation of mir-200 family microrna s and epithelial-mesenchymal transition markers in oral squamous cell carcinoma. *Oncology Letters*, October 2017.

[181] Rachel A. Battaglia, Samed Delic, Harald Herrmann, and Natasha T. Snider. Vimentin on the move: new developments in cell migration. *F1000Research*, 7:1796, November 2018.

[182] Shimrit Mayer, Tomer Milo, Achinoam Isaacson, Coral Halperin, Shoval Miyara, Yaniv Stein, Chen Lior, Meirav Pevsner-Fischer, Eldad Tzahor, Avi Mayo, Uri Alon, and Ruth Scherz-Shouval. The tumor microenvironment shows a hierarchy of cell-cell interactions dominated by fibroblasts. *Nature Communications*, 14(1), September 2023.

[183] Katarzyna Kamińska, Cezary Szczylik, Zofia F. Bielecka, Ewa Bartnik, Camillo Porta, Fei Lian, and Anna M. Czarnecka. The role of the cell–cell interactions in cancer progression. *Journal of Cellular and Molecular Medicine*, 19(2):283–296, January 2015.

[184] David B Brückner and Chase P Broedersz. Learning dynamical models of single and collective cell migration: a review. *Reports on Progress in Physics*, 87(5):056601, April 2024.

[185] David B. Brückner, Matthew Schmitt, Alexandra Fink, Georg Ladurner, Johannes Flommersfeld, Nicolas Arlt, Edouard Hannezo, Joachim O. Rädler, and Chase P. Broedersz. Geometry adaptation of protrusion and polarity dynamics in confined cell migration. *Physical Review X*, 12(3), September 2022.

[186] Themistoklis Zisis, David B. Brückner, Tom Brandstätter, Wei Xiong Siow, Joseph d'Alessandro, Angelika M. Vollmar, Chase P. Broedersz, and Stefan Zahler. Disentangling cadherin-mediated cell-cell interactions in collective cancer cell migration. *Biophysical Journal*, 121(1):44–60, January 2022.

[187] Caitlin M. Logan, Suren Rajakaruna, Caitlin Bowen, Glenn L. Radice, Michael L. Robinson, and A. Sue Menko. N-cadherin regulates signaling mechanisms required for lens fiber cell elongation and lens morphogenesis. *Developmental Biology*, 428(1):118–134, August 2017.

[188] Elena Scarpa, András Szabó, Anne Bibonne, Eric Theveneau, Maddy Parsons, and Roberto Mayor. Cadherin switch during emt in neural crest cells leads to contact inhibition of locomotion via repolarization of forces. *Developmental Cell*, 34(4):421–434, August 2015.

[189] Jakob Löber, Falko Ziebert, and Igor S. Aranson. Collisions of deformable cells lead to collective migration. *Scientific Reports*, 5(1), March 2015.

[190] Brian A. Camley and Wouter-Jan Rappel. Velocity alignment leads to high persistence in confined cells. *Physical Review E*, 89(6), June 2014.

[191] Verona Villar-Cerviño, Manuel Molano-Mazón, Timothy Catchpole, Miguel Valdeolmillos, Mark Henkemeyer, Luis M. Martínez, Víctor Borrell, and Oscar Marín. Contact repulsion controls the dispersion and final distribution of cajal-retzius cells. *Neuron*, 77(3):457–471, February 2013.

[192] Ravi A. Desai, Smitha B. Gopal, Sophia Chen, and Christopher S. Chen. Contact inhibition of locomotion probabilities drive solitary versus collective cell migration. *Journal of The Royal Society Interface*, 10(88):20130717, November 2013.

[193] Masayuki Hayakawa, Tetsuya Hiraiwa, Yuko Wada, Hidekazu Kuwayama, and Tatsuo Shibata. Polar pattern formation induced by contact following locomotion in a multicellular system. December 2019.

[194] Supriya Bajpai, Ranganathan Prabhakar, Raghunath Chelakkot, and Mandar M. Inamdar. Role of cell polarity dynamics and motility in pattern formation due to contact-dependent signalling. *Journal of The Royal Society Interface*, 18(175), February 2021.

[195] Jonathan E. Ron, Joseph d'Alesandro, Victor Cellerin, Raphael Voituriéz, Benoit Ladoux, and Nir S. Gov. Polarization and motility of one-dimensional multi-cellular trains. July 2023.

[196] Nizar N Batada, Larry A Shepp, David O Siegmund, and Michael Levitt. Spatial regulation and the rate of signal transduction activation. *PLoS Computational Biology*, 2(5):e44, May 2006.

[197] Randall Marsh and Robert Brackenbury. *Molecules of cell adhesion and recognition: An overview*, page 1–32. Elsevier, 1996.

[198] Gregory F. Weber, Maureen A. Bjerke, and Douglas W. DeSimone. A mechanoresponsive cadherin-keratin complex directs polarized protrusive behavior and collective cell migration. *Developmental Cell*, 22(1):104–115, January 2012.

[199] Brenton D. Hoffman, Carsten Grashoff, and Martin A. Schwartz. Dynamic molecular processes mediate cellular mechanotransduction. *Nature*, 475(7356):316–323, July 2011.

[200] Shreyansh Jain, Victoire M. L. Cachoux, Gautham H. N. S. Narayana, Simon de Beco, Joseph D'Alessandro, Victor Cellerin, Tianchi Chen, Mélina L. Heuzé, Philippe Marcq, René-Marc Mège, Alexandre J. Kabla, Chwee Teck Lim, and Benoit Ladoux. The role of single-cell mechanical behaviour and polarity in driving collective cell migration. *Nature Physics*, 16(7):802–809, May 2020.

[201] Tanay Bhatt, Abrar Rizvi, Surya Prakash Rao Batta, Sunny Kataria, and Colin Jamora. Signaling and mechanical roles of e-cadherin. *Cell Communication & Adhesion*, 20(6):189–199, November 2013.

[202] Olga Klezovitch and Valeri Vasioukhin. Cadherin signaling: keeping cells in touch. *F1000Research*, 4:550, August 2015.

[203] Weina Yu, Li Yang, Ting Li, and Yi Zhang. Cadherin signaling in cancer: Its functions and role as a therapeutic target. *Frontiers in Oncology*, 9, October 2019.

[204] Mitsutoshi Nakada, Eric M. Anderson, Tim Demuth, Satoko Nakada, Linsey B. Reavie, Kelsey L. Drake, Dominique B. Hoelzinger, and Michael E. Berens. The phosphorylation of ephrin-b2 ligand promotes glioma cell migration and invasion. *International Journal of Cancer*, 126(5):1155–1165, November 2009.

[205] Yao Zhao, Chenchen Cai, Miaomiao Zhang, Lubing Shi, Jiwei Wang, Haoliang Zhang, Ping Ma, and Shibao Li. Ephrin-a2 promotes prostate cancer metastasis by enhancing angiogenesis and promoting emt. *Journal of Cancer Research and Clinical Oncology*, 147(7):2013–2023, March 2021.

[206] Arvinder Singh. Eph/ephrin signaling in cell-cell and cell-substrate adhesion. *Frontiers in Bioscience*, 17(1):473, 2012.

[207] Tohru Yamazaki, Junko Masuda, Tsutomu Omori, Ryosuke Usui, Hitomi Akiyama, and Yoshiro Maru. Epha1 interacts with integrin-linked kinase and regulates cell morphology and motility. *Journal of Cell Science*, 122(2):243–255, January 2009.

[208] Dan Fero, Kuei-Chun Wang, Phu Nguyen, Sung Sik Hur, Yingli Hu, and Yi-Shuan Li. Ephrin-a1 regulates cell remodeling and migration. *Cellular and Molecular Bioengineering*, 4(4):648–655, November 2011.

[209] Matteo Parri, Francesca Buricchi, Elisa Giannoni, Giovanna Grimaldi, Tommaso Mello, Giovanni Raugei, Giampietro Ramponi, and Paola Chiarugi. Ephrina1 activates a src/focal adhesion kinase-mediated motility response leading to rho-dependent actino/myosin contractility. *Journal of Biological Chemistry*, 282(27):19619–19628, July 2007.

[210] Sarah E. Siegrist and Chris Q. Doe. Microtubule-induced cortical cell polarity. *Genes & Development*, 21(5):483–496, March 2007.

[211] Shereen Kadir, Jonathan W. Astin, Lubna Tahtamouni, Paul Martin, and Catherine D. Nobes. Microtubule remodelling is required for the front–rear polarity switch during contact inhibition of locomotion. *Journal of Cell Science*, 124(15):2642–2653, August 2011.

[212] Ksenija Drabek, Marco van Ham, Tatiana Stepanova, Katharina Draegestein, Remco van Horssen, Carmen Laura Sayas, Anna Akhmanova, Timo ten Hagen, Ron Smits, Riccardo Fodde, Frank Grosveld, and Niels Galjart. Role of clasp2 in microtubule stabilization and the regulation of persistent motility. *Current Biology*, 16(22):2259–2264, November 2006.

[213] Nives Pećina-Šlaus. *Cancer Cell International*, 3(1):17, 2003.

[214] Gerhard Christofori and Henrik Semb. The role of the cell-adhesion molecule e-cadherin as a tumour-suppressor gene. *Trends in Biochemical Sciences*, 24(2):73–76, February 1999.

[215] Dhananjay T. Tambe, C. Corey Hardin, Thomas E. Angelini, Kavitha Rajendran, Chan Young Park, Xavier Serra-Picamal, Enhua H. Zhou, Muhammad H. Zaman, James P. Butler, David A. Weitz, Jeffrey J. Fredberg, and Xavier Trepat. Collective cell guidance by cooperative intercellular forces. *Nature Materials*, 10(6):469–475, May 2011.

[216] Zhijun Liu, John L. Tan, Daniel M. Cohen, Michael T. Yang, Nathan J. Sniadecki, Sami Alom Ruiz, Celeste M. Nelson, and Christopher S. Chen. Mechanical tugging force regulates the size of cell–cell junctions. *Proceedings of the National Academy of Sciences*, 107(22):9944–9949, May 2010.

[217] Venkat Maruthamuthu, Benedikt Sabass, Ulrich S. Schwarz, and Margaret L. Gardel. Cell-ecm traction force modulates endogenous tension at cell–cell contacts. *Proceedings of the National Academy of Sciences*, 108(12):4708–4713, March 2011.

[218] Patricia Costa, Liisa M. Blowes, Ana C. Laly, and John T. Connelly. Regulation of collective cell polarity and migration using dynamically adhesive micropatterned substrates. *Acta Biomaterialia*, 126:291–300, May 2021.

[219] David Sarrió, José Palacios, Marta Hergueta-Redondo, Gonzalo Gómez-López, Amparo Cano, and Gema Moreno-Bueno. Functional characterization of e- and p-cadherin in invasive breast cancer cells. *BMC Cancer*, 9(1), March 2009.

[220] Yvonne L Chao, Christopher R Shepard, and Alan Wells. Breast carcinoma cells re-express e-cadherin during mesenchymal to epithelial reverting transition. *Molecular Cancer*, 9(1), July 2010.

[221] S. Lo Vecchio, O. Pertz, M. Szopos, L. Navoret, and D. Riveline. Spontaneous rotations in epithelia as an interplay between cell polarity and boundaries. *Nature Physics*, 20(2):322–331, January 2024.

[222] Linjie Lu, Tristan Guyomar, Quentin Vagne, Rémi Berthoz, Alejandro Torres-Sánchez, Michèle Lieb, Cecilie Martin-Lemaitre, Kobus van Unen, Alf Honigmann, Olivier Pertz, Guillaume Salbreux, and Daniel Riveline. Polarity-driven three-dimensional spontaneous rotation of a cell doublet. December 2022.

[223] Sangyoon J. Han, Kevin S. Bielawski, Lucas H. Ting, Marita L. Rodriguez, and Nathan J. Sniadecki. Decoupling substrate stiffness, spread area, and micropost density: A close spatial relationship between traction forces and focal adhesions. *Biophysical Journal*, 103(4):640–648, August 2012.

[224] Aapo Tervonen, Sanna Korpela, Soile Nymark, Jari Hyttinen, and Teemu O. Ihalainen. The effect of substrate stiffness on elastic force transmission in the

epithelial monolayers over short timescales. *Cellular and Molecular Bioengineering*, 16(5–6):475–495, July 2023.

[225] Michelle S. Liberio, Martin C. Sadowski, Carolina Soekmadji, Rohan A. Davis, and Colleen C. Nelson. Differential effects of tissue culture coating substrates on prostate cancer cell adherence, morphology and behavior. *PLoS ONE*, 9(11):e112122, November 2014.

[226] Jin-Young Lin, Kai-Yin Lo, and Yung-Shin Sun. Effects of substrate-coating materials on the wound-healing process. *Materials*, 12(17):2775, August 2019.

[227] Silvan Klein, Lukas Prantl, Jody Vykoukal, Markus Loibl, and Oliver Felthaus. Differential effects of coating materials on viability and migration of schwann cells. *Materials*, 9(3):150, March 2016.

[228] Carsen Stringer, Tim Wang, Michalis Michaelos, and Marius Pachitariu. Cellpose: a generalist algorithm for cellular segmentation. *Nature Methods*, 18(1):100–106, December 2020.

[229] Mithila Burute, Magali Prioux, Guillaume Blin, Sandrine Truchet, Gaëlle Letort, Qingzong Tseng, Thomas Bessy, Sally Lowell, Joanne Young, Odile Filhol, and Manuel Théry. Polarity reversal by centrosome repositioning primes cell scattering during epithelial-to-mesenchymal transition. *Developmental Cell*, 40(2):168–184, January 2017.

[230] Simon Brayford, Fiona N. Kenny, Toru Hiratsuka, Eduardo Serna-Morales, Lawrence Yolland, Andrei Luchici, and Brian M. Stramer. Heterotypic contact inhibition of locomotion can drive cell sorting between epithelial and mesenchymal cell populations. *Journal of Cell Science*, January 2019.

[231] E. M. Stephenson and N. G. Stephenson. Invasive locomotory behaviour between malignant human melanoma cells and normal fibroblasts filmed in vitro. *Journal of Cell Science*, 32(1):389–418, August 1978.

[232] Andreas Schoenit, Cristina Lo Giudice, Nina Hahnen, Dirk Ollech, Kevin Jahnke, Kerstin Göpfrich, and Elisabetta Ada Cavalcanti-Adam. Tuning epithelial cell–cell adhesion and collective dynamics with functional dna-e-cadherin hybrid linkers. *Nano Letters*, 22(1):302–310, December 2021.

Danksagung

An dieser Stelle möchte ich mich bei allen herzlich bedanken, die mir während meiner Promotion zur Seite standen und mich unterstützt haben:

Zunächst möchte ich mich bei **Prof. Joachim Rädler** dafür bedanken, dass er mir die Möglichkeit gegeben hat, an seinem Lehrstuhl zu promovieren. Vielen Dank für das Vertrauen und die Unterstützung bei der Betreuung dieser Arbeit und für die Freiheit, das Projekt eigenständig mitzugestalten.

Next, I would like to thank **Prof. Chase Broedersz** for many productive discussions and exciting ideas. This collaboration really brought this project to life.

Ich möchte mich auch bei **Dr. Andreas Roidl** und **Bianca Köhler** für die gemeinsame Arbeit an dem microRNA Projekt bedanken. Vielen Dank auch für die Bereitstellung vieler interessanter Zelllinien.

Ein riesengroßes Dankeschön geht an **Tom Brandstätter**. Ohne dich wäre diese Arbeit im wahrsten Sinne des Wortes nur halb so spannend. Deine Theorie passt zu meinen Experimenten wie der Aperol zum Spritz! Vielen Dank für die unzähligen hilfreichen Zoom Meetings (auch wenn die Internetverbindung uns oft im Stich gelassen hat), in denen wir stundenlang über unser Projekt diskutiert und philosophiert haben.

Ein großes Dank geht an die gesamte **Rädler-Gruppe** für eure Unterstützung während der letzten drei Jahre. Durch eure Hilsfbereitschaft wurde schon das ein oder andere Experiment gerettet. Besonders in Erinnerung bleiben die lustigen Wandertage, Volksfestbesuche und die legendären Skikeller-Antholz Partys.

Ein besonderer Dank geht an meine 'Gurls' **Judith** und **Nathalie** für eure Unterstützung, wenn der Western Blot zum wiederholten Male nicht klappte, die langen Zellkultursessions mit guter Musik und die zahlreichen Aperolabende. Ohne euch wäre es nur halb so lustig gewesen!

Vielen Dank auch an **Stefan** für die oft lustigen 'glühenden' Slack-Chats und die umfassenden Analysen des letzten Formel 1 Rennens beim 'early bird'-Kaffee mit obligatorischen Schokocroissant.

Zusätzlich möchte ich mich bei der Gossip-Queen aka **Chris** bedanken, für die lustigen Kaffeepausen, das Triton-treatment meiner Zellen und die Diskussionen übers Patentwesen.

Ein herzliches Dankeschön gilt auch **Gerlinde** für die E-Cadherin mRNA. Nach gut 2 Jahren leuchtete dann endlich die erste MDAMB231 Zelle grün mit meinem Lieblingsprotein E-Cadherin. Danke auch an **Susi** und **Charlott**, die dafür sorgen, dass das Labor überhaupt funktioniert.

Nicht zu vergessen sind natürlich meine fleißigen Korrekturlesern, ohne die der ein oder andere Satz doch recht wenig Sinn ergeben hätte. Danke!

Ein weiterer Dank geht an meine Freunde abseits des Labors: **Jackie**, **Anna** und die Handballcrew **Lotta**, **Lara** und **Carmen**. Ihr habt dafür gesorgt, dass der Spass abseits des Labors nicht zu kurz kommt!

Zu guter Letzt möchte ich mich bei meiner **Familie** für die Unterstützung der letzten Jahre bedanken! Ihr seid immer für mich da und habt mitgefiebert, dass die 'doofe' Zelle endlich grün wird.